

Joachim Espvik

NTNU
Norwegian University of
Science and Technology
Faculty of Information Technology and Electrical
Engineering
Department of Electric Power Engineering

Joachim Espvik

Modeling of Multiterminal HVDC grids with Renewable Energy and Storage Integration by Open Source tools

June 2019





Norwegian University of
Science and Technology

Modeling of Multiterminal HVDC grids with Renewable Energy and Storage Integration by Open Source tools

Joachim Espvik

Energy and Environmental Engineering

Submission date: June 2019

Supervisor: Elisabetta Tedeschi

Co-supervisor: Santiago Sanchez Acevedo

Norwegian University of Science and Technology
Department of Electric Power Engineering

Preface

This Master's Thesis was produced by Joachim Espvik under the supervision of Professor Elisabetta Tedeschi at NTNU and co-supervisor Santiago Sanchez Acevedo, now at SINTEF Energy Research. The Thesis concludes Espvik's Master's degree in Energy and Environmental Engineering at the Department of Electric Power Engineering, Norwegian University of Science and Technology (NTNU). The work is a continuation of a specialization project completed late 2018, titled "*Modeling of an HVDC Two-Level Voltage Source Converter in the Open-Source Tool OpenModelica*".

The problem description for this Thesis was formulated in cooperation between Professor Elisabetta Tedeschi at NTNU and Dr. Yongtao Yang at DNV GL. Two students shared the same problem description, cooperating to some extent in getting to know a new modeling software. The other student is Erling Vatn Tranulis who submits his Thesis. The two Thesis' have more or less the same background using the same mathematical models. However, the final results have different areas of focus, which are both combined in a paper submitted and accepted for presentation at the Offshore Energy and Storage Summit conference in Brest, France, in July 2019.

Acknowledgements

I would like to thank my supervisor, Elisabetta Tedeschi at NTNU, for excellent supervision during the process of working with this Thesis. I want to thank her for the numerous hours spent in meetings, on proofreading and giving valuable feedback. She has given me the possibility to experience the whole process from problem description to final results as well as believing in me to provide the opportunity of writing a paper for and presenting at a conference, which is something I highly appreciate.

I would also like to thank my co-supervisor, Santiago Sanchez Acevedo, now at SINTEF Energy Research, for introducing the OpenModelica software and providing the opportunity of working with laboratory equipment and software. I want to thank him for the many hours spent in the lab troubleshooting, trying to understand how things work together and finally figuring it out.

I would also like to thank Dr. Yongtao Yang at DNV GL for providing an interesting problem description that has allowed me to study a very important and exciting topic for a highly respected company in DNV GL.

Last but not least, I would like to thank my fellow student and friend, Erling Vatn Tranulis, for cooperation over the last year. Erling has provided me new insight and angles to broaden my view of many different topics. I want to thank Erling for the many hours spent with me trying to tame OpenModelica and for writing the paper for the conference together. Without Erling, this Thesis would have been much harder to produce.

Trondheim, 07.07.2019
Joachim Espvik

Summary

The world is in urgent need of low emission renewable energy production to meet the limits set for temperature increase in the Paris Climate Change agreement. Offshore wind power is one of the most promising technologies to reduce greenhouse gas emissions and meet this target to secure a safe future for generations to come. When the amount of offshore wind power installed increases, it is useful to connect offshore wind farms in a grid to increase the flexibility and reliability of the system to ensure the security of supply to shore.

At long distances of large-scale electrical power transmission by sub-sea cables, high-voltage direct current (HVDC) is often preferred over high-voltage alternating current (HVAC). In future and present offshore HVDC grids for large scale wind power integration, the modular-multilevel converter (MMC) is a key component to convert between AC and DC power, providing fast control and the possibility to change the paths of the power flows in the HVDC grid. Additionally, energy storage systems can be integrated in HVDC grids to deliver power and absorb power from offshore wind farms to complement the varying power production due to the intermittency of the wind.

HVDC grids are expected to develop into large and complex systems, and therefore it is useful to study the interactions between the various components such as wind farms, energy storage systems and the HVDC grid including converters and cables. To perform such studies, simulation tools using models that emulate the physical components can be used to gain knowledge on the operation of the system. One emerging modeling tool is the open-source software OpenModelica, which is based on the Modelica modeling language. In this Thesis, OpenModelica was used to model a multi-terminal HVDC system with offshore wind and energy storage integration.

Before building the final simulation system, some aspects of OpenModelica were studied closer. The first aspect was a preliminary assessment of the performance of the software with the accuracy of results and speed of simulations as criteria and Simulink as a benchmark. The results showed that OpenModelica could reproduce the fast dynamics in the current waveforms on the AC-side of a 10kHz 2L-VSC switching model that was implemented in both OpenModelica and Simulink. Additionally, the speeds of simulations in OpenModelica were similar to the speed of Simulink for most of the solvers in OpenModelica. The second aspect was on how OpenModelica could be used with one of Opal-RT's real-time simulators, facilitating hardware-in-the-loop simulations of HVDC systems modeled in OpenModelica. No such guides were found in the literature, and the built-in guide in Opal-RT's software was lacking details. Therefore, a guide on how to build and prepare models for Opal-RT's real-time simulator, ePHASORSIM, was included in the Thesis. The guide included models of a resistor, a voltage source converter (VSC) and a point-to-point MMC based HVDC model. OpenModelica models were successfully tested with the real-time simulator in the National Smart Grid Laboratory

Next, a three-terminal MMC based HVDC system was modeled with two wind farms where one of the wind farms was complemented by an energy storage system. Three

simulation cases were studied. The first case, Test case 1, showed that the three terminal HVDC system had a stable step response to changes in power references in both directions. Test case 2 focused on the dimensioning of the energy storage system using real wind speed data. A configuration where the power from the wind farm was filtered, and the difference in power was delivered and absorbed by the energy storage system, was used. Test case 3 combined the wind farm models and the energy storage configuration at one of the wind farms to study the difference in responses of the HVDC system to events at the two wind farms.

The simulation results of Test case 3 showed that having a fast and somewhat well dimensioned energy storage at the same MMC converter station as one of the wind farms improved the responses and operation of the HVDC system. It was observed that during large drops in wind speed, the DC-voltages and the internal energies of the converters had transients of lower magnitude than the case without an energy storage system connected. At sudden losses of wind farms, the response of the internal energies of the converters also had improved responses with transients of lower magnitude.

Overall, the experience of using the OpenModelica tool for this Thesis was positive, and the software is recommended for similar studies in the future.

Sammendrag

Verden har et akutt behov for energiproduksjon med lave utslipp av klimagasser for å nå grensene for temperaturøkning satt i Parisavtalen. Energiproduksjon fra havvind er en av de mest lovende teknologiene til å redusere utslippene av klimagasser for å nå dette målet og sikre en trygg framtid for fremtidige generasjoner. Når mengden installert effekt av havvind øker, er det nyttig å koble vindparker sammen i et elektrisk nett for å øke fleksibiliteten og påliteligheten og dermed sikre forsyningssikkerheten til land.

Ved lange distanser med overføring av store mengder elektrisk effekt er høyspent likestrøm (HVDC) ofte foretrukket framfor høyspent vekselstrøm (HVAC). I eksisterende og fremtidige HVDC-nett for storskala integrasjon av havvind, er modulær multಿನಿವå-omformerer (MMC) en avgjørende komponent for å omforme mellom likestrøm og vekselstrøm, og den bidrar med rask kontroll og muligheten til å endre retningen og veiene til effektflyten i HVDC-nettet. I tillegg kan et energilagringssystem integreres i HVDC-nett for å både produsere og absorbere effekt som kan komplementere den varierende effektproduksjonen fra vindparker som følger av variabiliteten i vinden.

HVDC-nett er vanligvis store og komplekse, og derfor er det nyttig å studere interaksjonene mellom de forskjellige komponentene som vindparker, energilagringssystemer og HVDC-nettet som inkluderer omformere og kabler. Til å utføre slike studier er det utviklet programvare der man kan bygge modeller som etterligner de fysiske komponentene slik at man kan opparbeide kunnskap om drift av systemet. Ett av de fremadstormende programvarene for slike studier er det åpen kilde-baserte programmet OpenModelica som er basert på modelleringsspråket Modelica. I denne avhandlingen er OpenModelica brukt til å modellere et flerterminal HVDC-nett med integrasjon av havvind og energilagring.

Før dette systemet ble bygd, ble det gjort noen nærmere undersøkelser av enkelte aspekter ved OpenModelica. Det første aspektet som ble undersøkt er en innledende evaluering av ytelsen til programvaren med kriteriene nøyaktighet i resultatene og hastighet av simuleringer med Simulink som sammenligningsgrunnlag. Resultatene viste at OpenModelica greide å gjenskape den raske dynamikken forbundet med strømmene på AC-siden av en 10kHz tonivå VSC (2L-VSC) via en svitsjemodell som ble implementert i både OpenModelica og Simulink. I tillegg viste resultatene at hastigheten på simuleringene i OpenModelica var relativt lik hastigheten til Simulink for de fleste problemløserne i OpenModelica. Det andre aspektet som ble undersøkt er hvordan OpenModelica kan brukes med en av Opal-RTs sanntidssimulatorer, noe som muliggjør det som kalles hardware-in-the-loop (HIL) simuleringer av HVDC systemer modellert i OpenModelica. Det ble ikke funnet noen guide i litteraturen for hvordan dette skulle gjøres, og den innebygde guiden i Opal-RTs programvare manglet detaljer. Derfor er det inkludert en guide som forklarer hvordan man skal bygge og klargjøre modeller i OpenModelica for sanntidssimuleringer i Opal-RTs sanntidssimulator ePHASORSIM. Denne guiden inkluderer en modell av en resistans, en spenningskildeomformer (VSC) og en punkt til punkt MMC-basert HVDC kobling.

Videre ble et tre-terminal MMC-basert HVDC system modellert med to havvindparker

hvorav en havvindpark var komplementert med et energilagringssystem. Tre caser ble simulert og studert. Den første casen, Test case 1, viste at modellen av HVDC systemet med tre terminaler hadde en stabil sprangrespons ved endringer i effektreferanse i begge retninger. Test case 2 fokuserte på å dimensjonere energilagringssystemet ved hjelp av faktisk målte vinddata. En konfigurasjon der effekten fra en vindpark ble filtrert for så at energilagringssystemet dekte forskjellen i filtrert og faktisk effekt ble brukt. Test case 3 kombinerte vindparkmodellene og konfigurasjonen med energilagring ved den ene vindparken for så å studere responsen til HVDC systemet til hendelser ved de to vindparkene.

Simuleringsresultatene av Test case 3 viste hvordan et raskt og relativt ordentlig dimensjonert energilagringssystem ved den samme MMC-terminalen som en vindpark kan forbedre responsen og driften av HVDC-systemet den er koblet til. Det ble observert at ved store fall i vindstyrke, hadde DC-spenningene og den internt lagrede energien i omformerne lavere transienter enn ved tilfellet uten energilagringssystem. Ved plutselige utfall av vindparkene ble det observert at responsen til den internt lagrede energien i omformerne var forbedret med lavere transienter.

Alt i alt er opplevelsen av å bruke OpenModelica for denne avhandlingen positiv, og programvaren kan anbefales til lignende studier i framtiden.

Table of Contents

Preface	1
Acknowledgements	2
Summary	i
Sammendrag	iii
Table of Contents	ix
List of Tables	xi
List of Figures	xvii
Nomenclature	xviii
1 Introduction	1
1.1 Background	1
1.1.1 The challenge of climate change	1
1.1.2 Offshore wind power resources	2
1.1.3 Storage integration for reduced intermittency	3
1.1.4 Offshore wind integration by HVDC grids	3
1.1.5 Open-source modeling tools	3
1.2 Objectives	4
1.3 Limitations of scope	5
1.4 Methodology	5
1.5 Document structure	6
1.6 Relation to specialization project and IEEE paper	6
2 HVDC Transmission Systems	7
2.1 HVDC transmission	7
2.2 Offshore HVDC applications	9

2.3	Multi-terminal HVDC grids	10
2.3.1	The Zhoushan Islands HVDC Grid	11
2.3.2	The North Sea Supergrid	12
2.4	The HVDC power electronic converter	12
3	The Modular Multilevel Converter	15
3.1	The MMC converter	15
3.2	MMC modeling	17
3.2.1	Overview of MMC models in the literature	17
3.2.2	Desired model characteristics for this Thesis	18
3.2.3	Compensated modulation	18
3.2.4	Energy-Based SSTI MMC Model	19
3.2.5	Detailed model	20
3.2.6	Simplified zero-sequence MMC model	21
3.3	Control structure of the MMC	23
3.3.1	Power control	23
3.3.2	Energy control	25
3.3.3	Additional control schemes	26
3.4	Advantages of the MMC	26
3.4.1	Harmonic content	26
3.4.2	Modularity	27
3.4.3	Fault-handling capabilities	28
3.4.4	Energy storage capabilities	28
4	The OpenModelica Modeling Tool	31
4.1	The OpenModelica software	32
4.1.1	The standard library of components	32
4.1.2	Acausal modeling in OpenModelica	33
4.1.3	Solvers in OpenModelica	33
4.1.4	Model exchange through the Functional Mockup Interface	34
4.2	Preliminary assessment OpenModelica's performance	35
4.2.1	Test description	36
4.2.2	Resulting current waveforms compared to Simulink	36
4.2.3	Simulation speeds compared to Simulink	39
4.3	Using OpenModelica for real-time simulations	40
4.3.1	Real-time simulations	40
4.3.2	Hardware-in-the-loop testing	40
4.3.3	Building models in OpenModelica for ePHASORSIM	41
4.3.4	HVDC model for ePHASORSIM	50
5	Simulation System Description	51
5.1	The complete system configuration	51
5.2	Wind farm model	52
5.2.1	Turbine control regions	54
5.3	MMC model	57
5.4	Energy storage model	57

5.5	HVDC cable model	59
5.5.1	Frequency dependency of series impedance elements	60
5.6	Transformer model	60
5.7	Description of test cases and simulation setups	61
5.7.1	Test case 1: Three-terminal HVDC system	61
5.7.2	Test case 2: Wind farm and energy storage	62
5.7.3	Test case 3: Complete system configuration	63
6	Results	65
6.1	Test case 1: Three-terminal HVDC system	65
6.1.1	Results with reversed power flows	68
6.2	Test case 2: Wind farm and storage	69
6.3	Test case 3: Complete system configuration	71
6.3.1	Sudden drop in wind speeds	72
6.3.2	Sudden loss of wind farms	74
7	Discussion	77
7.1	Test case 3 simulation setup	77
7.2	The offshore energy storage system	78
7.2.1	Effects of adding the energy storage to wind farm 1	78
7.2.2	Dimensioning of the energy storage	79
7.2.3	Offshore versus onshore placement of the energy storage	80
7.2.4	On solving the challenge of intermittency	80
7.3	Tuning of controllers	81
7.4	The HVDC real-time simulation OpenModelica model	81
7.5	Using the OpenModelica software	82
7.5.1	Developing real-time simulation models	82
7.6	Separating the area of focus in two Theses	83
7.7	Achieving the objectives	83
8	Conclusion	85
8.1	Suggestions for future work	86
	Bibliography	89
A	Transformations	97
A.1	Amplitude invariant Park transformation	97
A.1.1	abc to dq transformation	97
A.1.2	dq to abc transformation	97
A.2	Park transformation with zero-sequence component	97
A.2.1	abc to dqz transformation matrix	97
A.2.2	dqz to abc transformation matrix	98
A.3	Transformation between global and local ref. frame	98

B	AC-side switching models	99
B.1	Model parameters	99
B.2	Simulink switching model implementation	99
B.2.1	PMW generator	100
B.2.2	Current controller	100
B.2.3	dq transformation	101
B.2.4	inverse dq transformation	101
B.2.5	Ideal PLL	101
B.3	OpenModelica switching model implementation	102
B.3.1	PWM generator	102
B.3.2	Current controller	103
B.3.3	dq transform	103
B.3.4	Inverse dq transform	104
B.3.5	Ideal PLL	104
C	OpenModelica and Opal-RT	105
C.1	Power Pin to 3ph grid interface	105
C.1.1	Reference frame transformation	105
C.1.2	Grid	106
C.2	Implementation of VSC_BASE block	107
C.3	HVDC model for ePHASORSIM	107
C.4	RT-LAB / ePHASORSIM guide	109
C.4.1	Excel implementation of example system	110
C.4.2	Preparing the system model in RT-LAB	111
D	OpenModelica implementation	117
D.1	MMC model	117
D.2	AC-side	118
D.2.1	dq current controller	118
D.2.2	Park transform	119
D.2.3	Inverse park transform	119
D.3	DC-side	119
D.4	Zero sequence energy sum	120
D.4.1	Zero sequence energy dynamics	120
D.4.2	Energy controller	121
D.5	Power controller	121
D.6	Wind farm model	122
D.6.1	Turbine dynamics	122
D.6.2	Turbine speed controller	123
D.6.3	Turbine power/pitch controller	123
D.6.4	Region IV check	123
D.6.5	Coupling the wind farm model electrically	124
D.7	HVDC cable model	125
D.8	Energy storage model	125
D.8.1	Storage protection	126
D.9	Transformer model	126

E	System parameters	127
E.1	HVDC parameters	127
E.1.1	MMC parameters	127
E.1.2	Cable parameters	128
E.2	Wind farm parameters	129
E.3	Energy storage parameters	129
F	Additional results	131
F.1	Test case 2: Dimensioning of energy storage	131
F.1.1	Varying filter time constant with $P_{rated} = 250\text{MW}$	131
F.1.2	Varying P_{rated} with constant filter time constant	133
F.1.3	Increasing both filter time constant and P_{rated}	134
G	OSES2019 paper	137

List of Tables

4.1	Basic solvers in OpenModelica	34
4.2	Comparison of simulations speeds at $\Delta t = 1\mu s$	39
4.3	Information to register in the FMUGlossary file	47
6.1	Main parameters of Test case 1	65
6.2	Main parameters of Test case 2	69
6.3	Main parameters of Test case 3	71
B.1	2L-VSC parameters	99
E.1	MMC parameters	127
E.2	MMC controller parameters	128
E.3	Cable parameters	128
E.4	Wind farm parameters	129
E.5	Wind turbine controller parameters	129
E.6	Energy storage parameters	129

List of Figures

1.1	Greenhouse gas emissions per emission category up to 2017 [4, 5].	2
1.2	Actual and forecasted growth in offshore wind power installed worldwide [9].	3
1.3	A three-terminal HVDC system with renewable and storage integration. . .	5
2.1	Typical costs versus distance for high power AC and DC.	8
2.2	Planned and operating HVDC projects in China per 2017, connecting remote hydropower resources [20].	8
2.3	Transmitted power capacity versus distance for AC transmission at different voltage levels in a sub-sea cable [21, 22].	9
2.4	ABBs DolWin 2 offshore converter station [27].	10
2.5	Point to point connections of offshore wind farms to shore [30].	10
2.6	Conceptual meshed HVDC offshore grid [30].	11
2.7	The HVDC grid connecting the Zhoushan Islands [33].	12
2.8	Meshed North Sea HVDC grid scenario where the blue lines are expected early stage developments and the red lines are later stage developments [37].	13
3.1	The schematic of a three-phase MMC [45].	16
3.2	The AC voltage waveform of the 2-L VSC (upper) compared to an MMC (lower) [12].	16
3.3	Overview of the simplified zero-sequence MMC model.	23
3.4	Block diagram of the dq-current controller with feed-forward decoupling.	24
3.5	Block diagram of the per unit active power controller with DC voltage droop control.	25
3.6	Block diagram of the outer zero sequence energy controller with inner zero sequence circulating current controller.	25
3.7	Total harmonic distortion (THD) and maximum individual harmonic (D _{nm} x) in the voltage waveform when increasing the number of sub-modules per arm, N, from reference [58]	27

3.8	DC side fault current path of (a) a half-bridge sub-module (b) a full-bridge sub-module [55].	28
4.1	The OpenModelica standard library.	32
4.2	The difference of acausal modeling (a) using an electrical circuit and causal modeling (b) using generic blocks.	33
4.3	A circuit representation of the 2L-VSC used for the test with a constant DC-voltage on the DC-side.	35
4.4	Comparison of the dq-currents from switching model in Simulink and OpenModelica.	36
4.5	d-currents from OpenModelica and Simulink compared.	37
4.6	q-currents from OpenModelica and Simulink compared.	37
4.7	Comparison of the abc-currents from switching model in Simulink and OpenModelica.	38
4.8	Comparison of a phase currents from switching model in Simulink and OpenModelica.	38
4.9	Overview of the power hardware-in-the-loop (PHIL) process [82].	41
4.10	The Opal-RT Modelica Developer Library	42
4.11	The OpenModelica implementation of the Power Pin connector class.	43
4.12	The PIN2INOUT interface from the Opal-RT library.	44
4.13	The implementation of the RESISTOR model in the GenUnit library.	45
4.14	Implementation of the RESISTOR_BASE block in the Opal-RT library.	45
4.15	Implementation of a VSC in the GenUnit library to illustrate the use of the interface pin.	46
4.16	The interface of Opal RT's FMUCreator 1.0.	47
4.17	RESISTOR and VSC example implementation in the FMUGlossary file opened in Excel.	48
4.18	Excel implementation of the RESISTOR example with 1 parameter.	48
4.19	Excel implementation of the VSC example with 5 parameters.	49
4.20	Declaration of the interface pins in the Excel file.	49
4.21	Flowchart of the steps needed to prepare a Modelica model for ePHASOR-SIM.	49
5.1	The three-terminal MMC based HVDC system with wind farms and energy storage, reproduced from Figure 1.3 for convenience.	52
5.2	A general representation of a Type IV wind turbine with a synchronous generator and fully rated power electronic converters without a gearbox.	53
5.3	Control regions of a wind turbine [90].	54
5.4	A schematic of the wind turbine model with pitch controller and speed controller.	55
5.5	Block diagram of the turbine speed controller with anti-windup scheme.	56
5.6	Block diagram of the turbine pitch controller with anti-windup scheme.	56
5.7	Schematic of the energy storage model and positive power flow directions.	57
5.8	Generic representation of the frequency dependent cascaded pi-model of an HVDC cable with N parallel branches and p pi-sections from [91].	59
5.9	Frequency dependency of cable parameters.	60

5.10	Test case 1 simulation setup in OpenModelica.	61
5.11	Test case 2 simulation setup in OpenModelica.	62
5.12	The wind speed variation used for Test case 2.	63
5.13	Test case 3 simulation setup in OpenModelica.	64
5.14	The wind speed signals used to simulate a sudden drop in wind speeds for Test case 3.	64
6.1	The powers of all three MMCs when stepping the total power 0.4 pu. . . .	66
6.2	The response of the DC voltages when stepping the total power of 0.4 pu.	66
6.3	Response of the dq-currents when stepping the total power 0.4 pu.	67
6.4	The response of the circulating currents when stepping the total power 0.4 pu.	67
6.5	The response of the internal stored energy when stepping the total power 0.4 pu.	67
6.6	The response of the abc-currents when stepping the total power 0.4 pu. . .	68
6.7	The step response of the MMC powers when all power references are re- versed.	68
6.8	The step response of the DC voltages when the power flows are reversed.	69
6.9	Power from wind turbine, energy storage and combined power in the Test case 2 setup.	70
6.10	The state of charge (SOC) of the energy storage in Test case 2.	70
6.11	Variation of the rotational speed, ω , and blade angle, β of the turbine in Test case 2.	71
6.12	The response of the wind farm powers and energy storage powers when a sudden drop in wind speed is introduced.	72
6.13	Response of the MMC powers for test case 3 when a sudden drop in wind speeds is introduced.	73
6.14	The response of the DC voltages for Test case 3 when a sudden drop in wind speeds is introduced.	73
6.15	The response of the zero sequence energy of the MMCs at a sudden drop in wind speeds.	74
6.16	The response of the SOC when a sudden change drop in wind speeds is introduced	74
6.17	The response of the MMC powers at a sudden loss of wind farms.	75
6.18	The response of the DC voltages at a sudden loss of wind farms.	75
6.19	The response of the zero sequence energy of the MMCs at a sudden loss of wind farms.	76
A.1	Alignment of reference frames for transformation between global to local reference frame.	98
B.1	The implementation of the AC side in a 2L-VSC switching model in Simulink.	99
B.2	The implementation of a PWM signal generator in Simulink.	100
B.3	Implementation of the current controller in Simulink.	100
B.4	Implementation of the dq-transformation in Simulink.	101
B.5	Implementation of the inverse dq-transformation in Simulink.	101

B.6	Implementation of the ideal PLL in Simulink.	101
B.7	Implementation of the switching model in OpenModelica.	102
B.8	Implementation of the PWM generator in OpenModelica.	102
B.9	Implementation of the current controller for the switching model in Open- Modelica.	103
B.10	Implementation of the dq-transform for the switching model in OpenMod- elica.	103
B.11	Implementation of the inverse dq-transform for the switching model in OpenModelica.	104
B.12	Implementation of the ideal PLL in OpenModelica.	104
C.1	The outer level of the PowerPin to 3ph grid class.	105
C.2	Implementation of the reference frame transformation class.	106
C.3	Implementation of the Grid class used by the PowerPin to 3ph grid interface.	106
C.4	Implementation of the VSC_BASE block in OpenModelica including dq- current dynamics, controllers and transformation between local and global reference frame.	107
C.5	The example grid used to test the MMC based HVDC model.	107
C.6	The GenUnit implementation of the HVDC model.	108
C.7	The HVDC_BASE implementation in the Developer library.	108
C.8	The excel implementation of a grid containing the HVDC model built in OpenModelica.	109
C.9	Example system using the VSC model.	110
C.10	The complete excel implementation of the example system using the VSC.	111
C.11	The laboratory set up for real-time simulations.	112
C.12	The interface of RT-LAB.	112
C.13	The outer level of the VSC model in Simulink.	113
C.14	The SC_console sub-system of the VSC test model.	113
C.15	The SM_grid sub-system of the VSC test model.	114
C.16	Settings inside the "Solver" block for the Excel file and the FMU folder.	114
C.17	Settings under the "Simulation settings" tab in the "Solver" block.	115
C.18	The window that appears after the "Execute" button is clicked.	115
C.19	Screenshot during a successful real-time simulation containing the VSC model.	116
D.1	Implementation of the MMC model.	117
D.2	Implementation of the AC-side of the MMC model.	118
D.3	Implementation of the dq-current controller.	118
D.4	Implementation of the Park transform.	119
D.5	Implementation of the inverse Park transform.	119
D.6	Implementation of the DC-side of the MMC model	119
D.7	Implementation of the zero sequence energy sum block in the MMC model.	120
D.8	Implementation of the zero sequence energy dynamics	120
D.9	Implementation of the zero sequence energy controller.	121
D.10	Implementation of the active power controller with DC voltage droop.	121
D.11	Overview of the wind turbine model used to represent a wind farm.	122

D.12	Implementation of the turbine dynamics block.	122
D.13	Implementation of the speed controller in the turbine model.	123
D.14	Implementation of the power controller in the turbine model.	123
D.15	Logic block to turn off the power production when wind speed is above the limit for region IV.	123
D.16	Coupling of the wind farm model with electrical components.	124
D.17	Test of the wind farm model coupled with electrical components.	124
D.18	Implementation of a cable model with 3 parallel branches and 5 pi sections.	125
D.19	Implementation of the storage model.	125
D.20	Implementation of the storage protection.	126
D.21	Implementation of the transformer model in OpenModelica.	126
F.1	Effects on the combined wind farm and storage power when varying the filter time constant of Test case 2.	132
F.2	Effects on the SOC when varying the filter time constant of Test case 2.	132
F.3	Effects on the combined wind farm and storage power when varying the rated power of the energy storage in Test case 2.	133
F.4	Effects on the SOC when varying the rated power of the energy storage in test case 2.	134
F.5	Effects on the combined wind farm and storage power when increasing both the filter time constant and the rated power of the energy storage in Test case 2.	134
F.6	Effects on the SOC when increasing both the filter time constant and the rated power of the energy storage in Test case 2.	135

Nomenclature

i_u	=	Current in upper (u) arm
i_l	=	Current in lower (l) arm
i_c	=	Circulating current
i_v	=	AC grid current
w_u	=	Aggregated capacitor energy in upper (u) arm
w_l	=	Aggregated capacitor energy in lower (l) arm
w_Σ	=	Capacitor energy sum of upper and lower arm
w_Δ	=	Capacitor energy difference between upper and lower arm
n_u	=	Upper arm insertion index
n_l	=	Lower arm insertion index
$v_u^{SM_i}$	=	Voltage of the i th submodule in the upper arm
$v_l^{SM_i}$	=	Voltage of the i th submodule in the lower arm
v_u^σ	=	Upper arm capacitor voltage sum
v_l^σ	=	Lower arm capacitor voltage sum
v_u	=	Upper arm output voltage
v_l	=	Lower arm output voltage
u_c	=	Voltages driving circulating currents
e_v	=	Voltages driving AC-side currents
v_o	=	Voltage at the point of common coupling
v_g	=	Voltage of AC-grid Thvenin equivalent
v_{dc}	=	Voltage at the DC terminals of the MMC
R_a	=	MMC arm resistance
L_a	=	MMC arm inductance
R_f	=	Equivalent MMC output resistance
L_f	=	Equivalent MMC output inductance
R_{eq}	=	Equivalent AC resistance, $R_{eq} = R_a/2 + R_f$
L_{eq}	=	Equivalent AC inductance, $L_{eq} = L_a/2 + L_f$
C_{SM}	=	Capacitance of an MMC submodule
N	=	Number of submodules in an arm
C_{eq}	=	Equivalent MMC arm capacitance, $C_{eq} = C_{SM}/N$
C_{dc}	=	Capacitance at the DC terminals
abc	=	Natural three-phase coordinates
$dqz_{+\omega}$	=	Synchronous reference frame rotating at $+\omega$
$dqz_{-2\omega}$	=	Synchronous reference frame rotating at -2ω
$dqz_{+3\omega}$	=	Synchronous reference frame rotating at $+3\omega$

Chapter 1

Introduction

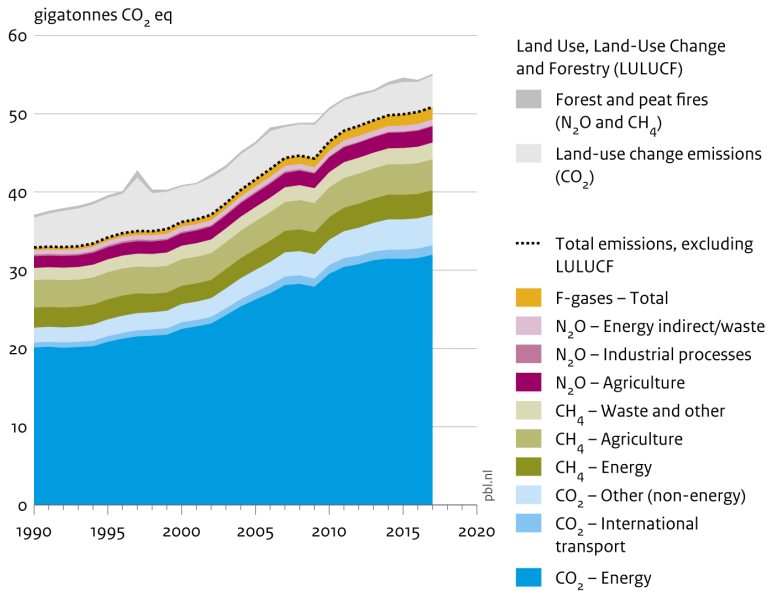
1.1 Background

1.1.1 The challenge of climate change

In October 2018, the report "Global Warming of 1.5°C" was published by The Intergovernmental Panel on Climate Change (IPCC). This report outlines what needs to be done to fulfill the Paris Climate Change agreement [1] of staying well below 2 degrees of global warming, which most of the nations of the world have ratified. The IPCC report was based on more than 6000 recent publications, and one of the conclusions is that greenhouse gas emissions must be 45% lower than 2010 levels by 2030 and net zero by 2050 to stay within 1.5 degrees of global warming [2].

From Figure 1.1 it can be seen that the emissions related to energy production and usage have the largest share of all greenhouse gas emission sources, making up a total of around 70% (CO₂ and CH₄). Therefore, it is clear that a transition to low emission energy systems is crucial to stay within the 1.5-degree limit. This transition was outlined in the IPCC report, which estimates that the shares of renewable energy sources in global electricity generation must be increased to between 50 and 60% within 2030 and between 60 and 80% within 2050 not to exceed the 1.5-degree limit [2]. For perspective, in 2017, the shares of renewable in global electricity production was 25% [3].

Global greenhouse gas emissions, per type of gas and source, including LULUCF



Source: EDGAR v5.0/v4.3.2 FT 2017 (EC-JRC/PBL, 2018); Houghton and Nassikas (2017)

Figure 1.1: Greenhouse gas emissions per emission category up to 2017 [4, 5].

1.1.2 Offshore wind power resources

In a comparison of emissions from renewable energy sources comparing 79 studies involving life cycle assessments, it was concluded that offshore wind power generates the lowest emissions of all renewable energy sources during its life cycle [6]. Offshore wind power is also currently the fastest growing renewable energy source [2] and has a global potential [7]. The interest around *offshore* wind farms is partly due to higher and more stable wind speeds compared to onshore wind sites [8] with more substantial potential for energy production. Figure 1.2 shows the historical growth during recent years and a forecast for the coming years on the growth of the installed offshore wind power capacity worldwide from reference [9]. During the last ten years, it has also been observed that the installed capacity of offshore wind power has a much higher growth rate than onshore wind power, although the total amount of installed offshore capacity is lower than onshore installed capacity [9].

Another crucial aspect related to wind power is its intermittent power production due to varying wind speeds. These variations in wind speeds make the power output from wind farms vary irregularly, while the load supplied by the wind farm is not necessarily varying in a correlated way [10].

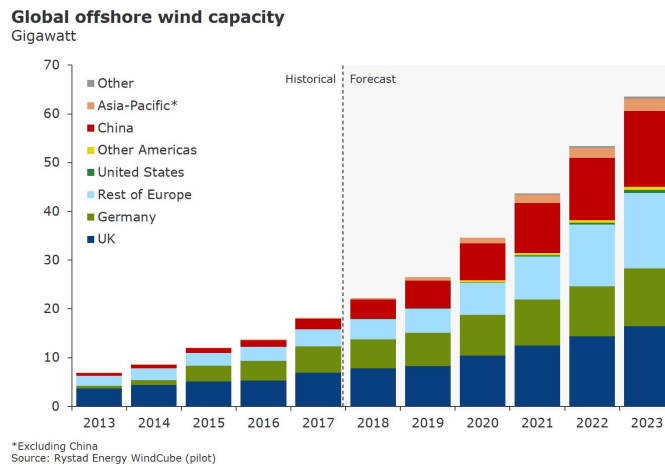


Figure 1.2: Actual and forecasted growth in offshore wind power installed worldwide [9].

1.1.3 Storage integration for reduced intermittency

One possible solution to the intermittency challenge is to integrate energy storage in the power system to complement the power production from the wind farm. This way, a storage unit can absorb power when the wind farm produces more power than the load consumes and release power when the wind farm produces less power than the load consumes [11]. Such possibilities will be further described and investigated in Chapters 5 and 6.

1.1.4 Offshore wind integration by HVDC grids

With increasing penetration of offshore wind power into the electrical power system, there are new requirements to the latter to secure the energy supply from the offshore wind resources. When wind farms are located far from shore, transmission systems based on long sub-sea cables are needed. For such long-distance transmission, high-voltage direct current (HVDC) technology is often preferred over high voltage alternating current (HVAC). Also, with an increasing number of wind farms, it is beneficial to connect them in a meshed HVDC grid to increase the reliability and flexibility of the transmission system.

In HVDC grids, the power converter that converts between AC and DC electrical power is a key component. Most future offshore HVDC grids will probably be based on the voltage source converter (VSC) technology, and more specifically the modular multilevel converter (MMC) topology [12].

1.1.5 Open-source modeling tools

When designing and developing technology for HVDC grids with renewable and storage integration, the topic of dynamic analysis to evaluate interactions among components plays an important role, as HVDC grids are expected to develop into large and complex systems.

Dynamic analysis is carried out through transient modeling and simulations to gain knowledge of the system dynamics to keep a stable and correct operation of the system. Such studies are performed through specialized software that can reproduce the dynamics of the physical components in the HVDC grid.

OpenModelica is an emerging tool for dynamic analysis of complex systems based on the Modelica language [13]. The software is open-source, meaning that the source code is available to anyone for any purpose for free. This way, anyone can change and improve the source code to, for example, improve the performance and perform bug fixes. Models developed in OpenModelica can be shared across multiple platforms and used for real-time hardware-in-the-loop (HIL) simulations, which allows laboratory experiments on HVDC grids without needing full-scale systems and can speed up the development processes of HVDC grids.

1.2 Objectives

This Thesis has multiple objectives, some of which have come as a feedback on the Specialization Project [14] as mentioned in the preface.

The first objectives of this Thesis relate to introducing and giving a basic understanding of HVDC systems, with particular focus on HVDC grids as well as introducing the modular multilevel converter (MMC) to provide the information needed to build a model of the MMC to be used in studies of HVDC grids.

The second group of objectives is related to the OpenModelica software, where one is to investigate how to use OpenModelica for real-time hardware-in-the-loop (HIL) simulations. The other objective, which was suggested in feedback from the Specialization Project, is to evaluate the performance of OpenModelica in replicating the fast dynamics of a 10kHz 2-L VSC switching model. These two objectives were also requested by the industrial partner, DNV GL, expressing an interest around open source tools in general and OpenModelica in particular in the project description for this Thesis.

The last objective is to model and study the interactions between components in a three-terminal MMC based HVDC system with offshore wind and energy storage integration as shown in Figure 1.3 using the OpenModelica software. The system includes two wind farms, WF1 and WF2, an energy storage system, ESS. As part of this objective, models of all components are implemented in OpenModelica, and the energy storage system has to be dimensioned using simulations with actual wind data. The system in Figure 1.3 is chosen because it is the system with the lowest complexity that allows studying the interplay of all key components in an offshore HVDC grid, and it can be further expanded using the models developed in this Thesis which are made publicly available.

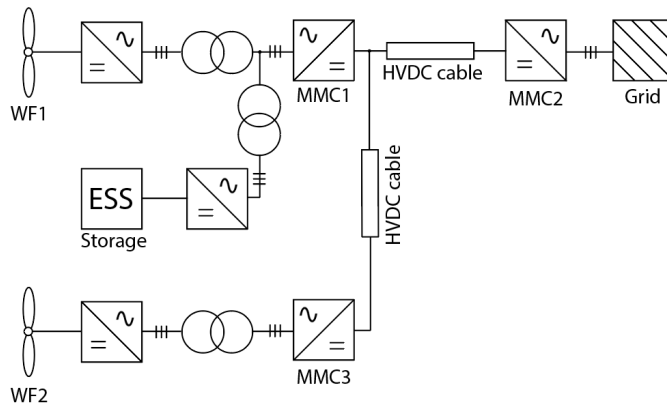


Figure 1.3: A three-terminal HVDC system with renewable and storage integration.

1.3 Limitations of scope

The main focus of this Thesis is the dynamics related to the HVDC system. Therefore, simplified but sufficient models are used for wind farms and energy storage. Also, the evaluation of the type of energy storage technology to be used is considered out of scope for this Thesis. When it comes to dimensioning of the energy storage used, a simple approach using real wind data and simulations is used, because more advanced methods for dimensioning of the storage are considered out of scope for this Thesis. Also, this approach was chosen to show an example of one practical use of simulation tools.

When it comes to HVDC systems, the comparison of LCC based and VSC based HVDC systems is left outside the scope of this work, as that was covered in the Specialization Project [14].

The internal storage capability of the MMC is modeled but not further explored during the simulations in this Thesis, as Erling Vatn Tranulis covers this topic in his Thesis [15].

Additionally, eigenvalue analysis of the system and further stability margins of the controllers used in the system are not considered, as the controllers are only tuned to give satisfactory responses. However, the system is properly tested to ensure that it is stable for a wide range of events.

Lastly, the models developed use ideal PLLs, meaning the topic of frequency stability is considered outside the scope of this Thesis.

1.4 Methodology

The work in this Thesis combines multiple methodologies; a literature review, mathematical modeling, simulations with an emerging modeling tool, development of packages for an emerging modeling tool and laboratory work with real-time simulators for future experimental validation.

The first part of this Thesis is a literature review to gain knowledge about HVDC grids and the modular multilevel converter (MMC), including modeling of the converter.

The next part contains simulations using the OpenModelica software and Simulink to evaluate the performance of OpenModelica. In the same chapter, work has been done in the National Smart Grid Laboratory using a real-time simulator to increase the knowledge and explore the potential of OpenModelica.

The last part of this Thesis uses mathematical modeling of multiple components combined in a package in OpenModelica. The models are combined in three different setups to study the dynamic interactions in an HVDC grid with offshore wind and energy storage integration.

1.5 Document structure

The document is structured as follows:

Chapter 2 gives an introduction to HVDC transmission with a focus on offshore applications for integration of offshore wind power. Chapter 3 introduces the modular multi-level converter (MMC) used in HVDC grids as well as the modeling of the MMC used for transient simulations. Chapter 4 introduces the OpenModelica simulation software used to model and simulate the system described in Chapter 5. Chapter 5 describes the modeling of a three-terminal offshore HVDC system with integration of two wind farms and an energy storage system. Chapter 6 shows the results from simulating the system, and Chapter 7 consists of a discussion on the results. Lastly, Chapter 8 provides the concluding remarks.

1.6 Relation to specialization project and IEEE paper

As mentioned in the Preface, this Thesis is a continuation of the Specialization Project titled *"Modeling of an HVDC Two-Level Voltage Source Converter in the Open-Source Tool OpenModelica"* where a literature study was done to give a state of the art description of HVDC systems. Some of the reference material used in describing HVDC systems and the MMC is also used in this Thesis. Additionally, the Specialization Project contained modeling of the AC-side of an average model of a 2L-VSC in OpenModelica with a comparison of results to Simulink, including a more detailed description of vector control of the AC-side currents than what will be provided in this Thesis. The Specialization Project also contains a discussion where the experience of using OpenModelica compared to Simulink is further explained.

As also mentioned in the Preface, the results from this Thesis are combined with the results from Erling Vatn Tranulis' Thesis [15] in an IEEE paper that was submitted and accepted for presentation at the Offshore Energy and Storage Summit 2019 conference held in Brest, France, in July 2019. The paper is titled *"Modeling of Multiterminal HVDC Offshore Grids with Renewable Energy and Storage Integration by Opensource Tools"* [16] and is appended in Appendix G.

HVDC Transmission Systems

The question on what transmission technology is more suitable for transferring electrical power spans back to the late 1800s with Thomas Edison's low-voltage direct current (DC) and Nikola Tesla's alternating current (AC). Since then, both technologies have improved due to technological advances, and although AC dominates most transmission networks, high-voltage DC (HVDC) is having increasing importance due to economic and technological reasons. When envisioning the role of power electronics in future power systems with a high penetration of photovoltaics and wind power already in 1988, Narain G. Hingorani stated the following: "The insertion of an HVDC link into the ac system will perhaps remain as the ultimate tool" [17].

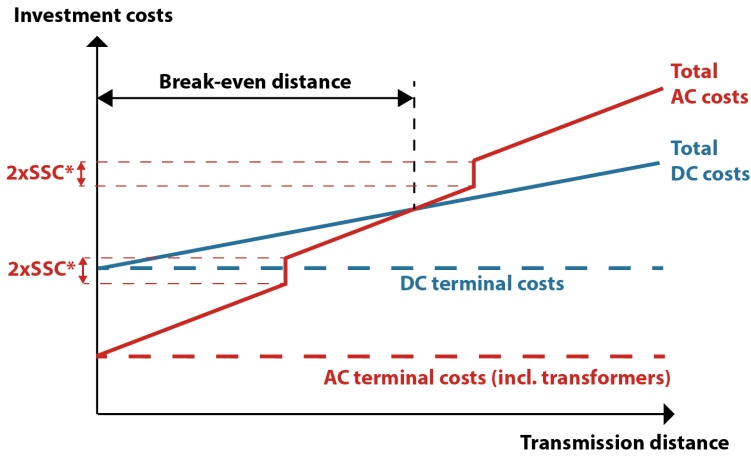
This chapter will give a perspective on some cases where HVDC is preferred over HVAC, and how multi-terminal HVDC grids can be used for the integration of offshore wind resources.

2.1 HVDC transmission

Today, HVDC transmission has increasing importance in the electrical power grid due to its advantages compared to HVAC when it comes to large power transfers over long distances.

The choice between AC and DC for transmitting large amounts of power is usually based on the costs, provided that both solutions are technically feasible. In this context, it should be mentioned that AC transmission is not possible above a certain distance and/or power level, which is to be explained later.

The cost of HVAC transmission tends to increase more rapidly with the increasing length of the transmission compared to HVDC. This makes HVDC the cheapest alternative for considerable distances. The distance where HVDC and HVAC costs are equal is called the break-even distance as can be seen in fig. 2.1. The break-even distance varies from project to project and is dependent on power levels, but as a rule of thumb, it is in the range of 500 to 800 km for overhead lines according to references [18]. Long AC connections require reactive compensation, which is shown by the vertical lines of the AC-curve in Figure 2.1.



*SSC = Series and shunt compensation of AC lines, which is required for each section of the line

Figure 2.1: Typical costs versus distance for high power AC and DC.

An example of connecting large amounts of renewable energy resources through HVDC is the connection of hydro resources in the west of China to the east of China where the population density is the highest. This is illustrated by The Economist in Figure 2.2. China is also where the currently largest HVDC project in the world is found, which is a 3284km hydropower connection from Changji to Guquan. The connection started successfully operating on December 31st, 2018, transmitting 12000MW of power at $\pm 1100\text{kV}$ [19].



Figure 2.2: Planned and operating HVDC projects in China per 2017, connecting remote hydropower resources [20].

2.2 Offshore HVDC applications

When using sub-sea cables for AC transmission, large charging currents are generated because of the much higher capacitances of sub-sea cables compared to overhead lines. Figure 2.3 shows how the increased transmission distance reduces the maximum transmitted power for AC in sub-sea cables at different voltage levels and compensation schemes at the end of the cables due to these charging currents. The compensation schemes used in the figure are Thyristor Controlled Reactors (TCR) at either one end or both ends of the sub-cable [21, 22].

The challenge with these charging currents can be further dealt with by installing additional compensation along the length of the cable connection by adding intermediate compensation platforms with shunt reactors [23]. Alternatively, the need for compensation can be entirely removed by using voltage source converter (VSC)-based HVDC. Therefore, HVDC is a well-suited technology for sub-sea connections to, for example, connect offshore power resources to shore.

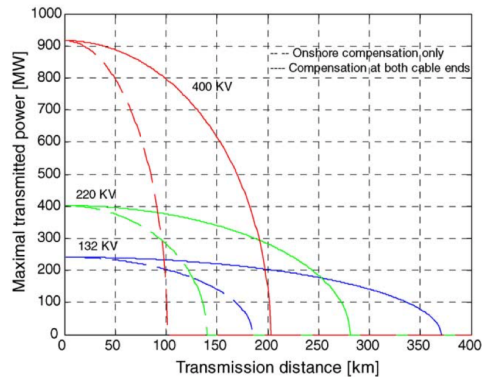


Figure 2.3: Transmitted power capacity versus distance for AC transmission at different voltage levels in a sub-sea cable [21, 22].

As a result of these charging currents, the break-even distance is drastically reduced, and it is typically lowered to the range of 50 to 70 km for sub-sea connections according to references [24, 18], depending on the project and power levels. However, it should also be mentioned that this break-even distance is increasing with recent advances in AC-cable technologies.

VSC-based HVDC, which is briefly explained later, is especially well suited for connecting wind farms due to its operational benefits and controllability, including fast and independent operation of active and reactive power. With these fast control mechanisms, VSC HVDC can, for example, allow wind farms to contribute in mainland frequency support in the future [25]. Additionally, VSC HVDC is well suited for being connected to weak grids. This fits connection of offshore wind farms, as they are weak grids by themselves. This also allows offshore wind power integration into weak onshore grids [26]. Also, VSC HVDC will be important in future and present HVDC grids due to its fast control and flexibility, as explained in the next section.

Figure 2.4 shows an offshore VSC HVDC converter station located in the North Sea, DolWin 2, connecting up to 916 MW of wind power to Germany at 320 kV [27].



Figure 2.4: ABBs DolWin 2 offshore converter station [27].

According to ABB, 90 offshore wind farms were operating in Europe in 2018 [28]. 40 of these wind farms were rated higher than 200MW. Around one-thirds of the 40 were connected through HVDC to shore, either combined in groups or individually. In total, seven HVDC systems were operating in the North Sea while three were under construction in 2018 [28].

Although most offshore wind farms today are connected by HVAC, the role of offshore HVDC will become increasingly important as the wind farms increases in size. Also, future projects are projected to be further from shore due to better wind speed profiles and and larger space demands [29].

2.3 Multi-terminal HVDC grids

The traditional way of connecting an HVDC-connected wind farm to shore is through point to point connections as shown in Figure 2.5.



Figure 2.5: Point to point connections of offshore wind farms to shore [30].

However, the traditional point to point connection is very dependent on the secure operation of the single connection between the wind farms and the shore. If there is a fault on either the cable or the one of the converters, the whole power supply may be lost. When having the expected increasing penetration of offshore wind resources in the power system, a more reliable transmission system for securing the power supply from offshore wind farms to shore is needed.

One way of ensuring the security of supply and increasing the system reliability and flexibility is to connect the wind farms in a meshed multi-terminal HVDC grid as shown in Figure 2.6. By adding HVDC connections between the wind farms to form a grid, additional paths for power flows to the shore are introduced which allow for rerouting of power flows in cases when a cable is out of operation. To have these changes in power flow directions without changing the DC voltage polarities of the system, VSC HVDC can be used as it allows power flow reversal by DC current reversal [31] without needing any additional switchgear [32].

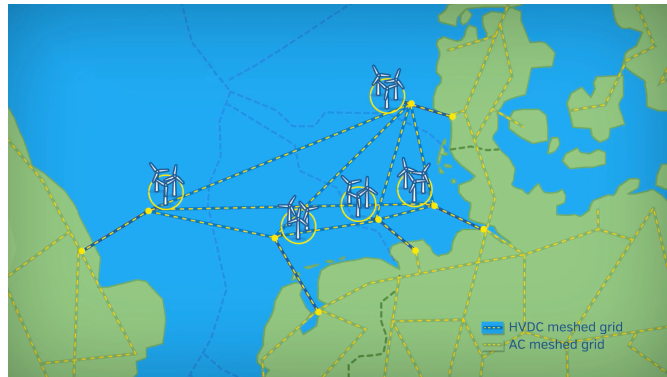


Figure 2.6: Conceptual meshed HVDC offshore grid [30].

The potential upsides of HVDC grids have facilitated a lot of research around the topic during recent years [32]. The two next sections will show an example of one of the first HVDC grids that was built and started operating in addition to an interesting possible future HVDC grid in the North Sea.

2.3.1 The Zhoushan Islands HVDC Grid

Recently, a five-terminal HVDC grid as shown in Figure 2.7 started operating in China, connecting the five Zhoushan Islands. The grid has a total capacity of 1000 MW at DC voltage levels of ± 200 kV where the largest HVDC converter has a rated power of 400 MW.

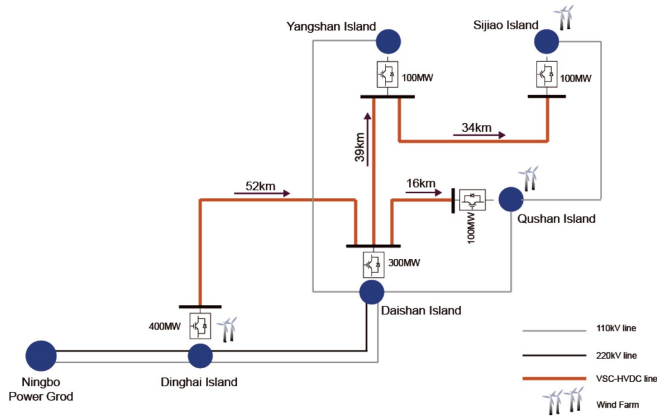


Figure 2.7: The HVDC grid connecting the Zhoushan Islands [33].

The old AC connections between the islands were having problems facing the increasing population and energy demand, yielding an unreliable and unstable power grid. The solution to increasing the system reliability was to introduce the VSC based HVDC, a grid which could provide reactive power support to stabilize the existing AC grid. Additionally, China is known for having large offshore wind resources outside their coast [34, 35]. The new HVDC grid on the Zhoushan islands did also open for integration of the large offshore wind potential in the area [36]. By adding the HVDC grid, the islands are now not relying only on small generator plants as before, but also on renewable offshore energy sources in addition to the added reliability and flexibility of the new grid.

2.3.2 The North Sea Supergrid

Another interesting area where an offshore HVDC grid can increase the system reliability and also interconnect otherwise separate markets to facilitate power exchange and trading is in the North Sea [37]. The area is known for having large amounts of offshore wind resources [38], which could be interconnected by HVDC to form a supergrid. Figure 2.8 shows a scenario combining early stage developments of single line connections and later stage developments connecting the wind farms in a grid. This grid is addressed by large projects as the Horizon 2020 project PROMOTioN [30]

2.4 The HVDC power electronic converter

The converter that converts the power between AC and DC is a key component in HVDC systems when it comes to operation and control.

The traditional converter is the well proven thyristor-based line commutated converter (LCC), which is still a reliable option in, for example, onshore point to point connections. However, due to limitations of the LCC [31] and the advances in semiconductor devices and converter topologies, the voltage-source converter (VSC) technology has emerged as a promising option.

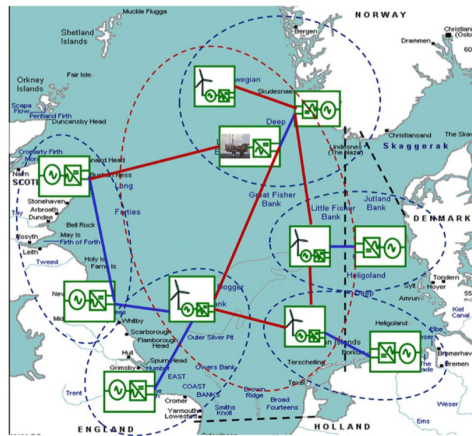


Figure 2.8: Meshed North Sea HVDC grid scenario where the blue lines are expected early stage developments and the red lines are later stage developments [37].

The VSC has multiple advantages compared to the LCC, including much faster control and more flexibility compared to the LCC [31]. The VSC is capable of fast and independent control of reactive and active power in all quadrants of the DC voltage-current plane, which makes it well suited for HVDC grids where current directions may change depending on power flow directions. A more in-depth comparison of LLC based and VSC based HVDC can be found in the Specialization Project [14].

The next chapter will introduce the most promising VSC topology for present and future HVDC grids, i.e., the modular multilevel converter (MMC).

The Modular Multilevel Converter

The Modular Multilevel Converter (MMC) has proven itself as the most promising converter technology for converting between AC and DC in modern HVDC systems, including grid integration of offshore wind farms [39]. The converter is based on the voltage source converter (VSC) technology, thus providing many benefits compared to the classical line commutated current source converters [31]. The MMC does also bring additional benefits compared to conventional VSCs such as two- and three-level VSCs.

The MMC was first introduced through a patent in 2001 [40] before being presented by Lesnicar and Marquardt in reference [41] in 2003. Today, the MMC is commercially available through for example ABB's HVDC Light [42] and Siemens's HVDC PLUS [43]. The latter is implemented in the interconnection INELFE which connects Spain and France through two MMCs, each at 1000 MW and a DC voltage of ± 320 kV [44].

This chapter will introduce the MMC topology and its benefits, and provide an overview of the control and a mathematical formulation of an energy-based model to be used in transient simulations of large HVDC systems.

3.1 The MMC converter

To understand the operation of the MMC, it is useful to consider the schematic of the MMC in Figure 3.1. The converter is built of multiple sub-modules which are usually either half bridges (as shown in Figure 3.1) or full bridges, with IGBTs and a capacitor. Additionally, there is an inductor in each arm (blue box in Figure 3.1) and one inductor for each phase on the AC side. The upper and lower arms in a phase form what is referred to as a leg. The three-phase MMC has three legs; one for each phase.

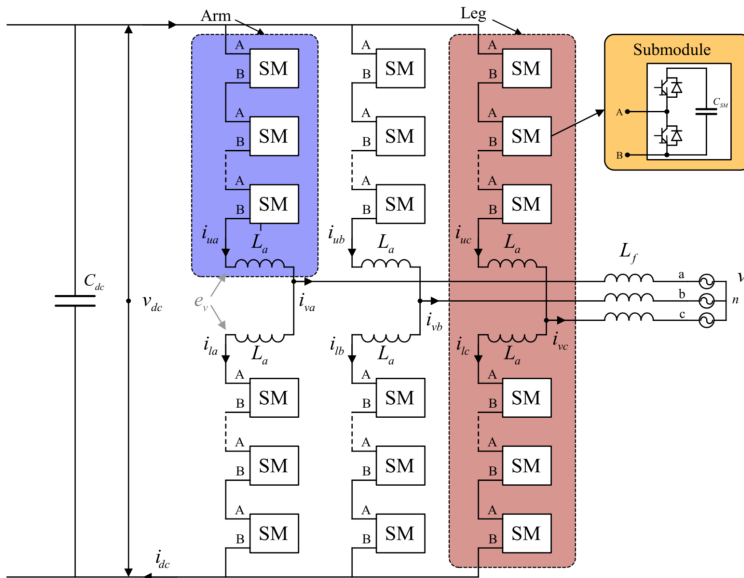


Figure 3.1: The schematic of a three-phase MMC [45].

When the upper IGBT in a sub-module is on, the voltage of the sub-module capacitor is inserted at the output voltage. The sub-module voltages are inserted at the output voltage in steps, as showed in Figure 3.2, where the AC-line voltage waveform of an MMC with 11 voltage levels is compared to the waveform of a two-level VSC. By increasing the number of sub-modules, the number of voltage levels is increased, and the output voltage of the MMC can be close to a perfect sine. In the literature, there are examples of MMCs with as many as 401 voltage levels [46].

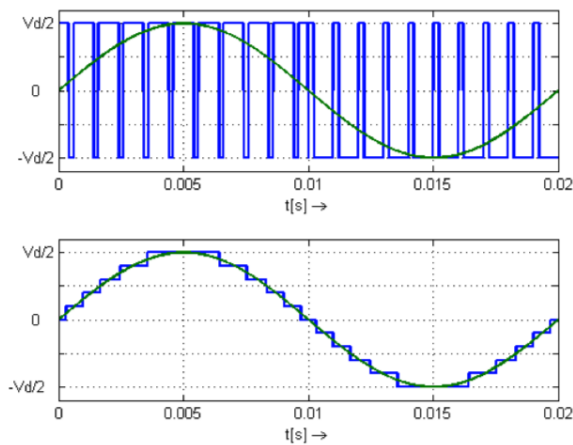


Figure 3.2: The AC voltage waveform of the 2-L VSC (upper) compared to an MMC (lower) [12].

3.2 MMC modeling

This section will describe an energy-based MMC model that is implemented in the simulation system described in Chapter 5. The nomenclature at the beginning of the document and Figure 3.1 can be used for further clarification of the conventions used for variables and parameters in this section.

First, an overview of the different ways to model an MMC found in the literature will be presented to explain further the choice of model used in the simulations later in this Thesis.

3.2.1 Overview of MMC models in the literature

There exist many MMC models with various levels of complexity to be used for different kinds of studies in the literature. The International Council on Large Electric Systems (CIGRÉ) has created a guide for developing MMC models to be used in HVDC grids, and in this guide, they categorize MMC models in seven different categories [47]. This section will give a brief overview of these seven categories, starting with the most complex type of models; Type 1 models.

Type 1 models, also referred to as "full physics-based models" are the most complex models where partial differential equations represent the IGBTs in the sub-modules. These equations give very precise results, but these models require extremely small time steps in the order of nanoseconds to be simulated. Therefore, Type 1 models are best suited for detailed analysis of sub-modules in for example the design stage.

Type 2 models, also referred to as "full detailed models", model the nonlinear nature of the IGBTs through simplified IGBT models. These models are well suited for studies of internal events as internal faults, blocked states and startup procedures. However, they may be too computational heavy to be used in HVDC grid models.

Type 3 models, also referred to as "models based on simplified switchable resistances", have a more simplified representation of the IGBTs compared to Type 2 models. The IGBTs are modeled as two-value switchable, bidirectional resistances with a small on-resistance and a large off-resistance.

Type 4 models, also referred to as "Detailed equivalent circuit models" or "Thevenin equivalent models", include a reduced Thevenin-equivalent of each arm to have a lower number of electrical nodes in the model. Type 4 models have high accuracy, including the impact of capacitor voltages of each sub-module, and are frequently used in the literature as reference models for further simplified models [39].

Type 5 models, also referred to as "average models based on switching functions", do not include any representation of the IGBTs. The MMC is represented by controllable voltage and current sources that contain the harmonic content which is generated from separate switching functions. These models still allow studying the harmonics in power quality studies of HVDC grids.

Type 6 models, also referred to as "average models based on the fundamental frequency", model the MMC with controllable voltage sources and current sources. These models only consider the fundamental frequency of the currents and voltages. Hence the harmonics are averaged out over the switching period. As these models do not capture

the fast switching dynamics, they can be simulated with a higher time-step than Type 5 models, resulting in faster simulations. Additionally, the simulation speed of Type 6 models is also independent of the number of sub-modules, whereas the more complex models become slower when the number of sub-modules is increased [39].

Type 7 models, also referred to as "RMS load-flow models", are the simplest kind of models which are to be used in load flow studies, describing the steady-state of the converter without any transients.

A study by S. Khan et al. has systematically compared MMC models in the literature and their performance in simulations of a point-to-point HVDC connection, where variations in power, AC-side faults, DC-side faults and simulation speeds are studied [39]. They conclude their work by recommending Type 3,4 and 5 models to be used for system-level studies where switching events are modeled. Further, average value models are recommended for network-level studies where the terminal characteristics of the MMC are of main interest and also for designing of control systems. Lastly, the most detailed models should be used for component design and analysis of switching characteristics [39].

3.2.2 Desired model characteristics for this Thesis

Based on the different model descriptions above and the recommendations from reference [39] for network-level studies, a Type 6, average model, is chosen for this Thesis. This is both because the simulations are performed on an average laptop requiring an efficient model, but also because of the relatively low complexity of average models compared to the more detailed models. The latter is also important when considering the fact that the model was to be implemented in a new and unfamiliar software, OpenModelica.

A model with steady-state operation of all variables without any oscillations, i.e. a steady-state time-invariant (SSTI) model, was desired for ease of controlling the MMC with techniques similar to those used for 2L-VSCs.

Finally, a model including the internal energy storage capabilities of the MMC was desirable for the kind of studies performed later in the Thesis.

All these desired characteristics led to the choice of the simplified zero-sequence model from reference [45].

The model will be presented after explaining one of the main assumptions it relies on, i.e. the use of compensated modulation, as well as the relations describing the variables such as voltages and currents used in the model.

3.2.3 Compensated modulation

This part will explain the concept of compensated modulation, as this is an underlying assumption for the energy-based model chosen. Also, understanding compensated modulation can lead to a better understanding of the operation of the MMC.

The modulation in the MMC is how the insertion indices n_u and n_l are calculated to determine how many sub-module capacitor voltages should be inserted in the upper and lower arm output voltages, respectively. By assuming the arm voltage is ripple-free, the simplest modulation can be applied; direct modulation [48]. Direct modulation calculates the insertion indices by dividing the reference voltages by the nominal DC voltage, $V_{dc,nom}$:

$$n_u = \frac{-e_v^* + u_c^*}{V_{dc,nom}}, \quad n_l = \frac{e_v^* + u_c^*}{V_{dc,nom}} \quad (3.1)$$

However, the arm voltages contain a dominant first and second order harmonic ripples. Thus the inserted voltages will have harmonics which will lead to circulating currents. This can be avoided by dividing the voltage references by the arm voltages, $v_{u,l}^\sigma$, instead, which is the technique called compensated modulation [48], and the expression for the insertion indices becomes:

$$n_u = \frac{-e_v^* + u_c^*}{v_u^\sigma}, \quad n_l = \frac{e_v^* + u_c^*}{v_l^\sigma} \quad (3.2)$$

In Equations (3.1) and (3.2), e_v^* is the output of the AC current controller as a reference for the voltage driving the AC side currents and u_c^* is the output of the circulating current controller as a reference for the voltages driving the circulating currents. These two controllers are presented later in this chapter.

3.2.4 Energy-Based SSTI MMC Model

An energy-based MMC model has the potential of capturing internal currents and energy dynamics of the MMC and starts with considering the energy stored within the MMC. In an energy-based model, the difference $w_{\Delta k}$ and the sum $w_{\Sigma k}$ of the energy between the two arms in a phase k are used as state variables, described by

$$w_{\Sigma k} = w_{uk} + w_{lk} \quad (3.3)$$

$$w_{\Delta k} = w_{uk} - w_{lk} \quad (3.4)$$

where the energy stored in the upper and lower arms, $w_{u,lk}$, is expressed by

$$w_{u,lk} = \frac{C_{SM}}{2N} (v_{u,lk}^\sigma)^2 \quad (3.5)$$

where C_{SM} is the capacitance of each sub-module, N is the number of sub-modules and $v_{u,lk}^\sigma$ is the sum of all sub-module voltages in the corresponding arm, which in turn can be expressed as

$$v_{u,lk}^\sigma = \sum_{i=1}^N v_{u,lk}^{SM_i} \quad (3.6)$$

Using the previously mentioned compensated modulation technique to generate the insertion indices, the output voltages of each arm, $v_{u,lk}$, can be approximated as

$$v_{u,lk} \approx n_{u,lk} \cdot v_{u,lk}^\sigma \quad (3.7)$$

where $n_{u,lk}$ is the insertion index for the corresponding arm.

Further, it is useful to define the grid side currents as

$$i_{vk} = i_{uk} - i_{lk} \quad (3.8)$$

and the circulating currents as

$$i_{ck} = \frac{i_{uk} + i_{lk}}{2} \quad (3.9)$$

where i_{uk} is the current in the upper arm and i_{lk} is the current in the lower arm according to Figure 3.1. These currents are driven by the voltages e_{vk} and u_{ck} respectively, which are defined through the arm voltages in a phase k as

$$e_{vk} = \frac{v_{lk} - v_{uk}}{2} \approx \frac{n_l \cdot v_{lk}^\sigma - n_u \cdot v_{uk}^\sigma}{2} \quad (3.10)$$

and

$$u_{ck} = \frac{v_{lk} + v_{uk}}{2} \approx \frac{n_l \cdot v_{lk}^\sigma + n_u \cdot v_{uk}^\sigma}{2} \quad (3.11)$$

where v_{lk} is the lower arm voltage and v_{uk} is the upper arm voltage.

The equivalent resistance and inductance seen from the AC which are used in the MMC model can be obtained from the equivalent grid resistance, R_f , the equivalent grid inductance L_f , the equivalent arm inductance, L_a , and the equivalent arm resistance, R_a , as

$$R_{eq} = \frac{R_a}{2} + R_f \quad (3.12)$$

$$L_{eq} = \frac{L_a}{2} + L_f \quad (3.13)$$

All the above equations are the basic equations describing each phase k of the MMC. The dynamics presented next are functions of these variables.

Both of the following models assume compensated modulation and balanced submodule voltages.

3.2.5 Detailed model

Two models are resulting from [45], both of which captures some of the internal dynamics of the MMC; one detailed model and one simplified model. The model that will be used in further in Chapter 5 is the simplified one. However, the detailed model will be presented first along with the simplifications and assumptions made to obtain the simplified model.

The detailed model is derived from the above equations. The derivation will not be repeated here, but it can be found in reference [45].

The detailed model takes into account the fact that the internal voltages and currents of the MMC have multiple frequency components. To deal with these components, three Park transformations of different frequencies, ω , -2ω and $+3\omega$, are applied to have steady-state operation of all variables without any oscillations. Therefore, the model is referred to as a steady-state time-invariant (SSTI) model. All oscillating model variables are transformed to a dqz reference frame that rotates with the corresponding oscillatory frequencies of the variable, where the z component is referred to as the zero sequence component. The transformation matrix for this transformation can be found in Appendix A.2.

The detailed model consists of the three dqz components describing the dynamics of the energy sum, w_Σ , the energy difference, w_Δ , the grid side currents, i_v , and the circulating currents, i_c for each phase k . The full model equations are presented in the

same form as in [45], where the superscripts represents the corresponding rotating dqz frame of the variable, rotating at ω , -2ω or $+3\omega$. The following equations are presented to later explain the simplifications made in the simplified zero-sequence model, which is described in the next section.

The first set of equations in the detailed model represents energy sum dq-dynamics rotating with -2ω :

$$\frac{d}{dt} \mathbf{w}_{\Sigma}^{dq-2\omega} = -\frac{1}{2} \mathbf{e}_v^{dq+\omega} \mathbf{i}_v^{dq+\omega} + 2(u_{cz} \mathbf{i}_c^{dq-2\omega} + \mathbf{u}_c^{dq-2\omega} i_{cz}) - j \cdot 2\omega \mathbf{w}_{\Sigma}^{dq-2\omega} \quad (3.14)$$

The next equation is describing the energy sum zero-sequence dynamics:

$$\frac{d}{dt} w_{\Sigma z} = -\frac{1}{2} \Re\{\bar{\mathbf{e}}_v^{dq+\omega} \mathbf{i}_v^{dq+\omega}\} + \Re\{\bar{\mathbf{u}}_c^{dq-2\omega} \mathbf{i}_c^{dq-2\omega}\} + 2u_{cz} i_{cz} \quad (3.15)$$

where the dash above the complex variables $\bar{\mathbf{e}}_v$ and $\bar{\mathbf{u}}_c$ marks the conjugate of the variables.

The next set of equations are describing energy difference dq-dynamics rotating with -2ω :

$$\frac{d}{dt} \mathbf{w}_{\Delta}^{dq-2\omega} = -\bar{\mathbf{e}}_v^{dq+\omega} \mathbf{i}_c^{dq-2\omega} + \frac{1}{2} \mathbf{u}_c^{dq-2\omega} \bar{\mathbf{i}}_v^{dq+\omega} - j \cdot \omega \mathbf{w}_{\Delta}^{dq+\omega} \quad (3.16)$$

Next, the energy difference zero-sequence dynamics rotating with $+3\omega$ is described by:

$$\frac{d}{dt} \mathbf{w}_{\Delta z}^{dq+3\omega} = -\mathbf{e}_v^{dq+\omega} \bar{\mathbf{i}}_c^{dq-2\omega} + \frac{1}{2} \mathbf{u}_c^{dq-2\omega} \mathbf{i}_v^{dq+\omega} - j \cdot 3\omega \mathbf{w}_{\Delta z}^{dq+3\omega} \quad (3.17)$$

The following set of equations describes the circulating currents dq-dynamics rotating with -2ω :

$$\frac{d}{dt} \mathbf{i}_c^{dq-2\omega} = -\left(\frac{R_a}{L_a} + j \cdot 2\omega\right) \mathbf{i}_c^{dq-2\omega} - \frac{1}{L_a} \mathbf{u}_c^{dq-2\omega} \quad (3.18)$$

Lastly, the circulating currents zero-sequence dynamics are described by:

$$\frac{d}{dt} i_{cz} = -\frac{R_a}{L_a} i_{cz} + \frac{1}{L_a} \cdot \frac{v_{dc}}{2} - \frac{1}{L_a} \cdot u_{cz} \quad (3.19)$$

3.2.6 Simplified zero-sequence MMC model

A simplified model of the MMC for power system-oriented studies is also proposed in reference [45] and it is validated against the detailed model in addition to a well-established reference model for analysis and simulation of the MMC. This reference model is a circuit-based average model of a three-phase MMC, where each arm is represented by a controlled voltage source and where the internal arm voltage dynamics are represented by an equivalent arm capacitance [49, 50, 51]. The reference model is also verified in laboratory-scale experiments in [49, 50]. The comparison showed that the simplified model captured the dynamic response of the reference model with high precision.

In the simplified model, the internal variables are only represented by the zero-sequence components. The model can be derived from the detailed model with the assumption that the dynamic equation for the zero-sequence energy sum, $w_{\Sigma z}$, is not dependent on the

product of the dq-components of \mathbf{u}_c and \mathbf{i}_c . This is a valid assumption because the dq-components of \mathbf{u}_c are much smaller than the zero sequence component and e_v . It should be noted that this simplified model assumes that all the neglected internal variables are properly controlled and do not cause any stability problems.

The five differential equations making the full simplified model including the dq-dynamics of the grid currents and the dc-link voltage are as follows:

The first equation describing energy sum zero sequence-dynamics per phase:

$$\frac{d}{dt}w_{\Sigma z} \approx -\frac{1}{2}(e_{vd}i_{vd} + e_{vq}i_{vq}) + 2u_{cz}i_{cz} \quad (3.20)$$

The second equation describing circulating current zero-sequence-dynamics:

$$\frac{d}{dt}i_{cz} = -\frac{R_a}{L_a}i_{cz} + \frac{1}{L_a}\frac{v_{dc}}{2} - \frac{1}{L_a}u_{cz} \quad (3.21)$$

The third equation describing d-current dynamics of the grid currents:

$$\frac{d}{dt}i_{vd} = \frac{1}{L_{eq}}(-R_{eq}i_{vd} + e_{vd} - v_{gd} - \omega L_{eq}i_{vq}) \quad (3.22)$$

The fourth equation describing the q-current dynamics of the grid currents:

$$\frac{d}{dt}i_{vq} = \frac{1}{L_{eq}}(-R_{eq}i_{vq} + e_{vq} - v_{gq} + \omega L_{eq}i_{vd}) \quad (3.23)$$

The fifth equation describing the DC-voltage dynamics:

$$\frac{d}{dt}v_{dc} = \frac{1}{C_{dc}}(i_{dc} - i_{load}) \quad (3.24)$$

where the relation between the dc-current and the circulating current is

$$i_{dc} = 3i_{cz} \quad (3.25)$$

All dq-quantities in these equations from the simplified model are rotating with $+\omega$, which is why a Park transformation between the measured three-phase abc-quantities and the dq-quantities (see Appendix A.1) is applied to perform vector control of the dq-currents, as also explained in more detail in the Specialization Project [14].

An overview of the circuit implementation of the simplified zero-sequence model including the associated control schemes is showed in Figure 3.3. Further details on the control of loops used in the model as well as block diagrams will be presented in the following sections.

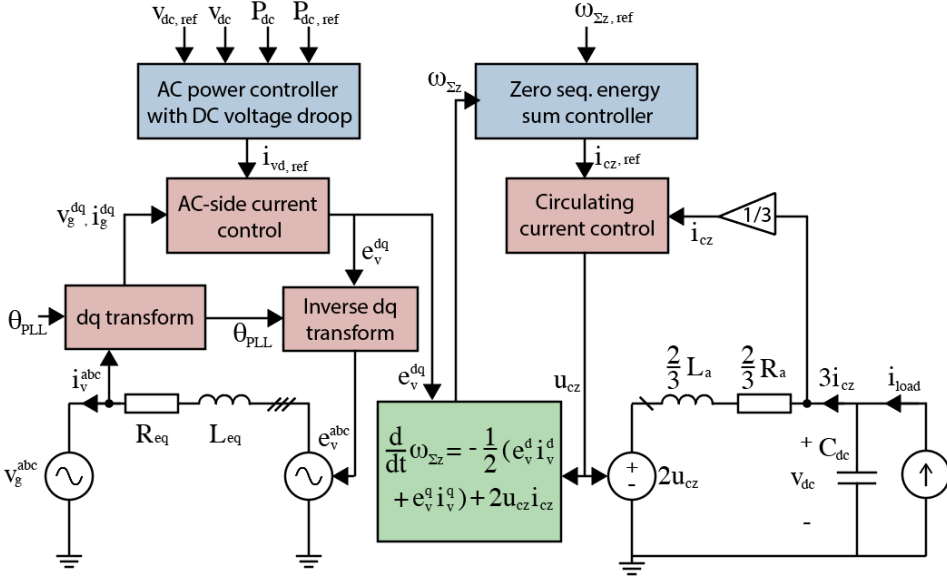


Figure 3.3: Overview of the simplified zero-sequence MMC model.

The load current in Figure 3.3 is included as a current source for illustration purposes. In an HVDC connection, this current will originate from another MMC or possibly from multiple MMCs in case of a multi-terminal HVDC system.

It is worth mentioning that the simplified model also has a simplified control system compared to the detailed model.

3.3 Control structure of the MMC

The control of the MMC is more complex compared to the control of the 2L-VSC, which was described in the Specialization Project [14], because of the increased complexity of the MMC structure.

This section will give an overview of the different control schemes used in the simplified zero-sequence MMC model, which are used for power control and energy control. Also, some additional control schemes are presented to show some of the added complexity of the MMC compared to the 2L-VSC.

3.3.1 Power control

The control of the AC currents in an MMC is important for the corresponding control of active and reactive power in the converter. The control scheme presented here has an outer power controller coupled with an inner current controller.

Inner AC current controller

The AC currents in an MMC can be controlled similarly to the two-level VSC through vector control of the dq-currents [52, 53, 14]. By applying the sine-based Park transform found in Appendix A.1 on the three-phase quantities and dynamic equations, the abc-currents are decomposed to dq components and vector control can be applied. The control scheme uses PI controllers for each current and feed-forward of the decoupling terms and the grid voltages, as shown in Figure 3.4, to obtain fast and independent control of the d- and q-currents.

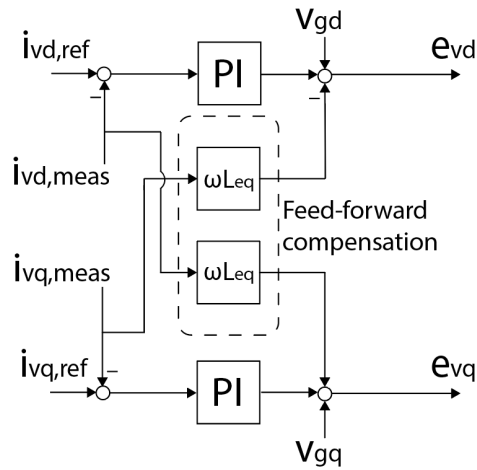


Figure 3.4: Block diagram of the dq-current controller with feed-forward decoupling.

Outer power controller with DC voltage droop

The outer controllers of the MMC use the q-component of the current to control reactive power and the d-component of the current to control the active power through the converter when a sine-based Park transformation is used. This leads to a fast and independent control of the active and reactive power through the converter.

An additional term can be added to the active power controller to control the DC voltage. Such DC voltage control is referred to as DC voltage droop control [54], and is often used in multi-terminal HVDC grids to distribute the DC-voltage control to multiple converters in the same grid, increasing the robustness of the system.

The block diagram of the power controller can be seen in Figure 3.5 using a constant K_P for the active power and a droop constant $1/K_{v,dc}$ for the DC voltage.

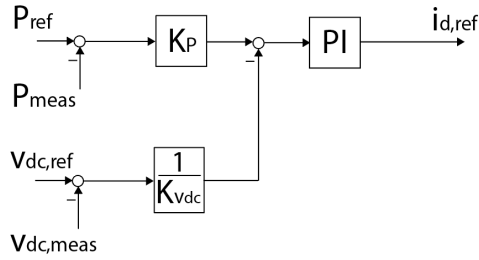


Figure 3.5: Block diagram of the per unit active power controller with DC voltage droop control.

3.3.2 Energy control

The control scheme presented here is based on the control scheme found in [45], which uses the dc-component of the circulating currents to control the energy balance of the MMC.

Inner circulating current controller

The MMC has one additional degree of freedom compared to the 2L-VSC that is the circulating current in each phase leg due to the two arms. The dc-component of these circulating currents play an important role in ensuring power balance in the converter. In [45], a control loop to control the DC component of the circulating current is implemented to control the active power flow in the converter.

Outer energy controller

The circulating currents in the MMC can be used to balance the energy stored in the converter. In this case, an outer energy controller is used to provide references for the inner circulating current controller. A constant reference for the energy controller means that the power entering the controller on the AC-side is transferred directly to the DC side and not stored within the converter.

The block diagram for this control scheme can be seen in Figure 3.6.

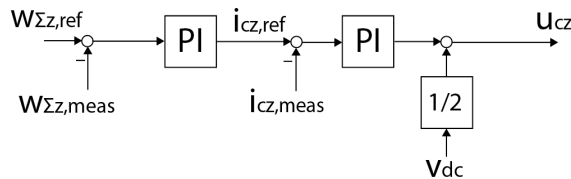


Figure 3.6: Block diagram of the outer zero sequence energy controller with inner zero sequence circulating current controller.

3.3.3 Additional control schemes

This section is included to explain some aspects of the increased complexity of control associated with an MMC. The MMC has additional control loops in order to operate efficiently. However, these control schemes will not be considered in any models used in this document.

Voltage balancing control

The MMC does also need a control scheme to ensure voltage balance within the rated limits of the capacitors in each sub-module to prevent damage [39]. The voltage balancing control is at the lowest level of control in the MMC and is present depending on the modulation technique to secure stable operation [55]. The control scheme which is most widely accepted for balancing the sub-module voltages is based on a sorting algorithm where the sub-module voltages are measured and sorted. This way, the sub-module with the lowest voltage is charged first and the sub-module with the highest voltage is discharged first [55]. However, this control scheme will not be considered any further in this document as the models used assume that the sub-module voltages are perfectly balanced.

Circulating current suppressing control

The circulating currents contain harmonics due to imbalances of the phase leg voltages. These harmonics need to be mitigated to reduce losses and rating requirements of the components inside the MMC [39]. An active filtering technique called circulating current suppressing control (CCSC) is therefore implemented in addition to the arm inductances to remove these harmonics from the MMC [56]. However, this control scheme should not be confused with the previously mentioned circulating current control that can control the energy of the converter, as the latter controls the DC component of the circulating current and not the harmonics, as CCSC do.

3.4 Advantages of the MMC

To conclude the chapter, this section will recall some advantages of the MMC compared to other VSC topologies, such as the 2L-VSC so that the reader can have a good understanding of why the MMC could be used over the other topologies, despite the increased control complexity. The relevance of such advantages to offshore applications will also be highlighted.

3.4.1 Harmonic content

The multilevel topology of the MMCs enables the nearly perfectly sinusoidal voltage generation, which reduces the harmonic distortion significantly compared to the 2L-VSC. By increasing the number of sub-modules, the need for harmonic filtering at the terminals of the MMC is effectively eliminated [57]. Figure 3.7 shows how two indices recommended by Standard IEEE 519 for voltage distortion, total harmonic distortion (THD) and maximum individual harmonic (D_n), are reduced by increasing the number of sub-modules in

an MMC [58]. The red dotted lines are commonly used maximum limits for HVDC systems with a THD of 2% and a D_{nmx} of 1%. From the figure, it can be seen that the MMC with 22 sub-modules or more per arm are within these limits, meaning that harmonic filtering is not needed [58].

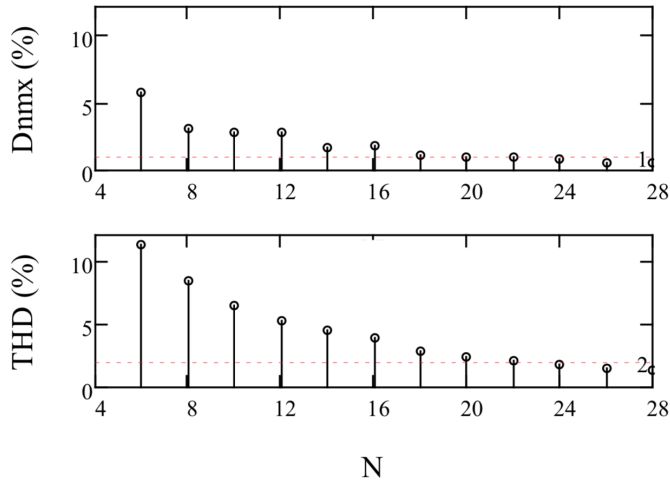


Figure 3.7: Total harmonic distortion (THD) and maximum individual harmonic (D_{nmx}) in the voltage waveform when increasing the number of sub-modules per arm, N , from reference [58]

In a 2L-VSC based on pulse-width modulation (PWM), the switching frequency needs to be increased to have lower harmonic distortion [12], which in turn would also increase the losses of the converter drastically. The MMC is capable of effectively eliminating the harmonic content without increasing the switching frequency, which means the losses are still at a low level. As an example of this, reference [59] compared the total losses of a 1000MW 2L-VSC with a switching frequency of 1kHz to the losses of a 1000MW MMC with 40 sub-modules per arm. The results in [59] showed that the total losses of the 2L-VSC was 17.711MW compared to 1.4713 MW for the MMC.

The lack of large filters at the converter station is also a significant advantage in offshore application because it gives a more compact design of the converter platforms [31]. Additionally, the execution time of projects can be shortened when components such as filters are not needed [57].

3.4.2 Modularity

Another advantage with the MMC is the modular aspect. Because each sub-module capacitor needs to be charged to a low value compared to the DC voltage, the sub-module capacitors can be rated for much lower voltage-levels than the DC-link capacitors in, for example, the 2L-VSC. Therefore, the MMC can be built of well proven standard components that are easily available [57]. This makes the MMC easily scalable to higher ratings by adding more sub-modules [12].

3.4.3 Fault-handling capabilities

When a DC fault occurs at the terminals of a 2L-VSC, the IGBT enters a blocked state for protection. However, the freewheeling diodes in the IGBTs provide a path for the fault current, which makes the converter feed the fault current as a diode rectifier. These fault currents through the freewheeling diodes can reach values around 15 p.u. for a couple of milliseconds and can potentially destroy the IGBTs [60]. In Figure 3.8a, it can be seen that the MMC with half bridge submodules has this freewheeling behavior.

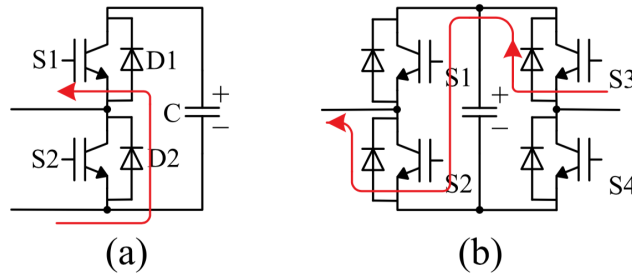


Figure 3.8: DC side fault current path of (a) a half-bridge sub-module (b) a full-bridge sub-module [55].

However, by considering the full bridge sub-module in Figure 3.8b, it can be seen how the full bridge sub-module can prevent freewheeling behavior. When a fault occurs on the DC side, the fault currents through the capacitors in the full bridge sub-module create a reversed voltage that blocks the AC-side currents and therefore clears fault current. This way, the full bridge MMC can provide fault blocking capabilities [61], which are useful to HVDC systems that are prone to fault, for example in overhead lines. Because the full bridge MMC is more expensive and has higher losses than the half-bridge MMC due to the higher number of semiconductors, other fault handling sub-modules are proposed [62] as a more cost-efficient alternative with lower losses.

However, for offshore transmission by sub-sea cables, the half-bridge based MMC is presently the most practical solution since the full-bridge MMC introduces additional complexity, additional costs, potential reliability issues, and additional losses.

3.4.4 Energy storage capabilities

Another advantage with the MMC topology is the inherent capability of storing energy inside the converter. This capability can be used to store or to release energy without affecting the DC voltage level to, for example, damp active power oscillations to enhance grid stability as proposed in references [63, 48]. Other possible utilizations of the internal storage capability includes, for example, inertia emulation for frequency regulation [64], improved voltage behaviour in HVDC grids [65] or increasing lifetime of MMC based energy storage systems [66].

This storage capability is related to the capacitors in each sub-module. Each sub-module is charged or discharged with an allowed variation around the average value,

which, with a sufficient number of sub-modules, can give energy storage capabilities of several megajoules [63].

The stored energy in the MMC can be described by the sub-module capacitance, C_{SM_i} , the number of sub-modules, N , and the sub-module voltages in the upper and lower arms, $v_{u,lk}^{SM_i}$ [48], as also explained earlier. The expression for the stored energy in joules in each arm can be expressed as

$$w_{u,lk} = \frac{C_{SM}}{2N} \left(\sum_{i=1}^N v_{u,lk}^{SM_i} \right)^2 \quad (3.26)$$

From this equation, it can be seen that the storage capabilities of the MMC can be increased by either increasing the number of sub-modules or by increasing the rated voltage of each sub-module.

If the converter is to use this storage capability, for example, for power oscillation damping, an additional controller is needed to provide references for the energy controller, as for example the controller proposed in reference [48].

The OpenModelica Modeling Tool

The use of modeling tools allows for modeling of systems through algebraic and differential equations to reproduce and study the dynamics found in real physical systems. There exist many modeling tools on the market, but many of them are usually specific for their application domain, which is a limitation when modeling complex multidisciplinary systems.

To overcome these limitations, the development of the Modelica modeling language started in 1996. The Modelica language was developed to combine multiple physical domains in one modeling language to model and simulate complex systems consisting of models from multiple physical domains such as electrical, mechanical, thermodynamic and hydraulic models [13].

When developing and designing HVDC grids, full scale testing on large systems is not feasible. Therefore, hardware-in-the-loop (HIL) testing is often used where parts of the physical components in the HVDC grid are combined with computer models of the rest of the system. Such computer models can be modeled in OpenModelica, which is a tool based on the Modelica language. This makes the OpenModelica tool interesting for modeling of HVDC grids, as it supports model exchange with external software, allowing OpenModelica models to be used in, for example, HIL testing using software and equipment developed by Opal-RT. To perform HIL testing, the computer model has to be compatible with a real-time simulator, which is an aspect that will be further investigated in this chapter.

The OpenModelica tool will be used to model the system shown in Figure 1.3 in the introduction, which is further described in Chapter 5. However, before using OpenModelica to model the multiterminal HVDC system in Figure 1.3, some aspects of the software needed to be further investigated.

This chapter starts with a short introduction to OpenModelica. Next, a preliminary assessment of OpenModelica's performance with Simulink as a benchmark using high frequency dynamics is included. The latter was requested through a feedback from the specialization project [14] and also by the industrial partner, DNV GL. Ultimately, work in the National Smart Grid laboratory led to a detailed guide on how to use OpenModelica

models with Opal-RT’s real-time simulator ePHASORSIM, which is included at the end of the chapter. The sections covering the assessment of performance and the guide are both related to the two objectives around the OpenModelica software, as mentioned in the introduction and requested by the industrial partner, DNV GL.

For a perspective on the usability of OpenModelica compared to Simulink, the reader can refer to the Specialization Project [14].

4.1 The OpenModelica software

Modelica is a vendor-independent standard, meaning that there are multiple tools supporting the Modelica language, like Dymola [67], MathModelica [68], and IDA [69]. However, one of the emerging tools is OpenModelica, which is an open-source implementation of Modelica. Being open-source, the source code of OpenModelica can be accessed by anyone for any purpose, like improvement of performance and bug fixes, which makes for a public collaboration of developing the software. Also, the software is completely license free, meaning users can save thousands of dollars from otherwise expensive licenses. The long-term development of OpenModelica is supported by the non-profit organization Open Source Modelica Consortium (OSMC) [70].

4.1.1 The standard library of components

The Modelica language is an object-oriented programming language based on algebraic and differential equations. The building blocks in object-oriented programming languages are objects. Objects are instances of their respective classes, which determine the general data and operations of an object. Multiple objects with different data can be declared from the same class in a model. This is an efficient way of reusing code and preventing repetitive work.

The OpenModelica software comes loaded with a standard library of components created as classes by default, including everything from maths to logical blocks to electrical and mechanical components. These libraries represent the many physical domains of the Modelica language, as seen in Figure 4.1.

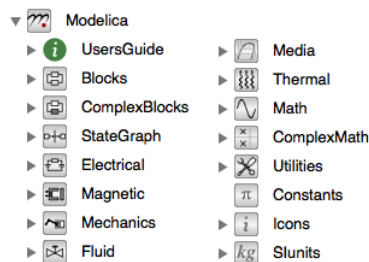


Figure 4.1: The OpenModelica standard library.

These components can, for example, be used to draw circuits or design control systems, where the user creates objects from the standard library classes to best represent the system

of interest.

For a description of some other OpenModelica libraries, the reader can refer to the specialization project [14].

4.1.2 Acausal modeling in OpenModelica

OpenModelica aims to be an intuitive modeling tool by using what is called acausal modeling [71]. Acausal modeling is when the dynamics of, for example, an electrical circuit can be represented by simply drawing the circuit in the software and connecting all components such as voltage sources and impedances. Then, the software will determine the differential equations based on the circuit drawn and solve them.

In causal modeling tools, the model needs to be represented explicitly by the differential equations through generic mathematical blocks. One example of a causal modeling tool is Simulink, which is causal by default. However, by installing additional libraries such as the Simescape Power Systems for additional license fees, acausal modeling can be activated in Simulink.

The differences between acausal and causal modeling is illustrated in Figure 4.2.

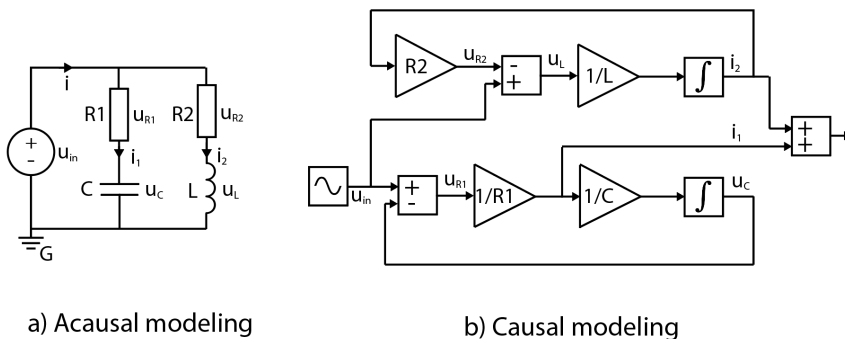


Figure 4.2: The difference of acausal modeling (a) using an electrical circuit and causal modeling (b) using generic blocks.

OpenModelica is acausal by default, which makes for a more intuitive modeling experience. The graphical modeling approach of an acausal modeling tool can be combined with written code and equations in OpenModelica for increased flexibility when modeling.

4.1.3 Solvers in OpenModelica

When running a simulation model, OpenModelica transforms the model into ordinary differential equations (ODEs) by default which are solved numerically using different integration methods. Table 4.1 shows the overview of the basic solvers that come with OpenModelica. The default solver of OpenModelica is Dassl, which is chosen as the default solver because of its features that make it stable for a wide range of models [72].

Table 4.1: Basic solvers in OpenModelica

Solver	Type	Step size	Integration order
Euler	Explicit	Fixed-step size	First
Heun	Explicit	Fixed-step size	Second
Runge-Kutta	Explicit	Fixed-step size	Fourth
Impeuler	Implicit	Fixed-step size	First
Imprungekutta	Implicit	Fixed-step size	Adjustable from first to sixth
Trapezoid	Implicit	Fixed-step size	Second
Dassl (default)	Implicit	Step size control	Adjustable from first to fifth
Ida	Implicit	Step size control	Adjustable from first to fifth

In addition to these eight basic solvers, there are five experimental solvers that come with the software (rungekuttaSsc, irksco, symSolver, symSolverSsc, qss). However, these are not currently very well tested.

Explicit solvers use the current states of a system to calculate the states at a later time, as described by the equation

$$X(t + \Delta t) = F(X(t)) \quad (4.1)$$

where $X(t)$ are the current states and $X(t + \Delta t)$ are the states at a later time $t + \Delta t$ where Δt is the step size of the solver.

Implicit methods, on the other hand, find the solution by both the current state and the later state, as described by the equation

$$G(X(t + \Delta t), F(X(t))) = 0 \quad (4.2)$$

to calculate $X(t + \Delta t)$. Implicit solvers usually require more computation than explicit solvers, and the choice between explicit and implicit solver depends on the problem to be solved [73].

Step-size control is a method of adaptive time step size where the size of the time-step is increased if the error is too small according to the predefined tolerance and decreased if the error is too large [74]. Further, fixed-step time is when a constant time-step is used throughout the simulation.

4.1.4 Model exchange through the Functional Mockup Interface

Another aspect that makes OpenModelica a versatile modeling tool is ease of model exchange with other software. This is achieved through the support of the Functional Mockup Interface (FMI). The FMI is a standardized interface protocol that allows for sharing of pre-compiled models in C-code or binary code between different tools [75]. In OpenModelica, one can use the FMI standard through Functional Mockup Units (FMUs).

FMUs are files that include the binary code of a model and information about the model (number of parameters, states, inputs, outputs, etc.), which are required by the FMI standard to connect externally. An OpenModelica model can easily be exported to an FMU file in the software or through external tools such as Opal-RT's FMUCreator, which will be explained later, for such model sharing.

An example of the use of Modelica in the industry is by ABB, which is a company with good experience of model-based engineering in the HVDC field and is a world leader within the field. ABB uses Modelica for modeling thermal power plants through the thermal library and electrical systems through the electrical library for real-time simulations [76]. Before adopting the FMI feature of Modelica, ABB experienced a lot of tricky work to adapt each version of modeling tools to the real-time simulator in order to make it work. Now, ABB uses the FMI feature of Modelica for the real-time simulations, and have good experience with the standard. This standard makes for a seamless coupling of the modeling tool and the real-time simulator, which is expected it to work every time, according to Head of Optimization Technology in ABB, Dr. Rüdiger Franke [76].

This aspect of OpenModelica will be further investigated later in this chapter, where a detailed guide on how to use OpenModelica models in Opal-RT's real-time simulator, ePHASORSIM through the use of FMUs, will be included.

4.2 Preliminary assessment OpenModelica's performance

This section will include a description of the preliminary assessment of the performance of OpenModelica as well as the results associated with the assessment.

The preliminary assessment of the performance of the tool was executed in order to test the software before using it further in a larger system study as described later in Chapter 5. The criteria for this assessment were the accuracy of results and speed of simulations with Simulink as a benchmark.

To test the performance of the OpenModelica software with the given criteria, a simple switching model of the AC-side dynamics of a 2L-VSC was implemented in both Simulink and OpenModelica, as no such implementations or tests could be found in the literature. Figure 4.3 shows the circuit of a 2L-VSC connected to three-phase voltage sources with line resistances and inductances. As this model includes only the AC-side dynamics, the DC voltage is assumed to be constant from a constant voltage source, as seen in the figure.

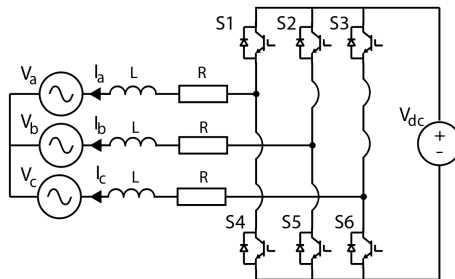


Figure 4.3: A circuit representation of the 2L-VSC used for the test with a constant DC-voltage on the DC-side.

The implementations can be found in Appendix B. The objective behind this was to investigate whether OpenModelica could reproduce the fast switching dynamics of a

switching model with a switching frequency of 10kHz, which in this document serves as an accuracy test of OpenModelica for high-frequency dynamics.

4.2.1 Test description

The event that was introduced to test the accuracy of the results from both models was a step change in the reference of $i_{q,ref}$ from -1 to 1 at $t = 0.7s$ while keeping $i_{d,ref} = 0$. In contrary to the MMC model presented in Chapter 3 where a sine-based Park transformation is used, i_q relates to active power and i_d relates to reactive power in this 2L-VSC model, as a cosine-based Park transformation is used.

This step in i_q allows studying the fast response of the current controller in addition to the harmonic components of the currents. The two last results will show how the harmonics in the dq -currents translate to the current of the a-phase in each software.

The simulations were performed with a time step of $\Delta t = 1\mu s$ and the Euler solver in both software.

4.2.2 Resulting current waveforms compared to Simulink

Figure 4.4 shows the responses of the dq-currents in both software when $i_{q,ref}$ is changed from -1 to 1 pu and $i_{d,ref}$ is kept constant at 0. Both currents follow their references, and the waveforms seem to be close to identical. Close-ups of the d - and q -currents will be added next to study the results closer.

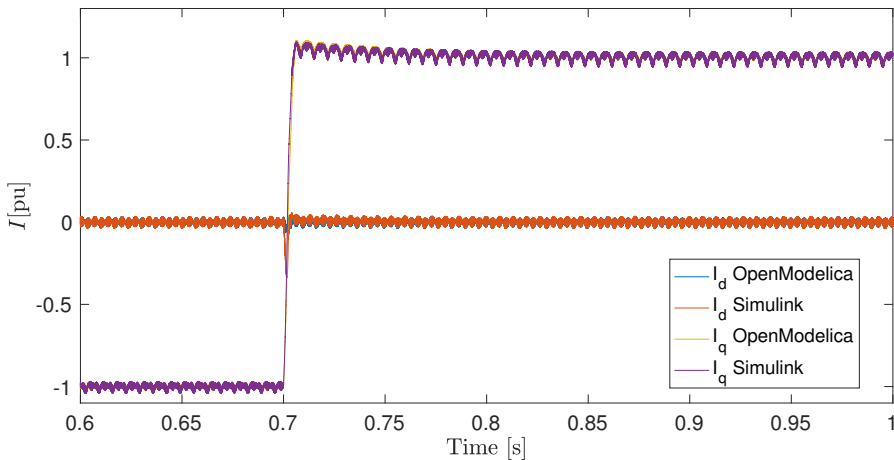


Figure 4.4: Comparison of the dq-currents from switching model in Simulink and OpenModelica.

Figure 4.5 shows a close-up of the d-currents in both software when $i_{q,ref}$ is changed from -1 to 1 pu and $i_{d,ref}$ is kept constant at 0. It can be seen how the OpenModelica implementation handles the decoupling better than the Simulink model, as the Simulink model makes a drop in the d-component of the current as the q-component is stepped at 0.7

s. Further, there seems to be a slight offset between the two waveforms until the transients settle, which could be caused by the different responses in the d-current when stepping the q-current.

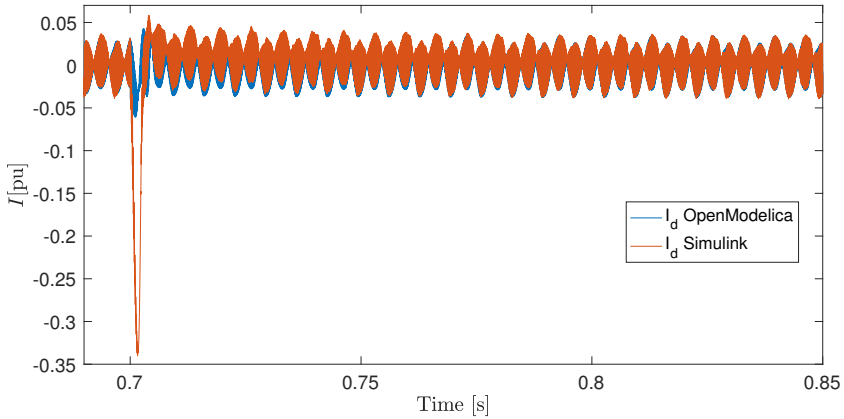


Figure 4.5: d-currents from OpenModelica and Simulink compared.

Figure 4.6 shows a close-up of the q-currents in both software under the same conditions as above. Also in the q-component, there seems to be a slight offset between the two waveforms until they reach a steady state, which also could be caused by the transient in the d-component of the current.

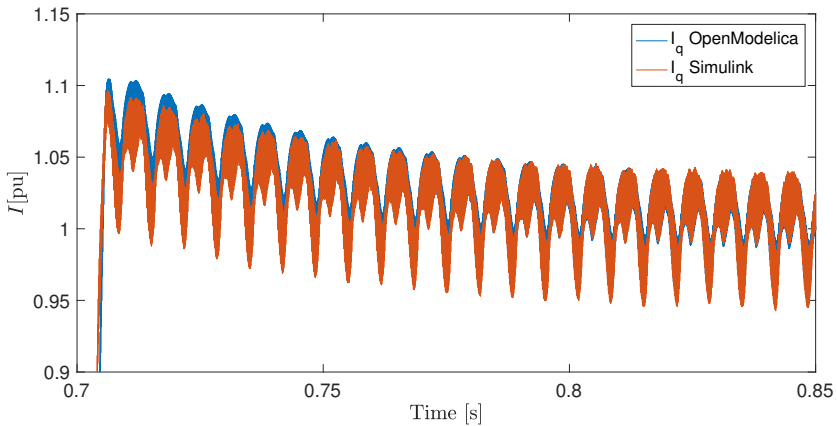


Figure 4.6: q-currents from OpenModelica and Simulink compared.

Figure 4.7 shows the waveforms of the a-phase current from OpenModelica (blue) and Simulink (red) containing the harmonics due to the switching of the 2L-VSC. The waveforms of the b- and c-phase have similar waveforms.

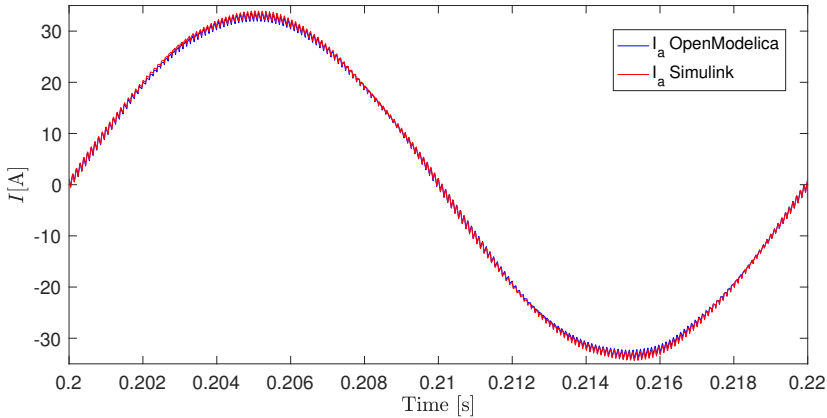


Figure 4.7: Comparison of the abc-currents from switching model in Simulink and OpenModelica.

Figure 4.8 shows a close-up of the current in the a-phase from both software, where it can be seen that the ripple has the same magnitude in both software. However, there seems to be a slight offset between the two waveforms, but as seen in Figure 4.7, this offset is small.

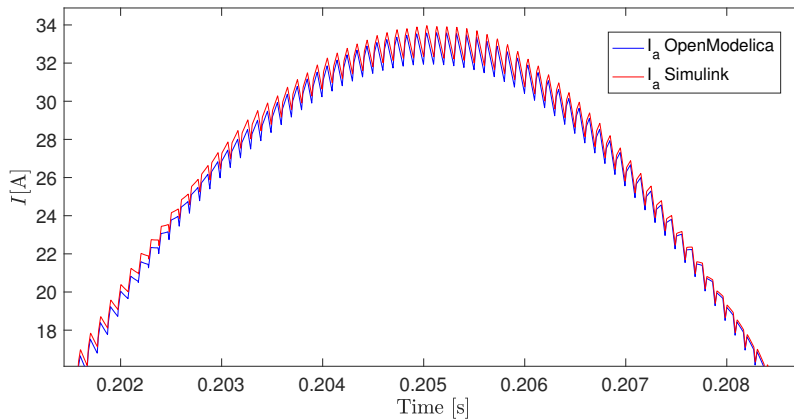


Figure 4.8: Comparison of *a* phase currents from switching model in Simulink and OpenModelica.

From these results, it is clear that OpenModelica can deal with the fast switching dynamics found in a 2L-VSC when switching at 10 kHz, as the current waveforms are close to identical compared to the waveforms from the corresponding Simulink model with some minor differences. This verifies the accuracy of the OpenModelica software for such fast dynamics.

Simulation models used later in this documents will consider average models with dynamics that are slower than these switching models, and hence they are expected to be

fully captured by the software, as also showed with an average model of a 2L-VSC in the Specialization Project [14].

4.2.3 Simulation speeds compared to Simulink

Another indicator of OpenModelica's performance is the simulation speed for different solvers. This section will compare the speed of different solvers in Simulink and OpenModelica for the previously mentioned switching models for a 1-second simulation at a time step of $\Delta t = 1\mu s$. The simulations were performed on a MacBook Pro, 13-inch, Mid 2014 with a 2.8 GHz Intel Core i5 processor with 2 cores and 16GB RAM. To increase the viability of the results, the CPU usage of the computer was monitored closely during all simulations to make sure that there were no conflicting processes.

The results in Table 4.2 shows the comparison of solvers in OpenModelica and Simulink. The results are the average of 3 simulations per solver, and the standard deviation for the 3 simulations, σ , is added in parenthesis for each solver.

Table 4.2: Comparison of simulations speeds at $\Delta t = 1\mu s$

Solver	Simulink	OpenModelica
Euler	51.48s ($\sigma = 3.61s$)	60.92s ($\sigma = 1.32s$)
Heun	62.87s ($\sigma = 2.06s$)	66.00s ($\sigma = 4.21s$)
Runge-Kutta (4h order)	78.87s ($\sigma = 8.52s$)	66.70s ($\sigma = 1.26s$)
Impeuler	-	97.77s ($\sigma = 2.09s$)
Imprungekutta	-	172.54s ($\sigma = 12.67s$)
Trapezoid	-	104.25s ($\sigma = 2.05s$)
Dassl	-	78.13s ($\sigma = 3.59s$)
Ida	-	83.33s ($\sigma = 2.10s$)
Bogacki-Shampine	68.94s ($\sigma = 1.09s$)	-
Dormand-Prince (RK5)	88.15s ($\sigma = 3.41s$)	-
Dormand-Prince (RK8)	127.73s ($\sigma = 2.14s$)	-
RungekuttaSsc	-	69.33s ($\sigma = 0.90s$)
Irksco	-	60.13s ($\sigma = 1.25s$)
SymSolver	-	*
SymSolverSsc	-	(53.04s ($\sigma = 0.49s$))†
qss	-	‡

* The SymSolver did not simulate the switching model at all and caused the model crashing.

† Despite simulating, the SymSolverSsc solver did not produce any accurate or usable results.

‡ When trying the qqs solver, a message was prompted saying the solver is still in development and should not be used.

Except for the problems with the three experimental solvers, all other solvers in OpenModelica produced similar results when running the switching model. Among the common solvers between OpenModelica and Simulink, the Euler and Heun solvers were slightly faster in Simulink. On the other hand, the fourth order Runge-Kutta method was slightly faster in OpenModelica compared to Simulink.

The implicit solvers in OpenModelica were significantly slower than the explicit solvers for this switching model. However, a warning was prompted to "*restart KINSOL and*

change linear solver to KINDense” when using Impeuler, Imprungekutta, and Trapezoid. A solution to these warnings was not found at the time, and the possibility that these solvers were not used optimally should be considered when considering these results. However, the implicit solvers were expected to be slower due to the increased computational effort of implicit solvers. It should also be noted that the default solver, Dassl, was almost 20 seconds ($\sim 28\%$) slower than the Euler solver in OpenModelica, which could be because it is an implicit solver.

Overall, the performance of OpenModelica in regards to simulation speeds was good compared to Simulink when considering the switching model.

4.3 Using OpenModelica for real-time simulations

This section will demonstrate how the previously mentioned FMI standard allows for model exchange from OpenModelica to an external software. This section will demonstrate the use of FMUs to make OpenModelica models work in the real-time simulator ePHASORSIM, based on work done in the National Smart Grid laboratory. The content in this section originates from the second objective related to the OpenModelica software, which was also requested by the industrial partner, DNV GL.

A literature review revealed that no guides on how to couple OpenModelica models with ePHASORSIM existed in the available literature. However, a description of the approach was found in the built-in user manual of the RT-LAB software, but that description was not complete and lacked important details. Therefore, this section will include a detailed guide of the necessary step needed to make OpenModelica models work with the real-time simulator ePHASORSIM based on work done in the National Smart Grid laboratory. Also, this section will have a more pedagogic approach than the previous, so that future student can follow the guide to build models in their work. The main steps of the approach are summarized in a flowchart at the end of the chapter.

However, before explaining the approach, some concepts need to be further explained.

4.3.1 Real-time simulations

Real-time simulations are simulations of computer models that replicate physical systems that are executed in the same rate as the actual physical system. Therefore, one can say that the simulations are performed in real-time using a real-time simulator.

An example of a real-time simulator used for studying transient stability in large power systems is Opal-RT’s ePHASORSIM [77, 78].

The use of real-time simulators to run simulation models in real-time facilitates the combined use of physical components and simulation models, as will be explained next.

4.3.2 Hardware-in-the-loop testing

Hardware-in-the-loop (HIL) testing includes parts of the physical hardware in the simulation loop along with a computer model of the rest of the system. This allows control loops to be tested on real physical components instead of a mathematical model and can also serve as a validation of mathematical models [79]. By coupling modeling tools

with hardware-in-the-loop (HIL) testing, development processes can be greatly accelerated without the need for producing prototypes [80].

In the context of multi-terminal HVDC grids, HIL tests offer testing without the need for full-scale systems. As testing of large and complex multi-terminal HVDC systems in full scale is not feasible, HIL provides a way to study multi-terminal HVDC systems with a good balance between fidelity and good test coverage [81]. Usually, simulation models have good test coverage, but the fidelity of simulation models, i.e. the degree of which the actual conditions are replicated, is limited because simulations are executed with models and not real equipment. Similarly, power test-beds with real equipment provide a high fidelity but have low coverage of tests and can be expensive.

The combined testing using both simulation models and physical hardware can be done in laboratory scale by using what is called power hardware-in-the-loop (PHIL) [82], where power amplifiers are used, as depicted in Figure 4.9, allowing testing at higher power levels. By using PHIL, simulations and power test-beds are combined to provide a good balance between the range of tests that can be performed and the fidelity of the tests, which is important for the development of multi-terminal HVDC grids.

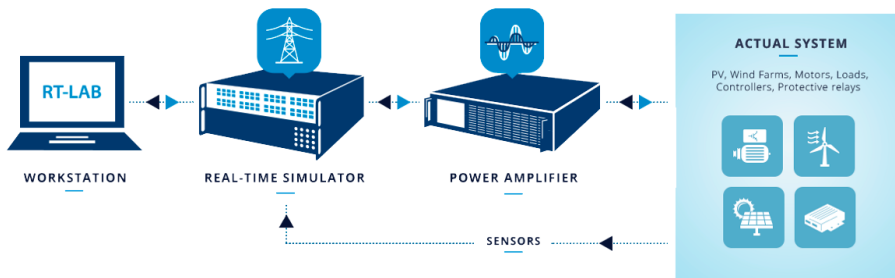


Figure 4.9: Overview of the power hardware-in-the-loop (PHIL) process [82].

Opal-RT is the leading developer of real-time simulators and HIL testing equipment for designing, testing and optimizing control and protection systems in, for example, power systems, power electronics and motor drives [83]. To fully utilize the OpenModelica tool to model HVDC grids, it is interesting to investigate how models developed in OpenModelica can be used for real-time HIL testing with Opal-RT's equipment.

4.3.3 Building models in OpenModelica for ePHASORSIM

As explained, real-time simulations are important to facilitate HIL simulations. Therefore, this section will explain how to build and export OpenModelica models for ePHASORSIM, which is one of Opal-RT's real-time simulators used for transient stability simulations in larger power systems. An example of use of ePHASORSIM can be found in reference [84]. No complete guide for this was found in the available literature, and therefore this section will have a pedagogic approach for future students and industrial actors to use it as a guide in their work. The main steps of the approach are summarized in a flowchart at the end of the chapter. The following is a result of work at the National Smart Grid laboratory, and additional explanations are added to the Appendix, including a

description of the RT-LAB environment in which ePHASORSIM is a part of.

ePHASORSIM is built for phasor domain simulations, which is explained next.

Phasor domain models

In phasor domain models, the currents and voltages are represented as phasors with a magnitude and angle, or by a real and imaginary component, depending on the coordinate system used. A key assumption in phasor domain models is that the quantities are varying more slowly than the fundamental frequency. This makes the currents and voltages time-invariant, meaning they are not oscillating as in time domain models. Such models are traditionally used to study larger power grids with the slow inertia responses of large machines and interactions in the time scale of seconds to minutes [85]. On the other hand, when considering the faster dynamics of, for example, power electronic converters and harmonic content, time domain models can become useful.

In such models consisting of multiple power system components, it is useful to distinguish between a local dq reference frame for each component and a global DQ reference frame which is a common reference frame for all components. Equations for each component and their respective control are expressed in the local dq reference frame. However, to find a solution to the whole system, all currents and voltages must be transformed to the common DQ reference frame [86]. A short explanation of this transformation and the equations needed can be found in Appendix A.3.

The Opal-RT Modelica developer library

The guide starts with describing the Modelica libraries that are necessary for building ePHASORSIM compatible models.

Opal-RT provides Modelica libraries for building models that are compatible with ePHASORSIM. These are two libraries, a developer library and a library called the GenUnit library. These libraries can be obtained by contacting Opal-RT's customer support after purchasing the license to their software, which was done in the National Smart Grid Laboratory.

The Opal-RT Modelica developer library comes with pre-built models of different components as seen in Figure 4.10, but the library also allows for user-defined models of components that are not existing to interface with ePHASORSIM through the Power Pin connector and the Interface Pin connector.

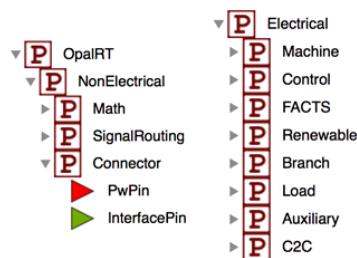


Figure 4.10: The Opal-RT Modelica Developer Library

In addition to the developer library, Opal-RT provides another library, the GenUnit library which contains models ready for use in ePHASORSIM or for example generators. It is important to note that any user-defined models must be built in the developer library and called in a model inside the GenUnit library. This is further clarified in an example model later.

The Power Pin

The red pin, "PwPin", in Figure 4.10 is called the Power Pin and comes with the Opal-RT Developer library. This pin is a connector type class that has variables for the real and imaginary components of both currents and voltages. The Power Pin is used as an interface between the power system buses in ePHASORSIM and the Modelica models. To properly interface with ePHASORSIM, the power pins must follow the naming conventions "bus0", "bus1", "bus2" and so forth in the GenUnit implementation of the model.

```

1365 connector PwPin
1366   Real vr;
1367   // real part of the voltage
1368   Real vi;
1369   // imaginary part of the voltage
1370   flow Real ir;
1371   // real part of the current
1372   flow Real ii;
1373   // imaginary part of the current
1374   annotation(Icon(coordinateSystem(extent = {{-100,
-100}, {100, 100}}, preserveAspectRatio = true,
initialScale = 0.1, grid = {2, 2}), graphics =
{Polygon(origin = {-0.39, 0.11}, fillColor = {255, 0,
0}, fillPattern = FillPattern.Solid, points = {{-99.613,
100.115}, {100.161, -1.01398}, {-99.613, -100.111},
{-99.613, 100.115}})}, Diagram(coordinateSystem(extent
= {{-100, -100}, {100, 100}}, preserveAspectRatio =
true, initialScale = 0.1, grid = {2, 2})));
1375 end PwPin;

```

Figure 4.11: The OpenModelica implementation of the Power Pin connector class.

Figure 4.11 shows the implementation of the Power Pin connector class. It can be noted that the variables are of type "Real", meaning the connector is not currently supported by the electrical library in the Modelica standard library. This means that the models must be implemented in equation form, or alternatively that an interface is used between electrical models and the Power Pin. For this purpose, an interface between the Power Pin and a three-phase electrical grid with voltage sources was designed and can be found in Appendix C.1. This interface allows three-phase time domain models to be used in ePHASORSIM.

ePHASORSIM interprets all components with at least one Power Pin as a current injector component. A current injector component is every component that can be modeled as a current source. Such components either generate, absorb or transfer electric energy to or from the system and can be, for example, generators, loads or lines.

The Interface Pin

The green pin, "InterfacePin", in Figure 4.10 is the interface with ePHASORSIM that allows changes to commands during simulations. This creates an input to the FMU model that allows to, for example, change current references in a VSC model while the real-time simulation is running.

Connecting to the Power Pin for model testing in OpenModelica

When building a model that is compatible with ePHASORSIM in OpenModelica, it is useful to test the model in OpenModelica before converting it to an FMU. The Opal-RT Developer library provides an interface that allows the user to connect to a Power Pin, define the real and imaginary part of the bus voltage and then investigate whether the user-defined current injector works as expected. This interface is implemented as the PIN2INOUT class, which can be found under SignalRouting in the Opal-RT library. The block is showed in Figure 4.12 and can give a better understanding of how ePHASORSIM interferes with the Power Pin.

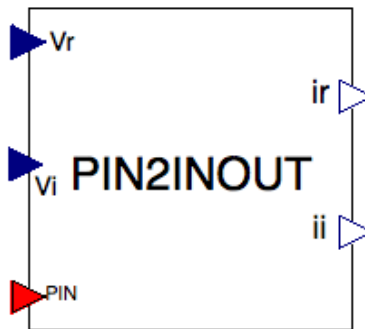


Figure 4.12: The PIN2INOUT interface from the Opal-RT library.

By connecting the Power Pin of the user-defined model built in OpenModelica to the "PIN" of the PIN2INOUT block and defining the input voltages, the model can, as mentioned, be tested without converting it to an FMU.

Example models

For illustration purposes, a simple example model of a resistor has been built in OpenModelica for use in ePHASORSIM. The outer layer of the model must be implemented in the GenUnit library, and the GenUnit implementation of the model can be seen in Figure 4.13.

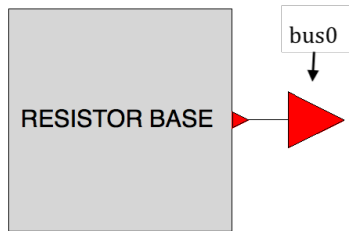


Figure 4.13: The implementation of the RESISTOR model in the GenUnit library.

The red power pin in Figure 4.13 must follow the naming convention, and it is therefore named "bus0". Any additional power pins should then be named "bus1", "bus2" and so on.

The RESISTOR_BASE block is defined in the Opal-RT library and contains a transformation from global to local reference frame and the equations for the local d- and q-currents forming the inner layers of the model. The implementation of the RESISTOR_BASE block can be seen in Figure 4.14. The implementation of the reference frame transformation block can be found in Appendix C.1.1. The resistor equations are simply $i_{qL} = 0$ and $i_{dL} = v_{dL}/R$.

It should also be mentioned that the Power Pin in the inner layers of the model does not need to follow the aforementioned naming convention, as this only applies to the outermost layer found in the GenUnit library.

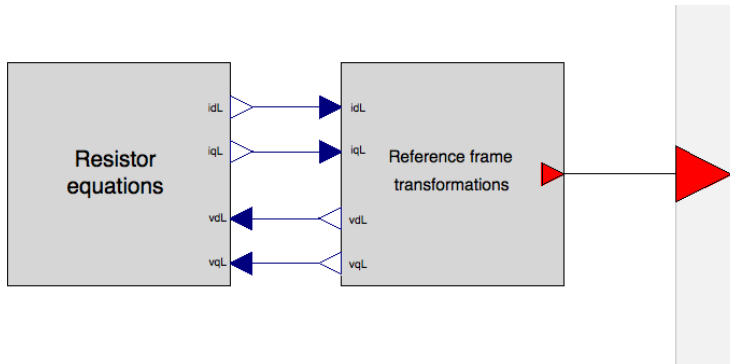


Figure 4.14: Implementation of the RESISTOR_BASE block in the Opal-RT library.

Further, to illustrate the use of the interface pin, a simple AC-side representation of a VSC was built using the same dynamic equations as for the dq-current dynamics of the MMC in Chapter 3 described by Equations (3.22) and (3.23). Figure 4.15 shows an example on how to properly use the interface pin in OpenModelica. This allows the user to change signals during simulations in ePHASORSIM, as in this case, the references for the d- and q-current controllers.

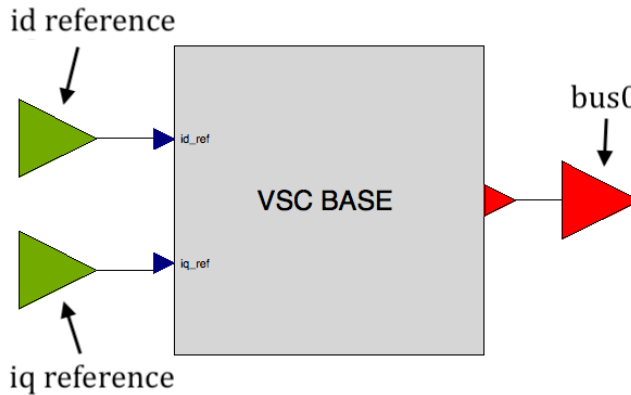


Figure 4.15: Implementation of a VSC in the GenUnit library to illustrate the use of the interface pin.

The details of the VSC_BASE block are not considered important in this context, but the implementation of the block can be found in Appendix C.2 for convenience.

Opal-RT's FMUCreator tool

ePHASORSIM comes with a tool called FMUCreator that converts a Modelica model (.mo) into an FMU (.fmu) that is to be used by ePHASORSIM.

For the FMUCreator to successfully generate an FMU, it is important that the model is implemented with a power pin that follows the naming convention and that the model is properly implemented in the GenUnit and Opal-RT libraries. The latter will be repeated here for further clarification.

Any user-defined model has to be part of the GenUnit library that comes with the Opal-RT Modelica developer library. The model must be declared as a block within the Opal-RT Developer library, named for example, "VSC_BASE" or "RESISTOR_BASE". Next, the base block, for example "VSC_BASE", must be called in a class named "VSC" in the GenUnit library. This is necessary for the FMUCreator to successfully create an FMU of the Modelica model. The path of both libraries is used as an input when using the FMUCreator, as showed in Figure 4.16.

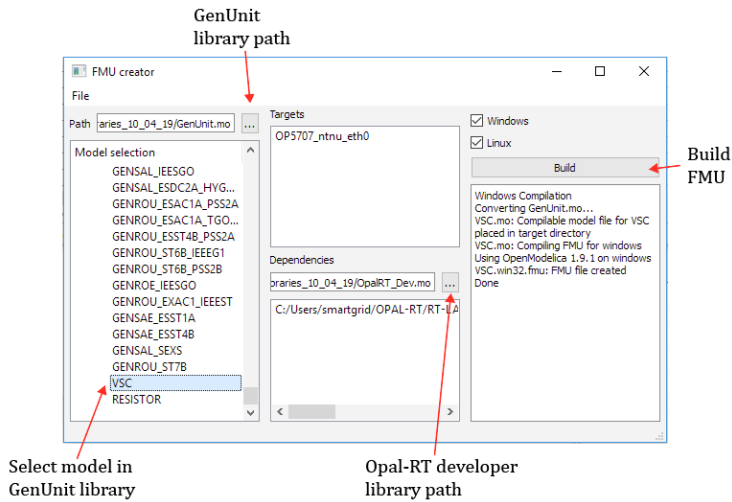


Figure 4.16: The interface of Opal RT’s FMUCreator 1.0.

It is important that both Windows and Linux are selected in the FMUCreator, as the computer running the real-time simulation in the National Smart Grid laboratory is a Linux-computer. If the Linux-version of the FMU is not created, the real-time simulation does not run.

Additionally, when a user-defined model is added to the GenUnit library, it has to be registered in the FMUGlossary file.

Registering a component in FMUGlossary

The FMUGlossary file is a .csv file that can be located in 'C:\opal-rt \RT-LAB \v11.3.x \FMUCreator \resources'. This file contains all necessary information for the FMUCreator, as showed in Table 4.3.

Table 4.3: Information to register in the FMUGlossary file

Entry	Information	Comment
1	ID	A unique ID generated from MATLAB
2	Name	Same as in the GenUnit library
3	Type	See below
4	Number of parameters	
5	Name of parameters	In any order

The unique ID needed in the file can be generated from the MATLAB command $UUID = java.util.UUID.randomUUID$.

The model type is established by Opal-RT and specified by the user as a number between 1 and 6 (1 for a machine, 2 for an exciter, 3 for a stabilizer, 4 for a turbine, 5 for an over-exciter, 6 for an under-excitation limiter and 7 for an HVDC model with 2 power pins). The VSC and RESISTOR example models would, for instance, be of type 1.

Figure 4.17 shows how the RESISTOR and VSC examples were implemented in the FMUGlossary file along with some preexisting models in the GenUnit library. To avoid confusion, it should be mentioned that the parameters of the preexisting models extend in columns beyond the figure.

	A	B	C	D	E	F	G	H	I	J
1	Version		1							
2	ID must be unique, containing numbers and characters									
3	Type 1 for machine, type 2 for exciter, type 3 for stabilizer, type 4 for turbine, type 5 for over-exciter, type 6 for under-excitation limiter, type 7 for hvdc									
4	Name of parameters must match with their corresponding names in FMUs.									
5	The order of components is not important, the order of parameters is important since other mapping files follow the same order									
6	Lines not starting with a GUID will be ignored in cimphony the mapping									
7	Entries right of the number of parameters declared in column 4 will be ignored and can be used for comments									
8										
9	ID	Name	Type	Number of Parameters	Parameters...					
10	3946f4d9-7a97-402e-91c2-b8d361743ad4	RESISTOR	1	1	R					
11	00785f15-f73c-4190-a2ea-bce4a55fe779	VSC	1	5	Vb	Sb	fb	Lpu	Rpu	
12	bfabdb20-b13b-443c-8203-f14505b4a466	GENROU	1	21	P_gen	Q_gen	Vt_abs	Vt_ang	SB	fn
13	8e2e0f49-8af4-4650-996c-ea8c8950f068	GENROE	1	21	P_gen	Q_gen	Vt_abs	Vt_ang	SB	fn
14	c558e72a-5e4c-411b-8da3-8576a5927d71	GENSAL	1	19	P_gen	Q_gen	Vt_abs	Vt_ang	SB	fn
15	a8c42ca4-3c62-4ebf-b354-578969d5b9de	GENSAE	1	19	P_gen	Q_gen	Vt_abs	Vt_ang	SB	fn
16	857a74f3-08fc-4294-a2fd-a2293a2b35e6	GENCLS	1	10	P_gen	Q_gen	Vt_abs	Vt_ang	SB	fn
17	d7de6bc0-e677-4392-a01f-16aee72cd9b7	WT4G1	1	16	P_gen	Q_gen	Vt_abs	Vt_ang	SB	fn
18	38c19cab-0f8c-4e9c-993d-368dba715513	CSVGN5	1	22	P_gen	Q_gen	Vt_abs	Vt_ang	SB	fn
19	1cf60197-9032-4b5f-a7b7-98a9b5715473	CSTCNT	1	22	P_gen	Q_gen	Vt_abs	Vt_ang	SB	fn

Figure 4.17: RESISTOR and VSC example implementation in the FMUGlossary file opened in Excel.

Defining the simulation system in Excel

Simulations in ePHASORSIM use data imported from an Excel file to define the power system to be simulated. The Excel file defines all the buses in the system, the components connected to the buses and which buses are connected together with all the corresponding parameters. A full Excel implementation of a system with corresponding single line diagram was created and can be found in Appendix C.4 for further clarification.

When creating a user-defined model in OpenModelica, an additional sheet in the Excel file has to be created to include the model in the power system. This new sheet must have the same name as the name of the model in the GenUnit library. The parameters of the model are then defined in this Excel sheet.

Figure 4.18 shows the Excel implementation of the RESISTOR example where the only parameter is R and Figure 4.19 shows the excel sheet of the VSC example and its parameters. The number under the "bus0" field in the excel files defines the bus in the power system that the Power Pin with name "bus0" in the component is connected to.

	A	B	C	D	E	F	G	H
1	name	bus0	R					
2	r1	1	1,1					
3								
4								
5								
6								

◀ ▶
General
Pins
Bus
Vsource
RESISTOR

Figure 4.18: Excel implementation of the RESISTOR example with 1 parameter.

	A	B	C	D	E	F	G	H	I	J
1	name	bus0	Vb	Sb	fb	Lpu	Rpu			
2	cnv1	2	400	20000	50	0,15	0,01			
3										
4										
5										

General Pins Bus Vsource Line VSC

Figure 4.19: Excel implementation of the VSC example with 5 parameters.

When using the green interface pins as explained with the VSC example, these have to be defined in the excel file under the "Pins" tab. This is illustrated in Figure 4.20, where "cnv1" is the name of the VSC defined in the VSC tab.

	A	B	C	D	E
1	outgoing	Vmag	1/Vmag	2/Vmag	
2	outgoing	Vang	1/Vang	2/Vang	
3	incoming	idref	cnv1/idref		
4	incoming	iqref	cnv1/iqref		
5					

General Pins Bus Vsource Line VSC

Figure 4.20: Declaration of the interface pins in the Excel file.

"iqref" and "idref" in Figure 4.20 correspond to the names of the interface pins defined in the Modelica model.

Summary of the approach

To summarize the overall approach, a flowchart of main steps was created. Figure 4.21 shows the flowchart on how to prepare a model built in OpenModelica for real-time simulations in ePHASORSIM.

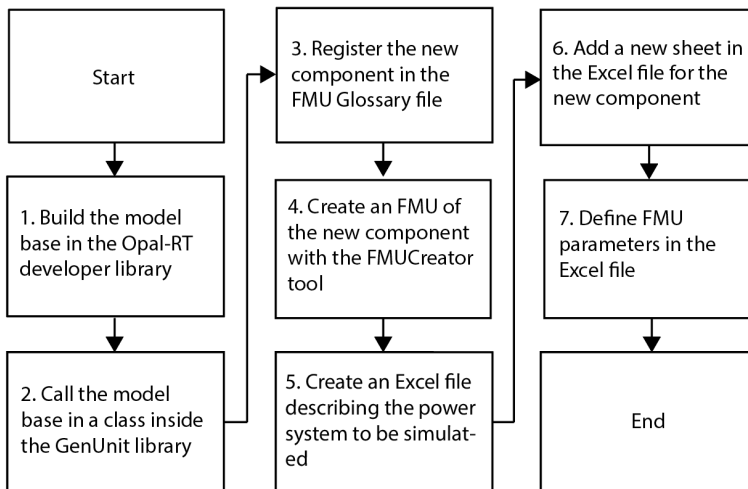


Figure 4.21: Flowchart of the steps needed to prepare a Modelica model for ePHASORSIM.

Following the steps in the flowchart should make the model work with the ePHASORSIM real-time simulator. ePHASORSIM is a part of the RT-LAB environment from Opal-RT. For further explanation on how to use ePHASORSIM, set up the model in the RT-LAB environment, and execute the real-time simulation, refer to Appendix C.4 where a guide for RT-LAB is added using an example system containing the VSC example model.

4.3.4 HVDC model for ePHASORSIM

To further explore models defined as Type 7 in the FMUGlossary file, a point-to-point HVDC model with two Power Pins was implemented in OpenModelica and successfully exported to FMU. The OpenModelica and Excel implementations of the model can be found in Appendix C.3.

This model will be further brought up in the discussion in Chapter 7, including some interesting observations related to the time step required by the real-time simulator. As it turned out, the model worked perfectly with a time step of $\Delta t = 100\mu s$ in OpenModelica using the Dassl and Rungekutta solvers. However, when testing the exported FMU in Simulink (according to the guide in Appendix C.4), the model only worked for a time step of $\Delta t = 25\mu s$ or smaller regardless of solvers.

Simulation System Description

As mentioned in the introduction, a simulation system was built to simulate the dynamics of the integration of offshore wind resources and offshore energy storage to the mainland power system through a three-terminal MMC based HVDC system.

This chapter describes the models used for the different components in this simulation system. All models are implemented in OpenModelica, and the implementations can be found in Appendix D. These models are made publicly available from the following URL: <https://github.com/joachimesp/OpenModelica-HVDC-NTNU>.

5.1 The complete system configuration

The complete simulation system used in this Thesis is showed in Figure 5.1. It includes two wind farms, WF1 and WF2, where WF1 is complemented with an energy storage system. The two wind farms are connected through a three-terminal HVDC system to shore where the HVDC converters are MMCs and the cable is represented by a frequency dependent cascaded pi-model, which is further explained later in this chapter.

A simplified wind farm model was included to reproduce the typical power profile delivered by a wind farm to the grid at realistically varying wind speeds. In addition, a simple energy storage model was implemented to study how energy storage can absorb and release power to study how it can complement the power production from an offshore wind farm.

The energy-based MMC model is chosen because of its accurate modeling of internal storage in the MMC. The model is chosen as an average-model since harmonic content is considered beyond the scope of this study, and average-models are more computationally efficient when used in larger system configurations. This allows the model to be efficiently used in possible model expansions with more HVDC terminals in the future.

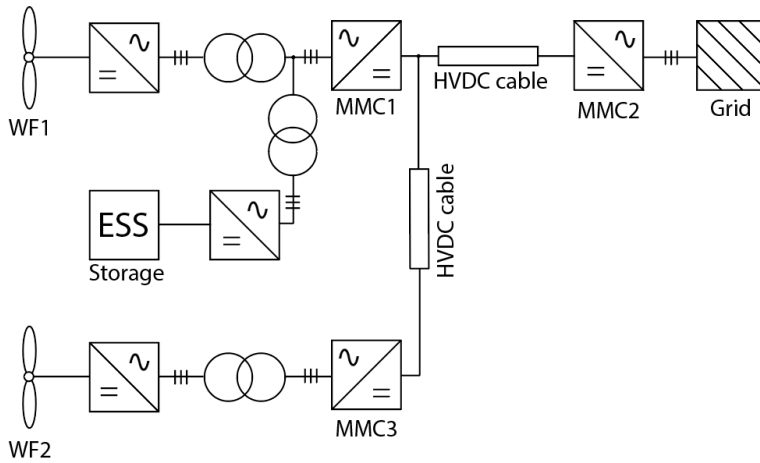


Figure 5.1: The three-terminal MMC based HVDC system with wind farms and energy storage, reproduced from Figure 1.3 for convenience.

A frequency dependent HVDC cable model is included to accurately capture the dynamics of the transmission of power between the HVDC terminals, as the HVDC cable is a very important passive element of the model.

Lastly, a transformer model is also included to represent the collector transformer which is the interface between the wind farm and the grid and also the step up transformer between the energy storage system and the offshore AC-grid.

5.2 Wind farm model

The wind farm model is represented in aggregated form by the dynamics of a single wind turbine. The physical quantities that form a basis for the dynamic model can be seen in Figure 5.2.

Figure 5.2 shows a general schematic of a Type IV wind turbine with a direct-drive synchronous generator without a gearbox and power electronic converters used for control of the turbine. These kinds of turbines have made their first inroads into the market as large turbines for offshore systems [87]. One feature that makes Type IV turbines suitable for offshore applications is the decreased maintenance requirements due to the lack of a gearbox in the turbine. The gearbox is usually needed to increase the shaft speed of the generator rotor; however it is not needed when using large synchronous generators with many poles. These generators can operate at low rotor speeds, matching the rotational speed of the turbine blades. One example of a Type IV turbine is Siemens Gamesa's SG 8.0-167 DD turbine with a rated power of 8MW, a rotor diameter of 167m and a direct-drive permanent-magnet synchronous generator [88].

In this context, it should be mentioned that Type III turbines with doubly-fed induction generators can provide flexibility in control (but with a lower range) at a lower cost including lower ratings of the power electronic converters ($\sim 30\%$ of rated generator power).

However, Type III turbines do not necessarily have the same low maintenance requirements as Type IV turbines [87]. This topic was only mentioned to give some general insight and will not be further discussed in this Thesis.

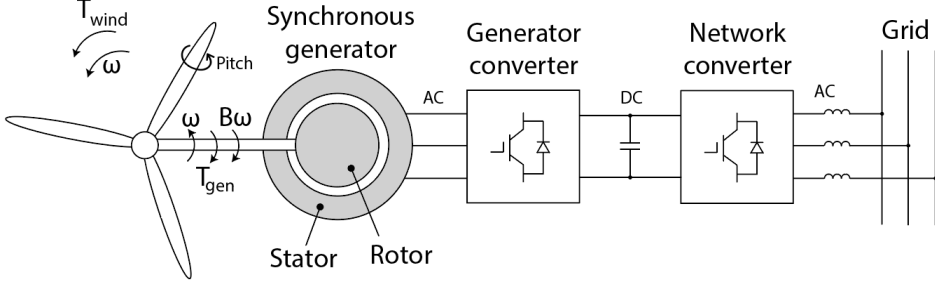


Figure 5.2: A general representation of a Type IV wind turbine with a synchronous generator and fully rated power electronic converters without a gearbox.

From Figure 5.2, a dynamic equation for torque balance between the turbine blades, T_{wind} , the electrical generator, T_{gen} and the frictional torque, $B\omega$ can be expressed as follows:

$$J \frac{d}{dt} \omega = T_{wind} - T_{gen} - B\omega \quad (5.1)$$

where J is the total inertia in turbine and the generator.

Further, the turbine mechanical power can be expressed by the turbine torque, T_{wind} , and rotational speed of the turbine, ω , as

$$P_{turbine} = \omega T_{wind} \quad (5.2)$$

Alternatively, the turbine power can be expressed as a fraction of the power available in the wind through the power coefficient C_p .

$$P_{turbine} = C_p P_{wind} = C_p \frac{1}{2} \rho A u^3 \quad (5.3)$$

where ρ is the air density, A is the area swept by the blades and u is the wind speed.

When considering the aerodynamics of the turbine blades, it is useful to define the tip speed ratio λ as:

$$\lambda = \frac{\omega \ell}{u} \quad (5.4)$$

where ℓ is the length of the turbine blades.

The power coefficient represents the aerodynamics of the turbine blades, and it can be expressed as a function of the tip speed ratio λ and the blade angle β representing the pitch of the blades in the pitch axis showed in Figure 5.2. The relationship is from reference [89] and is a well-established equation for simplified turbine models in the literature, expressed as:

$$C_p(\lambda, \lambda_{ai}, \beta) = 0.5176 \left(\frac{116}{\lambda_{ai}} - 0.4\beta - 5 \right) \exp \left(\frac{-21}{\lambda_{ai}} \right) + 0.0068\lambda \quad (5.5)$$

where

$$\lambda_{ai}(\lambda, \beta) = \left(\frac{1}{\lambda + 0.08\beta} - \frac{0.035}{\beta^3 + 1} \right)^{-1} \quad (5.6)$$

However, this relationship is just a numerical approximation, and the C_p curve will, in reality, vary from turbine to turbine.

By assuming all turbines in the wind farm are controlled equally and producing the same power, a scaling factor representing the number of turbines in the wind farm, $N_{turbines}$, is added to output the total power production of the wind farm.

5.2.1 Turbine control regions

For control purposes, the power curve of a wind turbine can be divided in four regions as showed in Figure 5.3.

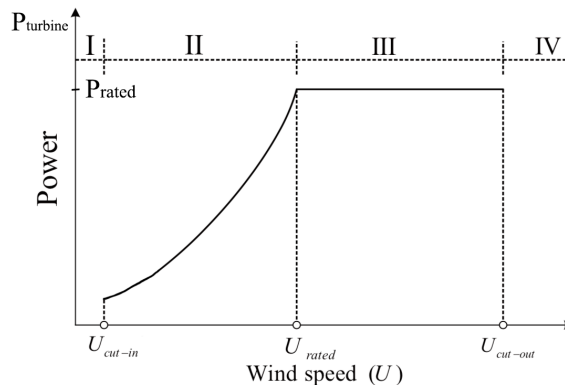


Figure 5.3: Control regions of a wind turbine [90].

In region I, the wind speed is too low to produce any torque to overcome the frictional torque; hence the turbine is shut down without any power production. In region II, variable speed control is applied to obtain optimal tip-speed ratio hence the optimal angle of attack to maximize C_p , thus the power production. In region III, the speed is kept constant while pitch control is applied to control the blade angle β to shed the excess power that exceeds the turbine generator ratings. The last region is region IV, where the turbine is shut down because of too high wind speed that can damage the turbine, and the power output is zero.

Model overview with the different control regions

Figure 5.4 shows a schematic of the complete turbine model used and the relationship between the two controllers and how they relate to the control regions.

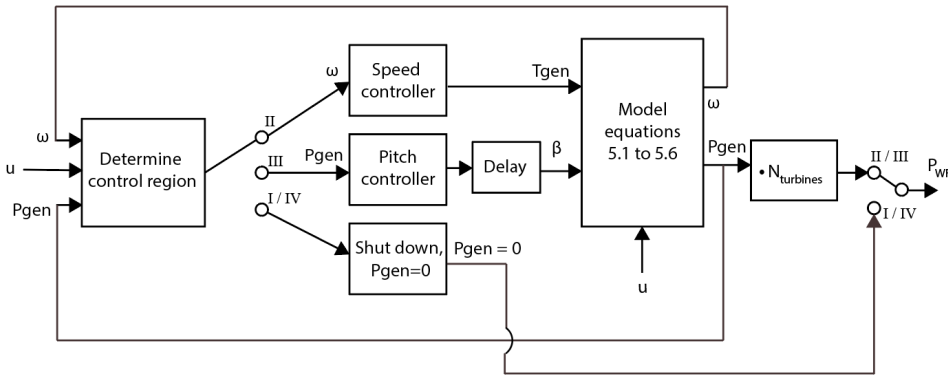


Figure 5.4: A schematic of the wind turbine model with pitch controller and speed controller.

The wind speed in Figure 5.4 is used to determine the control region and which controller to use. If region II is selected, the turbine rotational speed, ω , is used as feedback and if region III is selected, the turbine electrical power, P_{gen} , is used as a feedback. If the wind speed corresponds to region I or IV, the turbine dynamics are bypassed and the electrical power output is zero, which emulates the shutdown of the wind turbine.

A first-order delay is introduced between the pitch controller and the input of the blade angle, β , for the system equations. This delay, *bladeAngleTimeConstant*, represents the time it takes for the mechanical pitch system to rotate the turbine blades in the pitch axis of Figure 5.2. When operating in region II, the blade angle, β , is set to be constant at zero.

By using this model compared to the schematic in Figure 5.2, the electrical properties of the generator and the two converters are neglected. This leads to a more simplified control system compared to the real control system since the generator torque is controlled directly as a variable and not by the currents of the generator converter. Further details on the control will come in the next subsections. However, the simplified wind farm model allows studying how changes in wind speeds relates to changes in power production for a wide range of wind speeds.

To couple the wind farm model to electrical components, the power output can be translated to a DC current source at a certain voltage and combined with an MMC model as a simplification of the topology shown in Figure 5.2. This is a normal representation of wind farms in such HVDC grid studies [65], where the wind farm is simplified as a DC current source representing only the grid side converter in Figure 5.2 with a capacitor. An OpenModelica implementation of this can be found in Appendix D.6.5. However, the normal approach is taken one step further by introducing a some turbine dynamics in the power delivered from the DC current source through the aggregated wind farm model. However, this wind farm model assumes that all turbines are operating and that they are operating at the same speed and power production, which is unlikely in real wind farms.

The parameters used for both wind farm models in the system in Figure 5.1 can be found in Appendix E.2.

Wind turbine speed controller (region II)

The speed controller adjusts the speed of the turbine by controlling the generator torque to have optimal power production according to the C_p -curve in region II. To ensure correct region II operation, logic statements are combined with a PI controller with an anti-windup scheme as depicted in Figure 5.5. ω_{ref} is calculated using Equation (5.4) and $\lambda_{optimal}$.

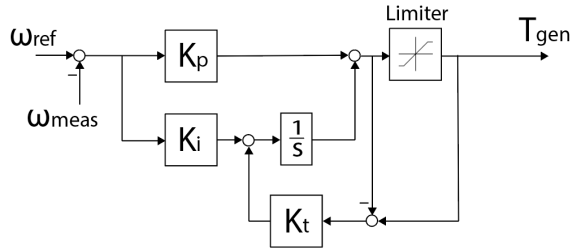


Figure 5.5: Block diagram of the turbine speed controller with anti-windup scheme.

In the physical model shown in Figure 5.2, the torque control is performed by controlling the currents of the generator converter.

The OpenModelica implementation of the speed controller can be found in Appendix D.

Wind turbine pitch controller (region III)

To ensure correct operation in region III, a set of logic statements is implemented along with a PI controller with an anti-windup scheme. The block diagram of the pitch controller is depicted in Figure 5.6. In region III, the power is controlled at its rated value by controlling the blade angle, β .

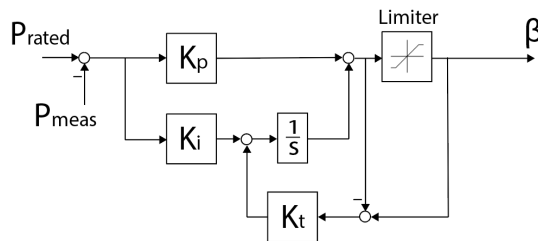


Figure 5.6: Block diagram of the turbine pitch controller with anti-windup scheme.

The OpenModelica implementation of the pitch controller can be found in Appendix D.

5.3 MMC model

The MMC model chosen for the HVDC converters in the simulation system is the simplified zero-sequence model that is described in Section 3.2.6. The control of the MMC is based on two control loops. The first cascaded control loop being inner vector control for the transformed AC currents with outer active power control with DC voltage droop. The second is the inner zero sequence circulating current control with outer zero sequence energy sum control. These control schemes were described with block diagrams in Section 3.3.

The MMC model used in this Thesis uses an ideal PLL representation where the angle used in the dq-transformations, ωt , is linearly increasing assuming constant electrical frequency on the AC-side.

The OpenModelica implementation of the model can be found in Appendix D, and the parameters used for the model, including tuning parameters, can be found in Appendix E.1.1.

5.4 Energy storage model

A schematic of the energy storage model used is depicted in Figure 5.7. The model consists of power flow from the storage unit, P_{es} , power flow from the power electronics controlling the storage unit, P_{pe} , and power loss in the storage unit and power electronics, P_{loss} . The directions of the power flows in Figure 5.7 defines the positive directions used in the model. A positive P_{pe} means that the energy storage is discharging, and a negative P_{pe} means that the storage unit is charging.

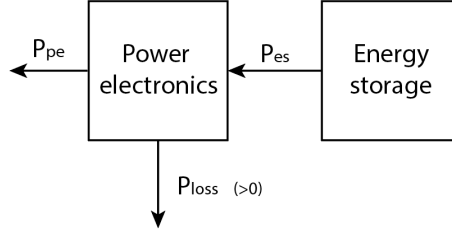


Figure 5.7: Schematic of the energy storage model and positive power flow directions.

The resulting equations describing the storage system are as follows:

$$P_{es} = P_{pe} + P_{loss} \quad (5.7)$$

$$W_{es} = \int -P_{es} \quad (5.8)$$

$$SOC = \frac{W_{es}}{W_{rated}} \quad (5.9)$$

$$1 \geq SOC \geq 0 \quad (5.10)$$

where SOC is the state of charge, describing to how much of the total capacity the storage unit is charged, and W_{es} is the accumulated energy stored in the unit.

Further, it is useful to distinguish the two charging states of the storage unit; whether it is charging or discharging. The equations describing the storage unit when it is discharging are:

$$P_{pe} > 0 \quad (5.11)$$

$$P_{pe} = \eta \cdot P_{es} \quad (5.12)$$

$$P_{loss} = \left(\frac{1}{\eta} - 1 \right) \cdot P_{pe} \quad (5.13)$$

where η is the efficiency of the energy storage system.

Next, the equations describing the unit when it is charging are:

$$P_{pe} < 0 \quad (5.14)$$

$$P_{es} = \eta \cdot P_{pe} \quad (5.15)$$

$$P_{loss} = (\eta - 1) \cdot P_{pe} \quad (5.16)$$

Additionally, a first-order transfer function with a time constant representing the delay in the storage system is added.

To keep the correct operation of the storage unit with regards to these two charging states, a protection system is implemented in the storage model.

Energy storage protection system

The protection system for the energy storage model is a set of logic statements implemented to prevent unwanted behavior from the model. The first protection mechanism is a limiter to prevent the storage system from charging beyond the rated power limits:

```

if  $P_{pe}^* > P_{pe,rated}$  then
  |  $P_{pe}^* = P_{pe,rated}$ 
end

if  $P_{pe}^* < -P_{pe,rated}$  then
  |  $P_{pe}^* = -P_{pe,rated}$ 
end

```

The second protection mechanism is included to prevent the storage system from overcharging when it is already fully charged:

```

if  $SOC \geq 1$  and  $P_{pe}^* < 0$  then
  |  $P_{pe}^* = 0$ 
end

```

The last protection mechanism is implemented to prevent a negative state of charge:

```

if  $SOC \leq 0$  and  $P_{pe}^* > 0$  then
  |  $P_{pe}^* = 0$ 
end

```

The OpenModelica implementation of the energy storage and protection system can be found in Appendix D, and the values used in the simulation setups that are described later can be found in Appendix E.3.

5.5 HVDC cable model

As mentioned before, a good model of the HVDC cable is needed to accurately reproduce the dynamics of the HVDC system that connects the wind farms to shore.

The cable model chosen for this study is a frequency-dependent cascaded pi-model based on [91], which is a combination of parallel branches and pi-sections, as shown in Figure 5.8, due to its accuracy for a wide range of frequencies.

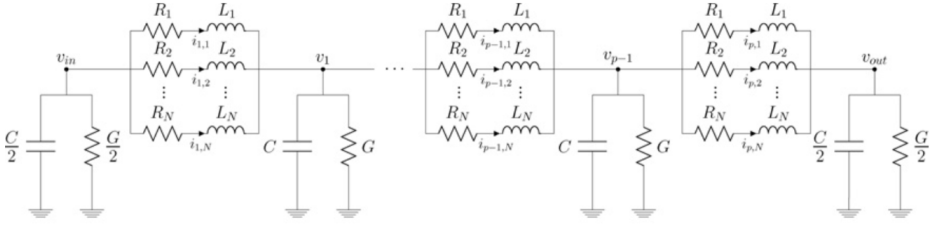


Figure 5.8: Generic representation of the frequency dependent cascaded pi-model of an HVDC cable with N parallel branches and p pi-sections from [91].

The elements of the pi-equivalent scheme are:

$$R_i = r_i \ell_\pi \quad (5.17)$$

$$L_i = l_i \ell_\pi \quad (5.18)$$

$$G = c \ell_\pi \quad (5.19)$$

$$C = g \ell_\pi \quad (5.20)$$

where $\ell_\pi = \ell/p$ is the length of a pi-section and p is the number of sections.

The model used in this study has 3 parallel branches and 5 pi-sections.

5.5.1 Frequency dependency of series impedance elements

This section is added to explain the frequency dependency of the cable by showing the frequency responses of an actual cable.

The typical frequency response of a DC cable can be seen in Figure 5.9. As the frequency increases above $f = 10^2$ Hz in Figure 5.9c and d, the magnitude and angle follow damped oscillations patterns. These oscillations are captured by splitting the series impedance elements into multiple parallel branches to include more poles in the model and replicate the magnitude and angle characteristics of Figure 5.9c and d.

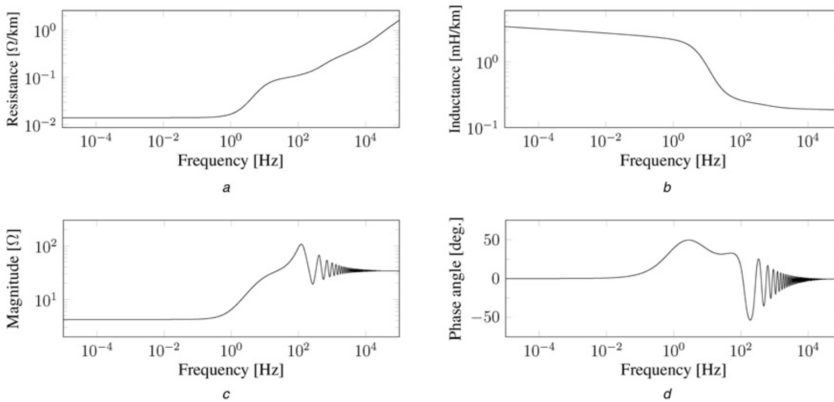


Figure 5.9: Frequency dependency of cable parameters.

To properly fit the model response to the actual response of the DC cable, a method called vector fitting, as proposed in [91], is applied to determine the value of the series impedance elements in the parallel branches. The vector fitting method is further explained in reference [92] for interested readers.

The values of the cable parameters used in this model can be found in Appendix E.1.2, and the OpenModelica implementation of the cable can be found in Appendix D.

5.6 Transformer model

The transformer in this system model represents the collector transformer in the wind farm and the step up transformer from the energy storage system, which transforms the voltages to a higher level to lower the losses in the transmission system [93].

The transformer model chosen for this study is a step-up star-star connected three-phase transformer with series impedances. The series inductances models the leakage flux in the core of the transformer and the series resistances models the conductor losses in the transformer due to the load current. These series losses include dc resistance losses, eddy current losses caused by the leakage flux and stray losses in the windings and the transformer tank [94].

By using this type of model, the parallel branch modeling the magnetization current of the transformer, core losses as eddy current losses and hysteresis losses are neglected.

These parameters are usually large parallel impedances resulting in relatively small contributions in steady state; thus they can be neglected for these kinds of network level studies.

The voltage transformation ratio, N , for this model is defined as

$$E_{HV} = N \cdot E_{LV} \quad (5.21)$$

where E_{HV} is the induced voltage on the high voltage side of the transformer and E_{LV} is the induced voltage on the low voltage side of the transformer.

The OpenModelica implementation of the transformer can be found in Appendix D. This implementation uses the built-in ideal transformers found in the OpenModelica standard library with added series impedance elements to transform the induced voltage levels.

5.7 Description of test cases and simulation setups

This section introduces the different test cases studied using the models described and the purpose of each test case. The results from the test cases are included in Chapter 6.

5.7.1 Test case 1: Three-terminal HVDC system

Test case 1 is introduced to show that the models in the HVDC system and their corresponding controllers are stable and working as expected. The simulation setup consists of three MMCs connected in a three-terminal HVDC system with HVDC cables between them, as seen in Figure 5.1 with positive power flow directions specified. The three MMCs are connected to a stiff grid on each of the AC sides. These stiff grids are three-phase voltage sources.

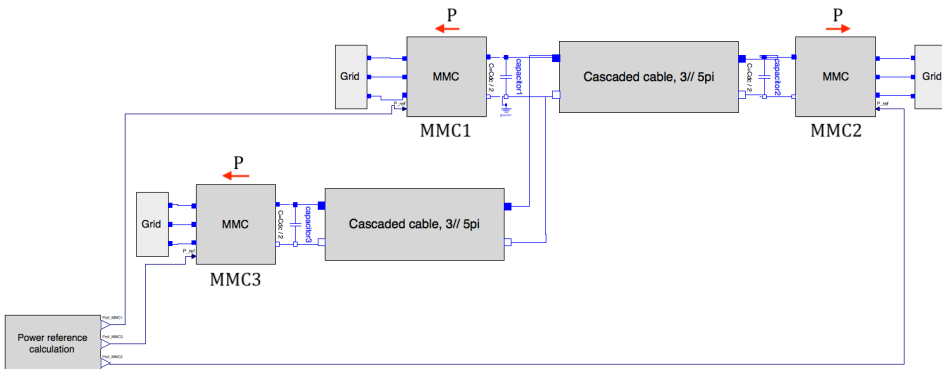


Figure 5.10: Test case 1 simulation setup in OpenModelica.

The event introduced to study the dynamics of the system is a step in the power reference for each of the three MMCs. MMC1 and MMC3, which are the offshore converters, are initially operating at 0.2 pu power each, and both have a step of 0.2 pu in their power reference at $t = 2s$. MMC2, which is the onshore converter, is initially operating at 0.4 pu power and has a step of 0.4 pu in the power reference at $t = 2s$.

As this test case focuses on the electrical HVDC system, the variables of interest are the DC voltages at each MMC terminal, the power at each MMC terminal, the zero sequence energy sum and the zero sequence circulating currents of each MMC. Additionally, the AC-currents of MMC2 are plotted to see the responses on the AC-side grid.

Because the stability of VSC based HVDC systems can be affected by the power flow direction, as studied in reference [95], a simulation where the power directions were reversed is added to see whether the system is stable with reversed power flows.

5.7.2 Test case 2: Wind farm and energy storage

Test case 2 has the purpose of testing the energy storage model and the wind turbine model combined and also provide a preliminary insight into the rating of the energy storage to be used in Test case 3.

The setup used in this test case is an example to show how the energy storage can smooth the power output from the wind farm. The setup for test case 2 can be seen in Figure 5.11, where the power output from the wind farm is filtered through a first-order filter with a large time constant. The difference between the filtered and the actual power is sent as a reference for the power from the energy storage device. The power from the energy storage is added to the filtered power from the wind farm to produce the combined power output.

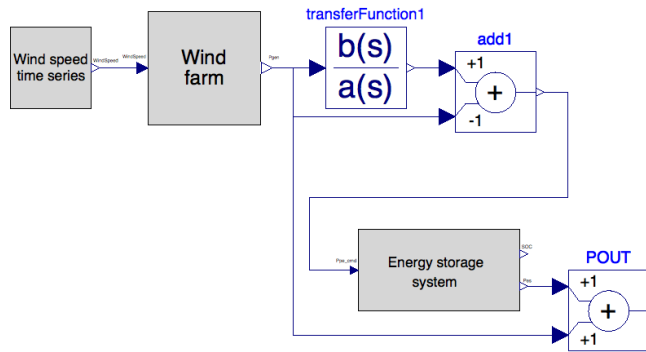


Figure 5.11: Test case 2 simulation setup in OpenModelica.

The wind farm used in this setup has the same parameters as wind farm 1 in the complete simulation system in Figure 5.1 and consists of 70 turbines with a rated power of 7 MW. The parameters correspond to wind farm 1 because wind farm 1 is the wind farm that is complemented with an energy storage system in Test case 3.

The variables of interest for this case are the power delivered and absorbed by the energy storage, the power output from the wind farm and the combined wind farm and energy storage power outputs. Additionally, the turbine speed, ω , and the turbine blade angle, β , will be studied to investigate the operation of the "aggregated wind turbine" according to the previously mentioned turbine control regions.

The energy storage state of charge (SOC) along with the energy storage power will, in this case, be used to dimension the energy storage unit.

To properly test all control regions of the wind turbine and also introduce realistically varying wind speeds, a time-series of actual measured wind speeds at Roosevelt station, as seen in Figure 5.12, was used. The data were originally provided in the course TET4175 Design and Operation of Smart Grid Power Systems at NTNU. These data were the best available data at the current time, and they provided the data needed to test the attributes of the wind farm model and the energy storage model. This way, the intermittency of the wind could be studied with the models built. However, the data were not from an offshore site, and this is further mentioned in the discussion in Chapter 7.

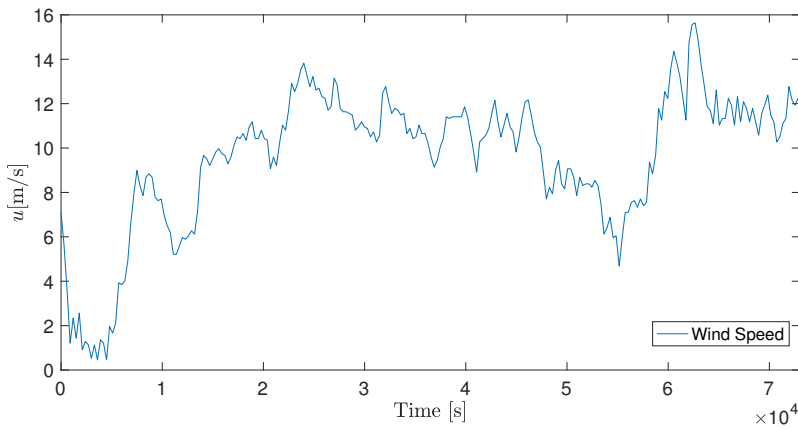


Figure 5.12: The wind speed variation used for Test case 2.

5.7.3 Test case 3: Complete system configuration

Test case 3 is introduced to study the combined short term effects of integrating two wind farms where one of them is complemented by an energy storage system, as illustrated in Figure 5.1. This test case will use the storage and filter time constant parameters that resulted from the simulations in Test case 2. Figure 5.13 shows the simulation setup used in OpenModelica to replicate the system in Figure 5.1. This configuration is slightly different from what was desired for this test case, as it does not include the transformer model or the circuit representations of the wind farm and energy storage system, and this will be further mentioned in the discussion in Chapter 7.

For this test case, two simulation cases are studied. The first simulation case is to study the dynamics when there is a sudden change in wind speed from 10m/s to 5m/s introduced at $t = 30$ seconds for wind farm 1 and $t = 60$ seconds for wind farm 2, as can be seen in Figure 5.14. This way, the effects on the HVDC system when having a wind farm with an energy storage system can be directly compared to a case without an energy storage system.

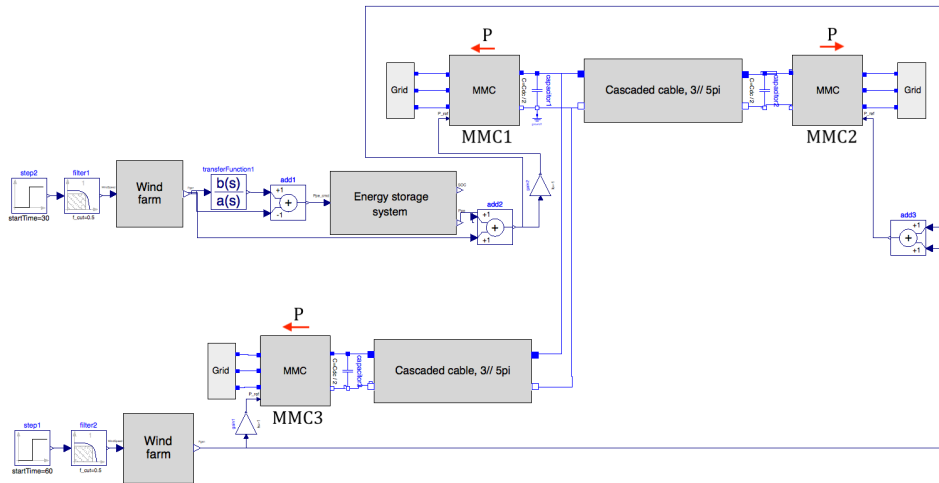


Figure 5.13: Test case 3 simulation setup in OpenModelica.

The wind speed signals in Figure 5.14 are steps filtered through a first order filter with time constant $T = 0.5s$ because the turbine model did not allow steps in the wind speed.

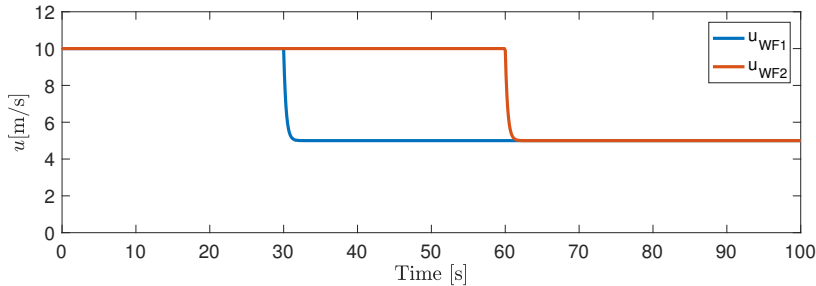


Figure 5.14: The wind speed signals used to simulate a sudden drop in wind speeds for Test case 3.

The second simulation case is to introduce a sudden loss of the two wind farms at $t = 30s$ and $t = 60s$, replicating, for example, a fault at the low voltage side of the collection transformers of each wind farm. This way, the dynamics of the system can be studied for large changes in power that occur when a wind farm is suddenly disconnected. A trigger mechanism to instantly set the power from the wind farms to zero was implemented in the OpenModelica simulation setup.

The variables of interest are related to the HVDC system, including MMC powers, DC voltages, and zero sequence energy sum of the MMCs to study how the energy storage affects the operation of the MMCs in the HVDC system. Additionally, the state of charge of the battery will be included to study the contribution of the energy storage at these events.

Results

6.1 Test case 1: Three-terminal HVDC system

This section includes the results from Test case 1. The simulations were executed with the default solver, Dassl, and a time step: $\Delta t = 100\mu s$ over the duration of 4 seconds. Table 6.1 shows the main parameters for Test case 1 for convenience.

Table 6.1: Main parameters of Test case 1

Parameter	Value
Rated power of MMCs	1059 MVA
Rated voltage of MMCs	333 kV
Base DC voltage	640 kV
Base internal stored energy	10.24 MJ
Length of HVDC cables	100 km

Figure 6.1 shows the response of the powers from the three MMCs in the simulation setup of Test case 1 when doing step changes in their power references. The power from MMC2 is double that of the power from MMC1 and MMC3, as it transfers the power from MMC1 and MMC3 combined to the onshore grid, hence the opposite sign. As can be seen, the power for each MMC reaches the reference value around 1 second after the step is introduced. The settling time of the powers can be shortened by tuning of the controllers. Some attempts of making the converters faster were made. However, when making the power controllers faster, oscillations started to appear in the DC-voltage responses. To avoid the worst oscillations, the final tuning of the controllers led to the responses showed here.

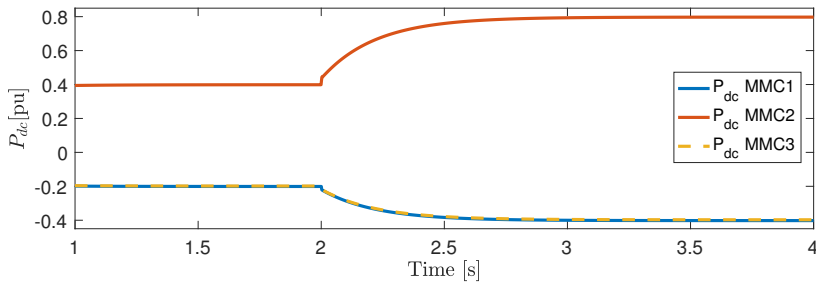


Figure 6.1: The powers of all three MMCs when stepping the total power 0.4 pu.

Figure 6.2 shows the response of the DC voltages at each MMC terminal when doing a step of the power references. The DC voltage reference for each MMC terminal is set constant at 1 pu. The voltages reach steady state value around 0.1 seconds after the step is introduced without any large oscillations. The voltages are at slightly different levels because of the voltage drops in the cable impedances between them. As can be seen from the plot, MMC2 is the converter with the lowest DC voltage. This makes sense because the power flows from high to low DC voltage levels, meaning the power flows *to* MMC2.

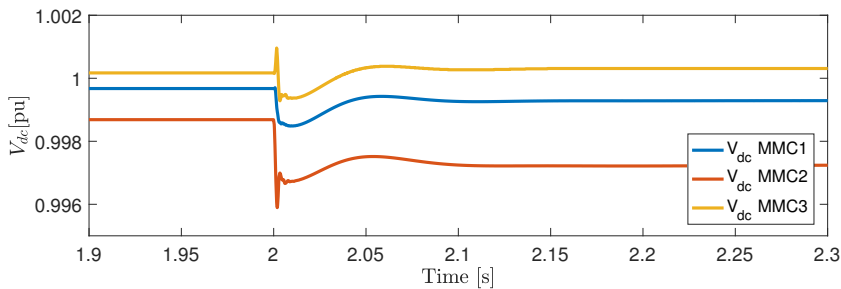


Figure 6.2: The response of the DC voltages when stepping the total power of 0.4 pu.

Figure 6.3 shows the response of the dq-currents after the step in power. The reference for the d-currents are calculated from the active power controllers, hence they follow the same response. The d-currents seem to follow the reference from the active power controller accurately. The inner dq-current controllers are tuned much faster than the active power controller so that they can follow the reference provided by the slower power controller. The reference for the q-current is set to zero for simplicity, and from Figure 6.3, it can be seen that the q-current for all MMCs are constant at zero. This effectively means that reactive power is controlled independently from the active power and that it is zero.

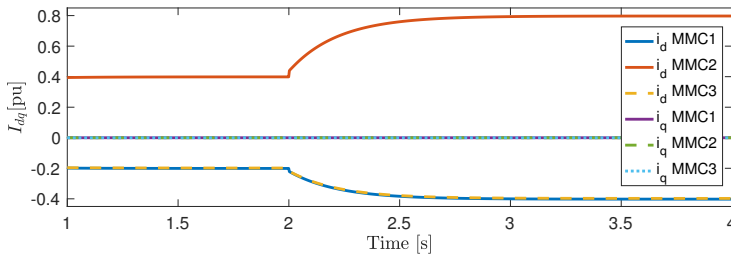


Figure 6.3: Response of the dq-currents when stepping the total power 0.4 pu.

Figure 6.4 shows the response of the circulating currents of each MMC after the step in power. The circulating currents reach a stable steady state value around 1 second after the step. As the circulating currents are closely related to the DC power, they also follow the same response as the active power.

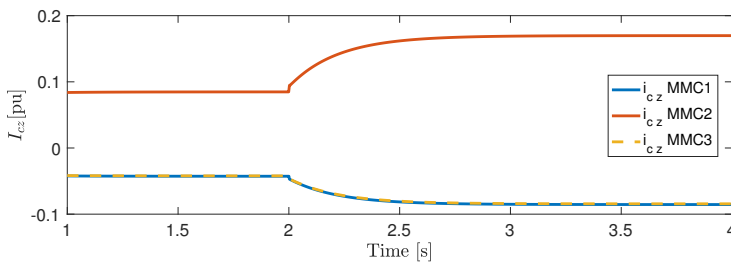


Figure 6.4: The response of the circulating currents when stepping the total power 0.4 pu.

Figure 6.5 shows the response of the zero sequence energy sum of each MMC after the power step. The reference for the energy for each MMC is set to a constant of 1 pu. The energy of MMC1 and MMC3 is slightly reduced right after the step, but reach a steady state value at the reference around 1.5 seconds after the step. The energy of MMC2 is increased right after the step but reaches a steady state value at the reference as the same time as the other MMCs.

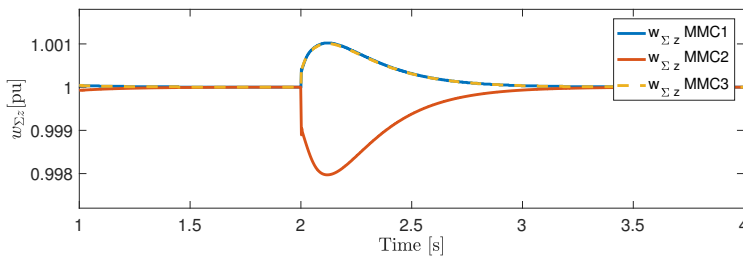


Figure 6.5: The response of the internal stored energy when stepping the total power 0.4 pu.

Lastly, Figure 6.6 shows how the three-phase AC currents of MMC2 are increased when the power of the MMC is increased. The magnitude of the currents are doubled as the power transmitted is also doubled.

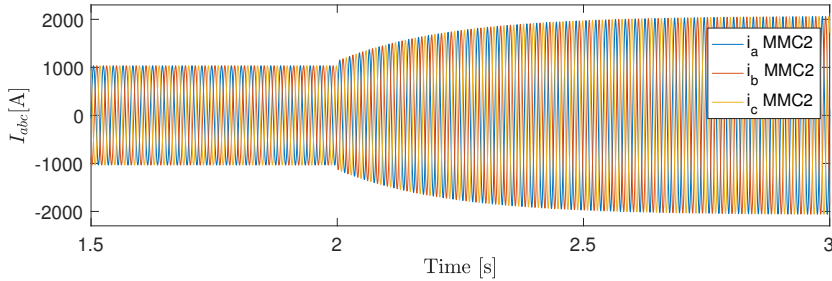


Figure 6.6: The response of the abc-currents when stepping the total power 0.4 pu.

Overall, the three-terminal HVDC system has a fast and stable response to sudden changes in power with the tuning parameters found in Appendix E.1.1.

6.1.1 Results with reversed power flows

As can be seen in Figure 6.7, the model is still stable when reversing all power flows and keeping the same step (with opposite sign) as in the previous simulation. All powers follow their references similarly to the previous simulations.

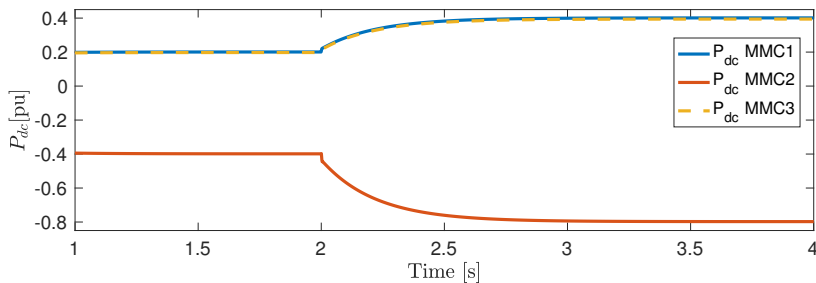


Figure 6.7: The step response of the MMC powers when all power references are reversed.

Figure 6.8 shows the response of the DC voltages when reversing the power flows. The response is quite similar to the previous simulation. However, the magnitude of the voltages is changed due to the reversed power flow. MMC3, which had the highest DC voltage previously, now has the lowest DC voltage. MMC2 now has the highest DC voltage, which makes sense since the power is flowing *from* MMC2 to the HVDC system.

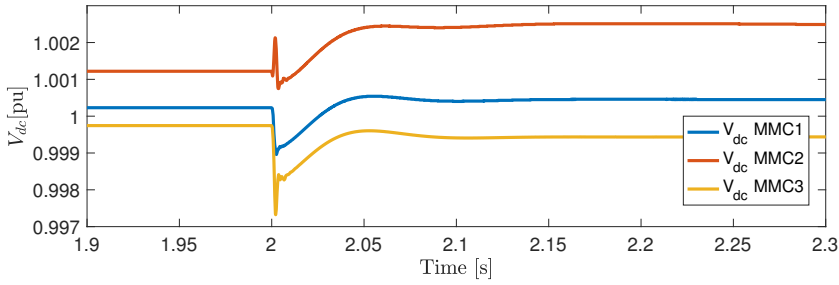


Figure 6.8: The step response of the DC voltages when the power flows are reversed.

These simulations show that the system is still stable when reversing the power flows, which is expected by MMC based HVDC systems to increase the flexibility, as discussed in Chapter 2. However, this power flow scenario is not realistic with the described system, as it means the wind farms would absorb power. Despite of this, the results show that the models and control technique can be used for future expansions where reversed power flows can be considered, or if large offshore loads are considered with the described system.

6.2 Test case 2: Wind farm and storage

This section includes the results for Test case 2. The simulations for Test case 2 were executed with the default solver, Dassl, and a time step of $\Delta t = 0.5s$ over the duration of 73000 seconds (approximately 20 hours), which corresponds to the length of the wind speed data set. The main parameters for Test case 2 are shown in Table 6.2

Table 6.2: Main parameters of Test case 2

Parameter	Value
Rated power of wind turbines	7 MW
Number of turbines, $N_{turbines}$	70
Rated power of wind farm	490 MW

After simulating the test case 2 setup with different values for the filter constant and the rated power of the energy storage, the final value of $T = 1000s$ for the filter constant and $P_{es,rated} = 250MW$ for the energy storage were obtained. For further explanation of the dimensioning process of the energy storage rated power and the filter time constant, additional results where both parameters are tweaked can be found in Appendix F.1. An example where the storage rated power is set to match the rated power of the wind farm is also included in Appendix F.1, and those results are further discussed in Chapter 7. However, the following results were obtained using $T = 1000s$ for the filter constant and $P_{es,rated} = 250MW$ for the energy storage.

Figure 6.9 shows the power from the wind farm, the power from the energy storage and the combined power from both the wind farm and the energy storage. The blue plot,

which is the combined power, is a much smoother power output than what would have been from the wind farm alone. It can, therefore, be seen how the energy storage can absorb and deliver the difference from the filtered wind farm power to remove the most rapid variations in the power from the wind farm. From Figure 6.9, it can also be seen that the energy storage never exceeds its limits of $\pm 250MW$.

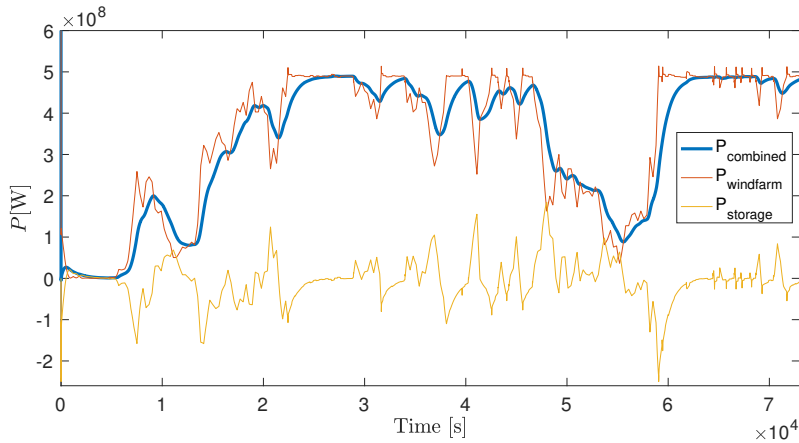


Figure 6.9: Power from wind turbine, energy storage and combined power in the Test case 2 setup.

Figure 6.10 shows the energy storage state of charge (SOC). The predefined upper limit for the SOC was 0.9, and the lower limit was 0.2. It can be seen that the SOC stays within these limits during the entire simulation. If the energy storage were to hit any of these limits during the simulation it could be an indication that the storage was not properly dimensioned for the task. This way, the SOC worked as an indicator when dimensioning the energy storage for the task of smoothing the wind farm power, which also led to a rated charge/discharge time of 1h.

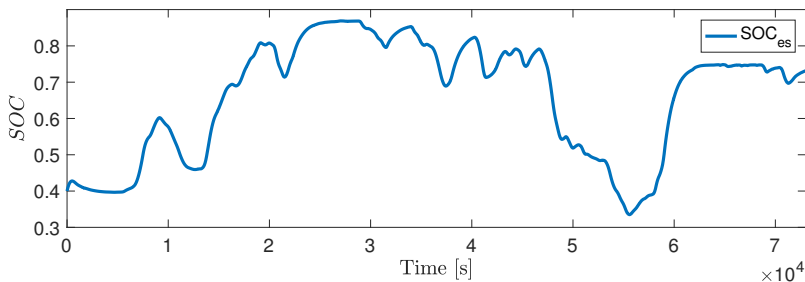


Figure 6.10: The state of charge (SOC) of the energy storage in Test case 2.

Figure 6.11 shows how the rotational speed, ω , and the blade angle, β of the turbine are varying during the simulation. The behavior of these two variables reflects the different control regions very well. When the wind speeds are according to region II, variable speed

control is applied. This can be seen in the areas where the rotational speed of the turbine is varying, and the blade angle is zero. Also, region III defines constant speed operation with variable pitch to limit the output power. When the rotational speed is capping in Figure 6.11 at around 1.4 rad/s, the blade angle starts to vary according to the pitch controller. This means that the turbine is operating in region III with variable pitch.

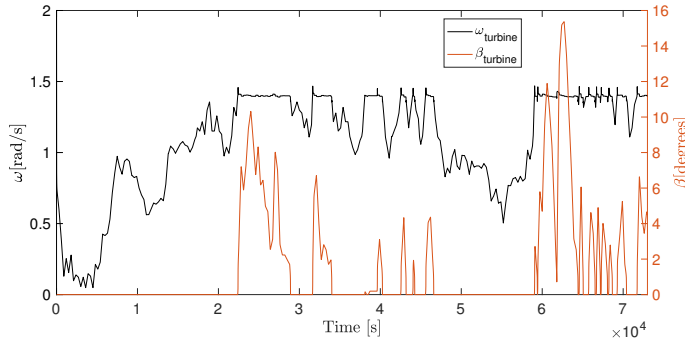


Figure 6.11: Variation of the rotational speed, ω , and blade angle, β of the turbine in Test case 2.

With these results, the correct operation of the wind turbine and energy storage models are verified. Additionally, the energy storage is dimensioned for the task of smoothing the variations in power output from the wind farm in the range of minutes to hours.

6.3 Test case 3: Complete system configuration

This section shows the results for Test case 3, where two simulation cases are considered. The first being a sudden drop in wind speeds and the last is a simulation case considering a sudden loss of wind farms.

The simulations were performed with a time step of $\Delta t = 100\mu s$ with the Dassl solver over a duration of 100 seconds. Table 6.3 includes the main parameters of Test case 3.

Table 6.3: Main parameters of Test case 3

Parameter	Value
Rated power of MMCs	1059 MVA
Length of HVDC cables	100 km
Rated power of wind turbines	7 MW
Number of turbines at WF1	70
Number of turbines at WF2	60
Rated power of WF1	490 MW
Rated power of WF2	420 MW
Rated power ESS	250 MW
Rated charge/discharge time of ESS	1 hour
Filter time constant	1000 s

6.3.1 Sudden drop in wind speeds

Figure 6.12 shows the response of the power outputs from the wind farms and energy storage at the sudden drop in wind speeds. The initial increase in the power output from the wind farms when the wind speed is suddenly dropped from 10m/s to 5m/s can be explained by looking at the inertia of the turbines. When the wind speed drops, the rotational speed of the turbines has to drop accordingly to maintain an optimal tip speed ratio as explained earlier for region II operation. This deceleration of the turbines releases the additional kinetic energy stored in the inertia of the turbine blades and machines in the wind farm, hence the initial increase in power output. It can also be seen how the energy storage has a very fast response and caps at its rated value.

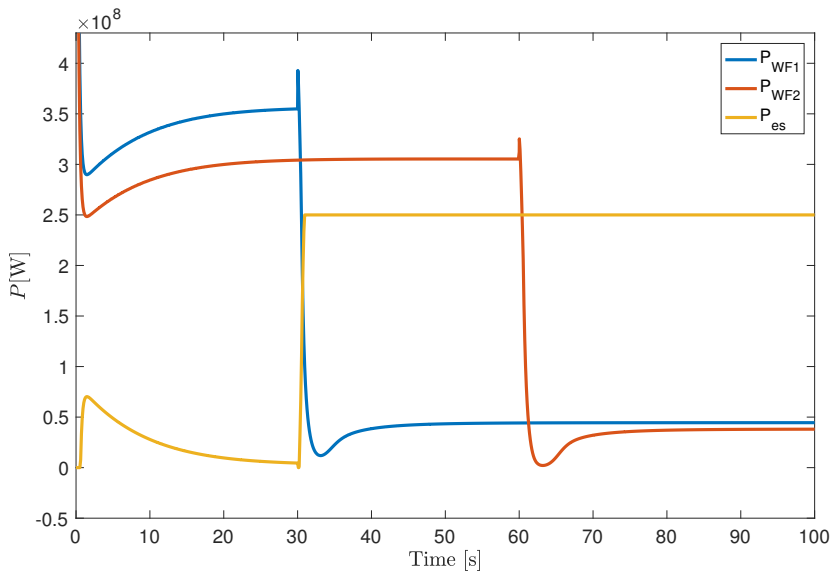


Figure 6.12: The response of the wind farm powers and energy storage powers when a sudden drop in wind speed is introduced.

Figure 6.13 shows how the powers from the MMCs respond to these events. It can be seen that the power of the MMC1, which has both a wind farm and a storage unit connected, has a much lower drop at $t = 30$ s than what MMC3, which only has a wind farm connected, has at $t = 60$ s. This is because the energy storage unit is producing the extra power up to its rated value from the event.

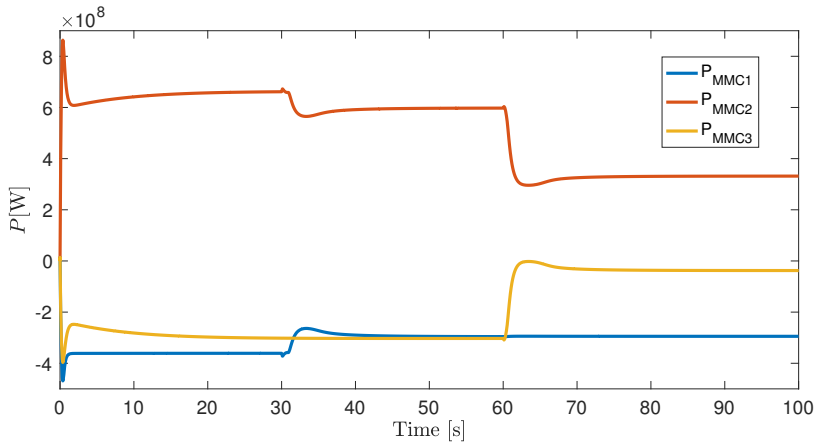


Figure 6.13: Response of the MMC powers for test case 3 when a sudden drop in wind speeds is introduced.

Figure 6.14 shows how the power profiles in Figure 6.13 translates to the DC voltages. The event at WF1 that has an energy storage unit connected has a smoother DC voltage response than that of the event where the other wind farm is affected. By having an energy storage unit connected at the wind farm, the DC voltage levels do not need to be adjusted as for the case without an energy storage device.

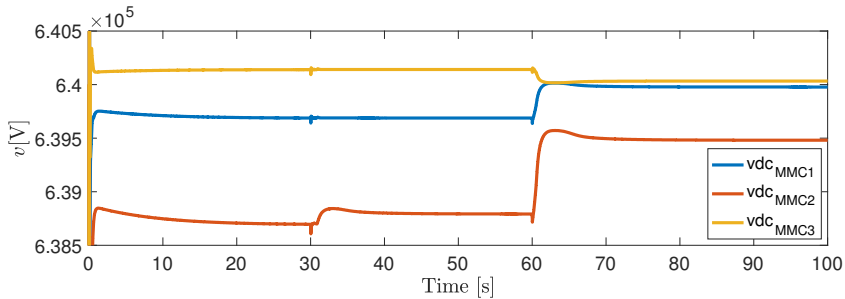


Figure 6.14: The response of the DC voltages for Test case 3 when a sudden drop in wind speeds is introduced.

Figure 6.15 shows the response of the internal zero sequence energy sum of the MMCs when the wind speeds are suddenly decreased. From the plot, one can see that the response at the change of wind speed at wind farm 1 has smaller transients than when the wind speed changes at wind farm 2. It can also be seen that the energy MMC1 is not affected by the change at MMC3 and vice versa.

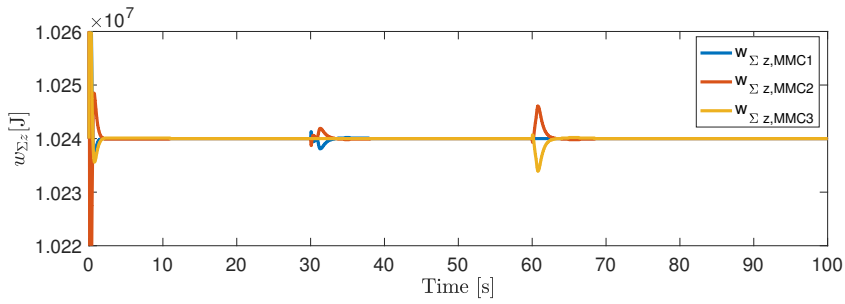


Figure 6.15: The response of the zero sequence energy of the MMCs at a sudden drop in wind speeds.

Lastly, Figure 6.16 shows how the SOC changes during this simulation. The change in SOC during the simulation is relatively small, which reflects that the storage can provide the rated power for a while in order for the wind speeds to increase. With at rated charge/discharge time of 1 hour, the energy storage system can deliver rated power for an hour if it is fully charged. However, with the limits of maximum SOC of 0.9 and minimum SOC of 0.2, the actual time the storage can provide rated power is somewhat shorter than 1 hour.

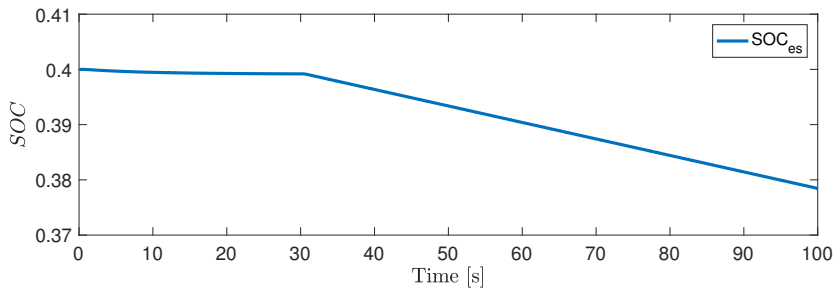


Figure 6.16: The response of the SOC when a sudden change drop in wind speeds is introduced

6.3.2 Sudden loss of wind farms

Figure 6.17 shows the response of the MMC powers when the two wind farms, WF1 and WF2, are lost at $t = 30s$ and $t = 60s$ respectively. One can see that the power from MMC1 is kept at the rated value of the energy storage device, and also that the dynamics of the turbine inertia is removed because the wind farm is disconnected.

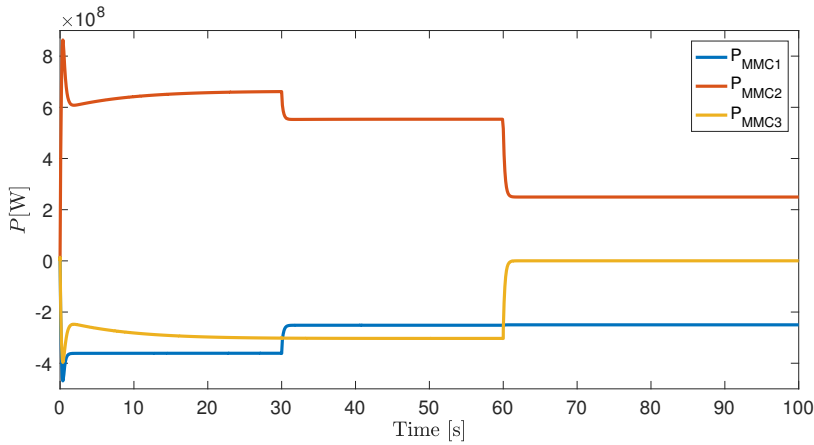


Figure 6.17: The response of the MMC powers at a sudden loss of wind farms.

Figure 6.18 shows the response of the DC voltages when the two wind farms are disconnected. The responses are faster than in the previous simulation because the delay caused by the inertia in the turbines is removed. Additionally, the responses have higher transients due to the faster change in power. It can be seen that the responses of both cases have around the same magnitude of transients, but the steady state of the voltages remain almost the same after the event at wind farm 1 with the energy storage. Even if the energy storage system is very fast, it is not fast enough to dampen the transients of the DC voltages in this case. It can also be seen how the voltages of MMC1 and MMC2 become equal after wind farm 2 is disconnected. This is because when the power from wind farm 2 is disconnected, there is no DC current flowing in the cable between the two MMCs causing any voltage drop between them.

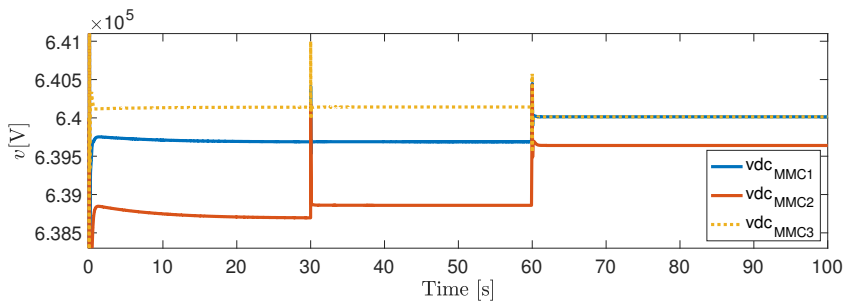


Figure 6.18: The response of the DC voltages at a sudden loss of wind farms.

Figure 6.19 shows how the response of the zero sequence energy sum in the MMCs also for this simulation is improved by including an energy storage unit. The transients at $t = 60$ s for loss of wind farm 2 are still larger than the transients at $t = 30$ s for loss of wind farm 1 due to the contribution of the energy storage system.

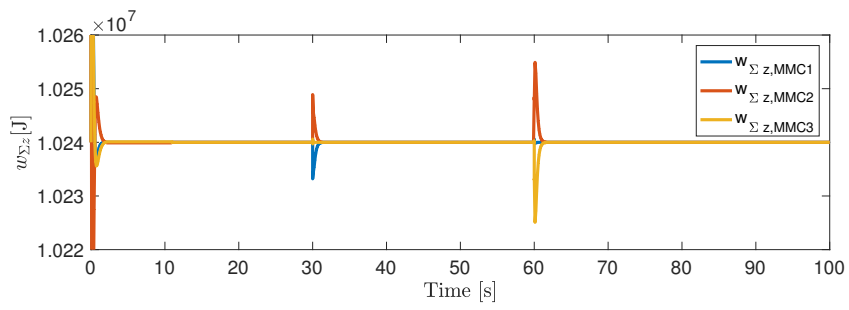


Figure 6.19: The response of the zero sequence energy of the MMCs at a sudden loss of wind farms.

Discussion

This chapter includes the discussion part of this Thesis. The main subjects of discussion will be related to the offshore energy storage system and the simulation results, the simulation setup used for test case 3, the HVDC model developed for ePHASORSIM and some additional experiences of using the OpenModelica software. Lastly, some experiences of sharing the topic with another student will be added and a discussion of whether the objectives of the Thesis were reached or not.

7.1 Test case 3 simulation setup

One of the main objectives for this Thesis was to develop a package with models of components in an HVDC grid. Models for all the described components were successfully implemented in OpenModelica. However, the final simulation setup for Test case 3 was slightly different from the desired setup. This section will discuss the Test case 3 simulation setup.

The goal when building the models in Chapter 5 was to use the wind farm and energy storage coupled with electrical components through DC current sources as showed in Appendix D.6.5 for the case with the wind farm. Using a DC current source is a normal way to model wind farms in such studies, as also done in, for example, reference [65]. This would allow using the electrical transformer model, which was described in Chapter 5, in the final Test case 3 simulation setup. However, this would require coupling of two MMCs front to front (AC-side to AC-side), which proved to be a challenge.

In order to connect the MMCs front to front, the MMC model and its control needed to be changed from the original model. The original model uses variable voltage sources on the AC-side that controls the voltage relative to the grid side voltages in order to obtain the desired currents. When connecting the MMCs front to front, the grid side voltages is replaced by the variable voltage sources of the other MMC. To make this configuration work, one of the MMCs must be controlled as a stiff voltage source on the AC-side. Due to lack of time, this configuration was not successfully implemented, and a simplified system was used instead. Some other workarounds were also tried without any success.

The simplified system using ideal grids connected to the MMCs and then using the power references to create the power from the wind farms and storage was ultimately used. By using this arrangement, the ideal grids can, in theory, deliver more power than what is available. However, since the controllers are tuned to follow the power references, this may be a valid simplification to some degree. This setup still allowed to study the dynamics of the HVDC system, which was the dynamics of interest for Test case 3. The main challenge for this setup would be the second part of test case 3, where the wind farms are suddenly lost, and the power is immediately set to zero. Because there is an additional delay in the MMC from the reference to the actual power is reached, the results provided for this part may not be the most accurate.

The transformer model is still included, as it is part of the package uploaded to GitHub for anyone to try.

7.2 The offshore energy storage system

This section provides discussions related to the energy storage system used in Test cases 2 and 3 and its attributes. The part related to the energy storage system was important to the objective of studying the interactions in a HVDC system in this Thesis. This allowed demonstrating the use of OpenModelica and also generating results for the paper accepted for presentation at the Offshore Energy and Storage 2019 conference.

7.2.1 Effects of adding the energy storage to wind farm 1

By using the selected rated power of around half that of the rated power from the wind farm, the energy storage system can not replace the power production from the entire wind farm, but only half the power at most. This introduces some interesting dynamics which were investigated in Test case 3. From the results from Test case 3, one can see that even though the energy storage cannot replace the wind farms power production at the events described, the operation of the HVDC converters are improved. This is especially apparent when studying the DC voltage responses and the internal zero sequence energy stored in the MMC. The responses after the two events at wind farm 1, where the energy storage system is connected are improved compared to the responses after the events at wind farm 2 with no energy storage connected. The energy storage unit makes the power from MMC1 more constant, which improves the DC voltage responses of all MMCs at both events. Also, the transients have smaller magnitudes for both the DC voltages and zero sequence energy sum of the MMCs when events occur at wind farm 1, due to the energy storage.

However, for the fastest changes, i.e. when a wind farm is suddenly lost, the transient in the DC-voltages are too fast for the energy storage system to reduce them due to the delay associated with the energy storage system. However, the energy storage system still improves the transients in the zero sequence energy sum of the MMCs, which are still lowered for also the case when wind farms are lost.

Response time

These results are probably influenced by the response time of the energy storage. In this Thesis, the storage was chosen to be very fast, with an almost immediate response in power with a time constant of $T = 10\text{ms}$ for the delay. This response time will be dependent on the energy storage technology used. For example, energy storage systems that are designed with large moving mechanical parts would not have the same fast response as the energy storage used in this study. On the other hand, electromchemical energy storage systems such as lead-acid or lithium-ion are capable of a near immediate response to changes in their power reference, and they usually have a response time in order of milliseconds [96, 97].

7.2.2 Dimensioning of the energy storage

This discussion part relates to the dimensioning of the filter and the corresponding rated power of the energy storage in Test case 2. For this Thesis, the energy storage rated time was set to be 1h, and it was not changed in any scenarios. As can be seen from the additional Test case 2 results in Appendix F.1, the balance between the filter time constant and the rated power of the energy storage is important to have a good operation and proper utilization of the battery. It was showed that a too high filter time constant could lead to worsened results as it demanded more of the energy storage, forcing it to reach its limits in SOC. A smaller time constant led to reduced utilization of the available power from the energy storage. Therefore, the rated power of the energy storage and the filter time constant had to be dimensioned according to each other.

The rated power of the energy storage unit was set to be around half of the rated power from wind farm 1 in this Thesis to investigate the effects of a storage unit with lower rated power than the wind farm. To have an energy storage system with lower rated power, in reality, would also reduce the costs of the energy storage system, so, therefore, it was considered interesting to investigate the effects of a lower rating. However, the effects of increasing the rated power of the energy storage to the rated power of the wind farm and filter time constant accordingly were also studied in the additional results in Appendix F.1. For this scenario, the effects of doubling the rated power of the storage was not considered satisfactory enough to further study the system with those values.

It should also be mentioned that the dimensioning of the energy storage according to Appendix F.1 may be very simple compared to the reality when building real wind farms with real energy storage systems. Such studies usually are much more extensive than what is performed in this Thesis. However, the dimensioning approach showed in this Thesis is also an example of what dynamic models can be used for, giving an indicator on how the system will perform in real life based on real data with a set of given parameters. Additionally, to increase the precision of the dimensioning, wind data from the actual offshore site where the wind farm is located should be used. However, the onshore wind speed data that was used still reflected every aspect needed to test the models and give an indication of the effects of the parameters to be dimensioned.

7.2.3 Offshore versus onshore placement of the energy storage

In the simulation system used in this Thesis, the energy storage system was placed offshore near one of the two wind farms to study the effects on the three terminal HVDC system. The improved operation of the HVDC system itself can, in this case, work as an argument for having the energy storage offshore.

Additionally, to make use of the increased flexibility of HVDC grids, one can argue that it may be beneficial to have the energy storage offshore. This would allow the same constant power will be delivered independently of the power flow path to the shore. This makes it able to move the combined power of the wind farm and storage system to any point in the system in case a connection to shore is lost. This can be further illustrated by using an example where multiple countries are connected by the same HVDC grid. By using an offshore energy storage system, the same power can be delivered to country x , as to country y without installing separate energy storage systems on the shore of both countries. The latter would require additional investments, making the overall system more expensive. On the other hand, by having the energy storage onshore, the energy storage can deliver power even if the HVDC connection to that point is out of operation.

Based on these reflections, it is apparent that the question of placing the storage offshore or onshore should be studied in detail separately, as placing the energy storage system offshore also will lead to maintenance challenges and introduce additional losses in the system. Also, the offshore placement can lead to space challenges if the energy storage systems are not hosted inside the turbines.

7.2.4 On solving the challenge of intermittency

In this Thesis, a configuration where a filtered power output from the wind farm was combined with the energy storage to cover the differences in power was used. This configuration was chosen to study one way in which energy storage can complement the power production from a wind farm with a particular focus on the short term dynamics. However, this configuration does not nearly solve the challenge of the intermittency in the wind, as mentioned in the introduction.

For an energy storage unit to fully complement the power production from a wind farm alone, making the combined output power nearly constant at all times, an energy storage system of much larger proportions must be used. That storage unit probably needs to be rated around the rated power of the wind farm in addition to having a very large capacity of stored energy. In this study, a rated charge/discharge time of 1 hour was used for the wind farm, meaning the storage unit can deliver rated power for an hour from it is fully charged at 1 SOC until it is fully discharged at 0 SOC. From the results in Test case 2, it can be seen that this amount of energy is no way near the capacity needed if the output power should remain constant at all times to solve the challenge of the intermittency. A more feasible solution could, for example, be to study the combined synergies between wind power and solar power or other renewables, instead of using extremely large energy storage systems.

However, the configuration used in this Thesis makes the output power *more* constant than the case without energy storage, at least in the hourly time frame. A more constant power output to shore would also benefit TSOs operating the onshore grid, as the effects

of changes in wind speed offshore are delayed by around 1 hour until the full effect takes place onshore. This would make it easier for TSOs to plan and schedule power production for the security of supply when the wind suddenly drops or increases.

7.3 Tuning of controllers

As mentioned in the Limitations of Scope, the topic of stability margins and optimal controller tuning was not considered in this Thesis. The controllers were tuned in such a way that they produced accurate and satisfactory responses. Therefore, there may be a possibility that the dynamics of the system can be slightly improved by simply improving the tuning of the controllers.

7.4 The HVDC real-time simulation OpenModelica model

This section relates to some interesting observations relating to the HVDC model developed for the real-time-simulator, which can be found in Appendix C.3. This is related to the objective of investigating how to use OpenModelica models in HIL simulations.

As mentioned, the model worked in OpenModelica using a time step of $\Delta t = 100\mu s$ with both the Dassel and the Rungekutta solvers. However, when testing it in Simulink after the FMU was exported, but before compiling the model for the real-time simulator, the model worked only for time steps of $\Delta t = 25\mu s$ or smaller regardless of solvers. It is interesting to note that the model worked at $\Delta t = 100\mu s$ with the Rungekutta solver but not in Simulink using the solver with the same name. To correctly answer why, a deeper knowledge of the solvers is needed, and the topic could be revisited in future work.

One hypothesis was that the model could contain dynamics that were simply too fast for the solver to compute. As a solution, all controllers were tuned slower without any effect; the model still did not work at larger time steps than $\Delta t = 25\mu s$. An additional solution to investigate this hypothesis could be to increase some of the parameters to make the model slower that way. However, the VSC model contained faster dynamics than what was found in the HVDC model. Since the VSC model worked at $\Delta t = 100\mu s$, the fast dynamics may be unlikely to cause the problem.

For the model to be properly tested with HIL simulations with hardware added, the model should be run at $\Delta t = 100\mu s$, as some of the processors in the hardware used for these kinds of simulations has a frequency that corresponds to $\Delta t = 100\mu s$. This is a topic that could be further addressed using the already developed model, or by attempting to make an HVDC model from scratch. The reason why exactly this model was used is that it was already built as a preparation for the Test case 1 setup, and the only real tweak to the model was to add the Power Pin to 3ph Grid interface as described in Appendix C.1. Additional efforts in making other implementations of the HVDC model was also made without any results.

7.5 Using the OpenModelica software

The work done in this Thesis and the corresponding specialization project [14] included one of the first attempts of using the OpenModelica software for such applications at NTNU. Therefore, it was considered part of the task to keep a pedagogic approach to this experience. A specific part of the task was to "advise" future students to ease their approach to OpenModelica with some time-saving findings. Therefore, some additional experiences and findings will be added in this discussion.

A thorough description of the experience of using OpenModelica compared to Simulink was included in the Specialization Project [14], and will not be repeated here. The experience of using OpenModelica has not changed drastically since then, and the software is still straightforward to use for the most part. However, some new experiences will be added here. These specific points relate to OpenModelica version 1.12.0 for Mac.

When starting using OpenModelica, most error messages were easy to understand, but some of the error messages were a bit harder to understand than others. However, after some experience of using OpenModelica, one can get used to some of the unclear error messages. Three of the most common unclear error messages that were encountered while using OpenModelica for the work in this Thesis will be explained here.

The first error message is "*Error: Model error. $0^{(-2)}$ is not defined*". This error message usually has to do with the initialization of the model. Usually, a variable or a parameter is initialized to zero when it is not supposed to. A good tip is to check whether all parameters are entered correctly in each class.

The second error message is "*The given system is mixed-determined. [index > 3] Please checkout the option +maxMixedDeterminedIndex*". Usually, this error message is also related to the initialization of the model, but this time when a variable is initialized to different values at different places in the model. For improved feedback, this error message should contain a hint to check the initialization of the model, as also expressed in a discussion forum at OpenModelica's website (follow reference [98] for link).

The third and last common error message is "*Error: Initialization problem is structurally singular, error found sorting equations*". When working with electrical components in OpenModelica, this problem usually appears when there is a problem with grounding. Either there is a ground element too much in the system, or the system is a ground short. This relates to both DC-side and AC-side when building HVDC models. For example, the error message was prompted when not using a ground element on the DC side of the HVDC models.

The solution to understanding these error messages was simply to google the error message, and usually a forum where a question regarding the error message could be found. These forums are used to add direct feedback for changes in the source code of OpenModelica, and this shows the strength of the open-source effort.

7.5.1 Developing real-time simulation models

This part of the discussion is related to the work in OpenModelica to develop models for the real-time simulator ePHASORSIM. This aspect reflects one of the objectives of this Thesis, which was to investigate how OpenModelica models could be exported and used

in other software, more specifically for HIL simulations.

As mentioned, Opal-RT provides libraries that can be expanded with user-defined models, as showed in Chapter 4. These libraries, the GenUnit library, and the Opal-RT Developer library, already contain a large number of models. A consequence of this is that the graphical model building approach becomes very slow, as OpenModelica has to save the whole library whenever a change occurs in one of the models. The software freezes whenever making a change to the graphical implementation of the model, like dragging and dropping a component from the standard library. At worst, the user had to wait almost a minute after dragging and dropping a component until the model could be further changed. It should be mentioned that the GenUnit library is slower to work in than the Developer library, but the Developer library tends also to freeze the software for several seconds.

A recommended workaround for this would be to develop and test the model outside the Developer library and then copy it into the Developer library once it is ready for FMU compilation.

7.6 Separating the area of focus in two Theses

As mentioned in Chapter 3, the MMC has the ability to store and release energy internally, basically working as a battery when needed. This aspect of the MMC was not further investigated in this Thesis as that topic is the main focus of the Thesis of Erling Vatn Tranulis [15]. The findings from the work in this Thesis were combined with the findings from Tranulis' Thesis to form the paper submitted for and presented at the Offshore Energy and Storage 2019 Conference in Brest, France [16].

The experience of separating the area of focus in two Thesis's around the same underlying topic (modeling of storage in HVDC grids using the OpenModelica software), was found to be very beneficial when working in an unfamiliar modeling environment as OpenModelica. During the work, the experience of having someone else working with the same software was very positive. Probably, this let to an even better understanding of both the underlying topic and models as well as the software than what would have been the case without being two students cooperating to some degree. As a recommendation to later years, if students are to write two separate Thesis's on the same topic, a clear separation in the of the area of focus between the two should be in place as early in the process as possible.

7.7 Achieving the objectives

The first objective of this Thesis was to give insight into HVDC systems and an introduction to the MMC. This objective was considered successfully achieved through a literature review.

The second group of objectives were related to the OpenModelica software. OpenModelica was successfully compared to Simulink for fast dynamics in order of several kHz. However, the model used was simple, and it was chosen to test the fast dynamics efficiently as it involved multiple simulations with many different solvers. It should be mentioned that an attempt of using a full bridge of switches and a constant DC-voltage on

the DC-side in OpenModelica was made. This exact configuration successfully simulated in Simulink, but the model was singular in OpenModelica. When placing a ground on the DC-side, the model was not singular, but the results had a significant DC-component in the resulting AC-currents due to the grounding. After using a lot of effort troubleshooting this model, a solution was not found. This led to the simplified model ultimately used. However, the results generated by the model at least allowed to compare Simulink and OpenModelica for the fast dynamics, which was the objective in the first place.

Secondly, the aspect of exporting FMUs from OpenModelica models to couple models with other software was investigated. The ultimate goal was to perform HIL-simulations, but due to the lack of time, this was not done. However, all the steps necessary to build and export the models were covered, and the last step to perform HIL simulations is more related to using ePHASORSIM and RT-LAB than to use OpenModelica. Therefore, also this objective was considered successfully achieved.

The last group of objectives was to study the interactions in the described three-terminal HVDC grid using a package of components developed for such use. Models were successfully implemented and tested both isolated and in the final system. As explained earlier in the discussion, the goal of connecting the wind farm and energy storage system electrically to the model was not reached. However, a workaround to make the models represent the final simulation system goal was made. Some interesting results describing the contribution of the energy storage system in the HVDC system were generated. Therefore, the overall objective was considered successfully achieved although one intermediate objective in the Test case 3 simulation setup was not achieved.

Conclusion

This Thesis started by introducing a three-terminal HVDC system with integration of two wind farms and an offshore energy storage system. One goal of the Thesis was to model this system in the open-source software OpenModelica and study the interactions between wind farms, energy storage and the three terminal HVDC system. The following chapters aimed to give all necessary information needed on HVDC systems, the modular multi-level converter, and OpenModelica to understand the background and purpose of the simulation system.

In Chapter 2, HVDC transmission systems were introduced, with a particular focus on explaining how offshore HVDC grids can be used to increase system flexibility and reliability when integrating large amounts of offshore wind power to shore. Next, a key component in HVDC grids, the Modular Multilevel Converter (MMC) was introduced. The general operation of the MMC was explained before introducing the different modeling approaches for the MMC. Next, an energy-based simplified zero sequence MMC model to be used later in the Thesis was introduced along with its control. Lastly, some of the added benefits from the MMC were mentioned for the reader to have a good understanding of the converter.

Then, the modeling and simulation tool OpenModelica was introduced, as that software was used later in the Thesis to model a three-terminal HVDC system with wind power and storage integration. In this chapter, a preliminary assessment of OpenModelica's performance was carried out with the accuracy of results and simulations speeds as criteria and Simulink as a benchmark. The results from the simulations of the AC-side of a 10kHz 2L-VSC showed that OpenModelica could accurately reproduce the current waveforms for high frequencies and that the simulation speeds were in the same range as in Simulink for most of the solvers. Additionally, a description of how to build models in OpenModelica for Opal-RTs real-time simulator ePHASORSIM was provided as no such description could be found in the literature. This description can be used by future students to ease the work of using OpenModelica models for future real-time HIL simulations. OpenModelica models were successfully tested with the real-time simulator in the National Smart Grid Laboratory.

In the next chapter, the three-terminal HVDC system with two wind farms and an energy storage system was presented as it contained all the necessary components to study the dynamic interactions in the HVDC system. The models used for the wind farms, energy storage, HVDC cable, and transformer were described. Lastly, three simulation cases were introduced to study different aspects of the system. The first case, Test case 1, focused on showing that the three terminal HVDC system was working and that controllers were stable for step responses in power. Also, a test with power reversal within the same test case was simulated. Test case 2 focused on dimensioning the energy storage system configuration where the power from the wind farm was filtered, and the difference in filtered and actual power was covered by the energy storage system using real wind speed data. Lastly, Test case 3 combined the three terminal HVDC system with two wind farms where an energy storage system complemented one of the wind farms. Two events, a drop in wind speeds and sudden losses of wind farms, were introduced to study the dynamics of the HVDC system and compare the differences in responses at events on the two wind farms.

The results showed that the overall operation of the HVDC system was improved when the events occurred at the wind farm with energy storage compared to the events at wind farm without an energy storage system. The added power from the energy storage led to a more stable power production that lowered the transients in the DC-voltages and the zero sequence energies stored in the MMCs due to the fast response of the energy storage model used.

In the discussion, it was mentioned that this configuration could benefit TSOs with opportunities for easier balancing and scheduling as the effects of changes in wind speeds are delayed by almost an hour with the energy storage parameters used. However, this configuration would not solve the intermittency challenge of the wind, as the rated energy capacity of the energy storage system used was too low. Some discussion of pros and cons related to having the energy storage offshore was also included.

Lastly, the experience of using OpenModelica to model and study the multiterminal HVDC system in this Thesis was very positive. The adaptation to the software from Simulink was relatively smooth and quick, however, this was not discussed in this Thesis as it was already covered in the Specialization Project.

8.1 Suggestions for future work

Future work should use the guide provided for building model in ePHASORSIM for real-time simulations and use it to include real hardware to perform hardware-in-the-loop (HIL) simulations with models developed in the software or with other user-defined models to be used, for example, for experimental verification.

Additionally, future work should go deeper in the solvers of OpenModelica and Simulink to try to explain why the HVDC model built for ePHASORSIM did not work at a time step of $\Delta t = 100\mu s$, and also try to use that knowledge to make the HVDC model ultimately work with $\Delta t = 100\mu s$.

Since the models used in this study are made publicly available, the models can be used and changed by anyone for any purpose. This could include the assessment of stability margins of the controllers in this system because these were not considered in this

Thesis. This way, the response of the system after re-tuning of the controllers could be studied. Alternatively, future studies could include changing the energy storage parameters or configuration. Another possibility is to use the models in an expanded HVDC grid with more MMC terminals to tune the DC-voltage droops of the active power controllers for either verification of results or experimentation.

The models provided could also be improved by replacing the ideal PLL used in this Thesis with a dynamic PLL model to prepare the models for studies on the effects of changes in electrical frequency.

Future work should also look at the front to front (AC-side to AC-side) arrangement of two MMCs in OpenModelica and try to find a way to make the arrangement work. This way, the electrical representation of the model can be built to have an even more accurate representation of the simulation system described, to make full use of the multi-physics aspect of OpenModelica.

To further increase the levels of detail in the system, a DFIG model, for example, including a more accurate representation of an induction generator and the back to back power electronic converters on the rotor, could be added to have a more accurate representation of the wind farms. Also, a more accurate representation of a real energy storage system could be implemented to increase the level of detail in the system, as the energy storage model used in this Thesis is very simple. This would allow studying the added effects of having more detailed models of the energy storage and the wind farms in the HVDC system. Alternatively, the FMU capability of OpenModelica can be investigated further to study the opportunities of coupling OpenModelica with external software used for wind turbine design.

Bibliography

- [1] United Nations. Framework Convention on Climate Change. *Adoption of the Paris agreement*. 2015.
- [2] Intergovernmental Panel on Climate Change. *Global Warming of 1.5°C*. 2018.
- [3] International Energy Agency. *Global Energy and CO₂ Status Report 2017*. 2018.
- [4] Jos GJ Olivier, KM Schure, and JAHW Peters. “Trends in global CO₂ and total greenhouse gas emissions”. In: *PBL Netherlands Environmental Assessment Agency* (2017), p. 5.
- [5] G. Janssens-Maenhout et al. “EDGAR v4.3.2 Global Atlas of the three major Greenhouse Gas Emissions for the period 1970–2012”. In: *Earth System Science Data Discussions* 2019 (2019), pp. 1–52. DOI: 10.5194/essd-2018-164. URL: <https://www.earth-syst-sci-data-discuss.net/essd-2018-164/>.
- [6] Nana Yaw Amponsah et al. “Greenhouse gas emissions from renewable energy sources: A review of lifecycle considerations”. In: *Renewable and Sustainable Energy Reviews* 39 (2014), pp. 461–475.
- [7] Xi Lu, Michael B McElroy, and Juha Kiviluoma. “Global potential for wind-generated electricity”. In: *Proceedings of the National Academy of Sciences* 106.27 (2009), pp. 10933–10938.
- [8] Bureau of Ocean Energy Management. *Offshore Wind Energy*. Available from: <https://www.boem.gov/Renewable-Energy-Program/Renewable-Energy-Guide/Offshore-Wind-Energy.aspx>. 2018. (Visited on 11/19/2018).
- [9] Rystad Energy. *New Tech Boosts Offshore Wind Growth Potential*. Available from: <https://www.rystadenergy.com/newsevents/news/press-releases/New-tech-boosts-offshore-wind-growth-potential/>. 2018. (Visited on 05/12/2019).
- [10] Guorui Ren et al. “Overview of wind power intermittency: Impacts, measurements, and mitigation solutions”. In: *Applied Energy* 204 (2017), pp. 47–65.

- [11] TR Ayodele and ASO Ogunjuyigbe. “Mitigation of wind power intermittency: Storage technology approach”. In: *Renewable and Sustainable Energy Reviews* 44 (2015), pp. 447–456.
- [12] R. Marquardt. “Modular Multilevel Converter: An universal concept for HVDC-Networks and extended DC-Bus-applications”. In: *The 2010 International Power Electronics Conference - ECCE ASIA* -. June 2010, pp. 502–507. DOI: 10.1109/IPEC.2010.5544594.
- [13] P. Fritzson et al. “OpenModelica - A free open-source environment for system modeling, simulation, and teaching”. In: *2006 IEEE Conference on Computer Aided Control System Design, 2006 IEEE International Conference on Control Applications, 2006 IEEE International Symposium on Intelligent Control*. Oct. 2006, pp. 1588–1595. DOI: 10.1109/CACSD-CCA-ISIC.2006.4776878.
- [14] Joachim Espvik. “Modeling of an HVDC Two-Level Voltage Source Converter in the Open-Source Tool OpenModelica”. Specialization Project. Norwegian University of Technology and Science, Dec. 2018.
- [15] Erling Vatn Tranulis. “Modeling MMC energy dynamics in offshore HVDC systems using OpenModelica”. Masters Thesis. Norwegian University of Technology and Science, June 2019.
- [16] Joachim Espvik et al. “Modeling of Multiterminal HVDC Offshore Grids with Renewable Energy and Storage Integration by Opensource Tools”. In: (July 10–13, 2019). Brest, France, 2019.
- [17] Narin G Hingorani. “Power electronics in electric utilities: role of power electronics in future power systems”. In: *Proceedings of the IEEE* 76.4 (1988), pp. 481–482.
- [18] AG Siemens. “High voltage direct current transmission-proven technology for power exchange”. In: *Energy Sector, Germany*. Accessed at <http://www.siemens.com/sustainability/pool/en/environmental-portfolio/products-solutions/power-transmission-distribution/hvdc-proven-technology.pdf> (2011).
- [19] China Electricity Council. *Changji-Guquan 1, 100 kV UHV DC Transmission Project Starts Power Transmission*. Available from: <http://english.cec.org.cn/No.106.1720.htm>. 2019. (Visited on 05/15/2019).
- [20] The Economist. *Electricity now flows across continents, courtesy of direct current*. Available from: <https://www.economist.com/science-and-technology/2017/01/14/electricity-now-flows-across-continents-courtesy-of-direct-current>. 2017. (Visited on 11/27/2018).
- [21] N Barberis Negra, Jovan Todorovic, and Thomas Ackermann. “Loss evaluation of HVAC and HVDC transmission solutions for large offshore wind farms”. In: *Electric power systems research* 76.11 (2006), pp. 916–927.
- [22] J Todorovic. “Losses Evaluation of HVAC Connection of Large Offshore Wind Farms”. PhD thesis. Master Thesis, Royal Institute of Technology, Stockholm, Sweden, 2004.

-
- [23] ENTSOE. *Offshore Transmission Technology*. Available from: https://www.entsoe.eu/fileadmin/user_upload/_library/publications/entsoe/SDC/European_offshore_grid_-_Offshore_Technology_-_FINALversion.pdf. 2011. (Visited on 05/29/2019).
- [24] ABB. *Why HVDC?* Available from: <https://new.abb.com/systems/hvdc/why-hvdc/economic-and-environmental-advantages>. 2019. (Visited on 05/07/2019).
- [25] B. Silva et al. "Provision of Inertial and Primary Frequency Control Services Using Offshore Multiterminal HVDC Networks". In: *IEEE Transactions on Sustainable Energy* 3.4 (Oct. 2012), pp. 800–808. ISSN: 1949-3029. DOI: 10.1109/TSTE.2012.2199774.
- [26] Lie Xu, Liangzhong Yao, and Christian Sasse. "Grid integration of large DFIG-based wind farms using VSC transmission". In: *IEEE Transactions on Power Systems* 22.3 (2007), pp. 976–984.
- [27] ABB. *DolWin2*. Available from: <https://new.abb.com/systems/hvdc/references/dolwin2>. 2018. (Visited on 11/25/2018).
- [28] ABB. *HVDC technology for offshore wind is maturing*. Available from: <https://new.abb.com/news/detail/8270/hvdc-technology-for-offshore-wind-is-maturing>. 2019. (Visited on 05/12/2019).
- [29] P. Bresesti et al. "HVDC Connection of Offshore Wind Farms to the Transmission System". In: *IEEE Transactions on Energy Conversion* 22.1 (Mar. 2007), pp. 37–43. ISSN: 0885-8969. DOI: 10.1109/TEC.2006.889624.
- [30] PROMOTioN. *Progress on meshed HVDC offshore transmission networks*. Available from: <https://www.promotion-offshore.net>. 2018. (Visited on 11/27/2018).
- [31] M. P. Bahrman and B. K. Johnson. "The ABCs of HVDC transmission technologies". In: *IEEE Power and Energy Magazine* 5.2 (Mar. 2007), pp. 32–44. ISSN: 1540-7977. DOI: 10.1109/MPAE.2007.329194.
- [32] R. Adapa. "High-Wire Act: HVdc Technology: The State of the Art". In: *IEEE Power and Energy Magazine* 10.6 (Nov. 2012), pp. 18–29. ISSN: 1540-7977. DOI: 10.1109/MPE.2012.2213011.
- [33] Hao Wang, Luo Lori, and Dianfeng Wu. *Hierarchical control in a 5-terminal VSC-HVDC project*. Available from: <http://www.ee.co.za/article/hierarchical-control-5-terminal-vsc-hvdc-project.html>. 2014. (Visited on 11/27/2018).
- [34] Jinjin Chen. "Development of offshore wind power in China". In: *Renewable and Sustainable Energy Reviews* 15.9 (2011), pp. 5013–5020.
- [35] Lixuan Hong and Bernd Möller. "Offshore wind energy potential in China: under technical, spatial and economic constraints". In: *Energy* 36.7 (2011), pp. 4482–4491.
-

- [36] The Energy Times. *China Upgrades Capacity to the Zhoushan Islands*. Available from: <https://www.theenergytimes.com/capacity/china-upgrades-capacity-zhoushan-islands>. 2017. (Visited on 11/27/2018).
- [37] T. M. Haileselassie and K. Uhlen. "Power System Security in a Meshed North Sea HVDC Grid". In: *Proceedings of the IEEE* 101.4 (Apr. 2013), pp. 978–990. ISSN: 0018-9219. DOI: 10.1109/JPROC.2013.2241375.
- [38] Michiel Müller et al. *Translate COP21 - 2045 outlook and implications for offshore wind in the North Seas*. July 2017.
- [39] Salman Khan and Elisabetta Tedeschi. "Modeling of MMC for Fast and Accurate Simulation of Electromagnetic Transients: A Review". In: 10 (Aug. 2017).
- [40] R Marquardt. "Stromrichterschaltungen mit verteilten energiespeichern". In: *German Patent DE10103031A1* 24 (2001).
- [41] A. Lesnicar and R. Marquardt. "An innovative modular multilevel converter topology suitable for a wide power range". In: *2003 IEEE Bologna Power Tech Conference Proceedings*, vol. 3. June 2003, 6 pp. Vol.3-. DOI: 10.1109/PTC.2003.1304403.
- [42] ABB. *HVDC Light (VSC)*. Available from: <https://new.abb.com/systems/hvdc/hvdc-light>. 2018. (Visited on 11/27/2018).
- [43] Siemens AG. *HVDC PLUS*. Available from: <https://www.siemens.com/global/en/home/products/energy/high-voltage/high-voltage-direct-current-transmission-solutions/hvdc-plus.html>. 2018. (Visited on 11/23/2018).
- [44] P. L. Francos et al. "INELFE ffdfffd Europe's first integrated onshore HVDC interconnection". In: *2012 IEEE Power and Energy Society General Meeting*. July 2012, pp. 1–8. DOI: 10.1109/PESGM.2012.6344799.
- [45] Gilbert Bergna-Diaz, Jon Are Suul, and Salvatore D'Arco. "Energy-based state-space representation of modular multilevel converters with a constant equilibrium point in steady-state operation". In: *IEEE Transactions on Power Electronics* 33.6 (2018), pp. 4832–4851.
- [46] Jaime Peralta et al. "Detailed and averaged models for a 401-level MMC–HVDC system". In: *IEEE Transactions on Power Delivery* 27.3 (2012), pp. 1501–1508.
- [47] Randy Wachal et al. *Guide for the Development of Models for HVDC Converters in a HVDC Grid*. Dec. 2014.
- [48] Abel A Taffese, Elisabetta Tedeschi, and Erik De Jong. "A control scheme for utilizing energy storage of the modular multilevel converter for power oscillation damping". In: *2017 IEEE 18th Workshop on Control and Modeling for Power Electronics (COMPEL)*. IEEE. 2017, pp. 1–8.
- [49] Lennart Harnefors et al. "Dynamic analysis of modular multilevel converters". In: *IEEE Transactions on Industrial Electronics* 60.7 (2013), pp. 2526–2537.
- [50] Steffen Rohner, Jens Weber, and Steffen Bernet. "Continuous model of modular multilevel converter with experimental verification". In: *2011 IEEE Energy Conversion Congress and Exposition*. IEEE. 2011, pp. 4021–4028.

-
- [51] Nilanjan Ray Chaudhuri, Rafael Oliveira, and Amirnaser Yazdani. “Stability analysis of vector-controlled modular multilevel converters in linear time-periodic framework”. In: *IEEE Transactions on Power Electronics* 31.7 (2016), pp. 5255–5269.
- [52] V. Blasko and V. Kaura. “A new mathematical model and control of a three-phase AC-DC voltage source converter”. In: *IEEE Transactions on Power Electronics* 12.1 (Jan. 1997), pp. 116–123. ISSN: 0885-8993. DOI: 10.1109/63.554176.
- [53] Chandra Bajracharya et al. “Understanding of tuning techniques of converter controllers for VSC-HVDC”. In: *Nordic Workshop on Power and Industrial Electronics (NORPIE/2008), June 9-11, 2008, Espoo, Finland*. Helsinki University of Technology. 2008.
- [54] Wen-ning Yan et al. “Priority control strategy of VSC-MTDC system for integrating wind power”. In: *Journal of Electrical and Computer Engineering* 2015 (2015), p. 49.
- [55] S. Debnath et al. “Operation, Control, and Applications of the Modular Multilevel Converter: A Review”. In: *IEEE Transactions on Power Electronics* 30.1 (Jan. 2015), pp. 37–53. ISSN: 0885-8993. DOI: 10.1109/TPEL.2014.2309937.
- [56] Q. Tu, Z. Xu, and L. Xu. “Reduced Switching-Frequency Modulation and Circulating Current Suppression for Modular Multilevel Converters”. In: *IEEE Transactions on Power Delivery* 26.3 (July 2011), pp. 2009–2017. ISSN: 0885-8977. DOI: 10.1109/TPWRD.2011.2115258.
- [57] B. Gemmell et al. “Prospects of multilevel VSC technologies for power transmission”. In: *2008 IEEE/PES Transmission and Distribution Conference and Exposition*. Apr. 2008, pp. 1–16. DOI: 10.1109/TDC.2008.4517192.
- [58] Udana N Gnanarathna, Aniruddha M Gole, and Sanjay K Chaudhary. “Multilevel modular converter for VSC-HVDC transmission applications: control and operational aspects”. In: *16th National Power Systems Conference, NPSC-2010*. 2010.
- [59] PA Gbadega and AK Saha. “Loss Assessment of MMC-Based VSC-HVDC Converters Using IEC 62751-1-2 Std. and Component Datasheet Parameters”. In: *2018 IEEE PES/IAS PowerAfrica*. IEEE. 2018, pp. 1–9.
- [60] J. J. Mesas et al. “Cable fault characterization in VSC DC systems”. In: *2016 International Symposium on Fundamentals of Electrical Engineering (ISFEE)*. June 2016, pp. 1–5. DOI: 10.1109/ISFEE.2016.7803210.
- [61] E Spahic et al. “Impact of the DC technology on transmission grids”. In: (2015).
- [62] J. Qin et al. “Hybrid Design of Modular Multilevel Converters for HVDC Systems Based on Various Submodule Circuits”. In: *IEEE Transactions on Power Delivery* 30.1 (Feb. 2015), pp. 385–394. ISSN: 0885-8977. DOI: 10.1109/TPWRD.2014.2351794.
- [63] CD Barker et al. “Low Frequency Active Power Oscillation Damping Using a MMC-VSC HVDC link”. In: (2017).
- [64] Andres E Leon. “Short-term frequency regulation and inertia emulation using an MMC-based MTDC system”. In: *IEEE Transactions on Power Systems* 33.3 (2017), pp. 2854–2863.
-

BIBLIOGRAPHY

- [65] Julian Freytes et al. “Dynamic Analysis of MMC-Based MTDC Grids: Use of MMC Energy to Improve Voltage Behavior”. In: *IEEE Transactions on Power Delivery* 34.1 (2019), pp. 137–148.
- [66] Ishaan Puranik, Lei Zhang, and Jiangchao Qin. “Impact of Low-Frequency Ripple on Lifetime of Battery in MMC-based Battery Storage Systems”. In: *2018 IEEE Energy Conversion Congress and Exposition (ECCE)*. IEEE. 2018, pp. 2748–2752.
- [67] Dassault Systèmes. *DYMOLA Systems Engineering*. Available from: <https://www.3ds.com/products-services/catia/products/dymola/>. 2019. (Visited on 06/03/2019).
- [68] Peter Fritzson, Johan Gunnarsson, and Mats Jirstrand. “MathModelica-an extensible modeling and simulation environment with integrated graphics and literate programming”. In: *2nd International Modelica Conference, March 18-19, Munich, Germany*. 2002.
- [69] Equa AB. *The IDA simulation tool*. Available from: <https://www.equa.se/en/>. 2019. (Visited on 06/03/2019).
- [70] Adeel Asghar. *Open Source Modelica Consortium*. Available from: <https://openmodelica.org/home/consortium>. 2019. (Visited on 06/03/2019).
- [71] Raphaël Valyi and Enrique Ortega. “Energy simulator, an open source simulation platform dedicated to systems ecology and Energy studies”. In: (July 2002), pp. 349–360.
- [72] Open Source Modelica Consortium. *Solving Modelica Models*. Available from: <https://openmodelica.org/doc/OpenModelicaUsersGuide/latest/solving.html>. 2019. (Visited on 03/19/2019).
- [73] François E Cellier and Ernesto Kofman. *Continuous system simulation*. Springer Science & Business Media, 2006.
- [74] HA Watts. *Step size control in ODE solvers*. Tech. rep. Sandia National Labs., Albuquerque, NM (USA), 1984.
- [75] Open Source Modelica Consortium. *Functional Mock-up Interface - FMI*. Available from: <https://openmodelica.org/doc/OpenModelicaUsersGuide/v1.11.0/fmi.html>. 2019. (Visited on 03/12/2019).
- [76] Modelon. *Modelica FMI are crucial for ABB real-time simulation*. Available from: <https://www.youtube.com/watch?v=-G55yIF1ujs>. 2014. (Visited on 03/20/2019).
- [77] Opal-RT Technologies Inc. *Innovative Large-Scale Electromechanical Power System Real-Time Simulation*. Available from: <https://www.opal-rt.com/systems-ephasorsim/>. 2018. (Visited on 03/20/2019).
- [78] Vahid Jalili-Marandi et al. “A real-time dynamic simulation tool for transmission and distribution power systems”. In: *2013 IEEE Power & Energy Society General Meeting*. IEEE. 2013, pp. 1–5.
- [79] Marko Bacic. “On hardware-in-the-loop simulation”. In: *Proceedings of the 44th IEEE Conference on Decision and Control*. IEEE. 2005, pp. 3194–3198.

- [80] Dietmar Winkler, Clemens Gühmann, et al. “Synchronising a modelica real-time simulation model with a highly dynamic engine test-bench system”. In: *In 5th International Modelica Conference, Vienna*. Citeseer. 2006.
- [81] Raymundo E. Torres-Olguin. *HVDC system and laboratory analysis*. Available from: https://www.sintef.no/globalassets/project/nowitech_new/final-seminar-august2017/presentations/olguin_sintef.pdf. 2017. (Visited on 05/10/2019).
- [82] OPAL-RT. *Power Hardware-in-the-loop - A Revolution in the Industry*. Available from: <https://www.opal-rt.com/power-hardware-in-the-loop/>. 2019. (Visited on 06/02/2019).
- [83] Opal-RT Technologies Inc. *Opal-RT*. Available from: <https://www.opal-rt.com>. 2018. (Visited on 03/12/2019).
- [84] Siqi Wang and Kevin Tomsovic. “Quantitative control approach for wind turbine generators to provide fast frequency response with guarantee of rotor security”. In: *2018 IEEE Power & Energy Society General Meeting (PESGM)*. IEEE. 2018, pp. 1–5.
- [85] Dmitry Baimel et al. “Dynamic modeling of networks, microgrids, and renewable sources in the dq0 reference frame: A survey”. In: *Ieee Access* 5 (2017), pp. 21323–21335.
- [86] Prabha Kundur, Neal J Balu, and Mark G Lauby. *Power system stability and control*. Vol. 7. McGraw-hill New York, 1994.
- [87] Gilbert M Masters. *Renewable and efficient electric power systems*. John Wiley & Sons, 2013.
- [88] Siemens Gamesa Renewable Energy. *SG 8.0-167 DD Offshore wind turbine*. Available from: <https://www.siemensgamesa.com/en-int/products-and-services/offshore/wind-turbine-sg-8-0-167-dd>. 2019. (Visited on 05/29/2019).
- [89] Siegfried Heier. *Grid Integration of Wind Energy Conversion Systems*. John Wiley & Sons, 1998.
- [90] Mohammed Khair Al-Solihat and Meyer Nahon. “Flexible multibody dynamic modeling of a floating wind turbine”. In: *International Journal of Mechanical Sciences* 142 (2018), pp. 518–529.
- [91] Jef Beerten, Salvatore D’Arco, and Jon Are Suul. “Frequency-dependent cable modelling for small-signal stability analysis of VSC-HVDC systems”. In: *IET Generation, Transmission & Distribution* 10.6 (2016), pp. 1370–1381.
- [92] Bjorn Gustavsen and Adam Semlyen. “Rational approximation of frequency domain responses by vector fitting”. In: *IEEE Transactions on power delivery* 14.3 (1999), pp. 1052–1061.
- [93] Stephen Chapman. *Electric machinery fundamentals*. Tata McGraw-Hill Education, 2005.
- [94] LP Teshmont Consultants and Shaarbafi Karim. “Transformer Modelling Guide”. In: *AESO, Alberta Electric System Operator, Revision* (2014).

BIBLIOGRAPHY

- [95] Mohammad Amin et al. “Impact of power flow direction on the stability of VSC-HVDC seen from the impedance nyquist plot”. In: *IEEE Transactions on Power Electronics* 32.10 (2017), pp. 8204–8217.
- [96] Holger Hesse et al. “Lithium-ion battery storage for the grid: A review of stationary battery storage system design tailored for applications in modern power grids”. In: *Energies* 10.12 (2017), p. 2107.
- [97] Brian B McKeon, Jun Furukawa, and Scott Fenstermacher. “Advanced lead–acid batteries and the development of grid-scale energy storage systems”. In: *Proceedings of the IEEE* 102.6 (2014), pp. 951–963.
- [98] olivleno. *4451 assigned enhancement Unspecific error message: The given system is mixed-determined*. Available from: <https://trac.openmodelica.org/OpenModelica/ticket/2721>. 2018. (Visited on 05/13/2019).
- [99] Santiago Sanchez, Gilbert Bergna, and Elisabetta Tedeschi. “Tuning of control loops for grid-connected modular multilevel converters under a simplified port representation for large system studies”. In: *2017 Twelfth International Conference on Ecological Vehicles and Renewable Energies (EVER)*. IEEE. 2017, pp. 1–8.

Transformations

A.1 Amplitude invariant Park transformation

A.1.1 abc to dq transformation

$$x_d = \frac{2}{3} \left(x_a \sin(\omega t) + x_b \sin\left(\omega t - \frac{2\pi}{3}\right) + x_c \sin\left(\omega t + \frac{2\pi}{3}\right) \right) \quad (\text{A.1})$$

$$x_q = \frac{2}{3} \left(x_a \cos(\omega t) + x_b \cos\left(\omega t - \frac{2\pi}{3}\right) + x_c \cos\left(\omega t + \frac{2\pi}{3}\right) \right) \quad (\text{A.2})$$

A.1.2 dq to abc transformation

$$x_a = x_d \sin(\omega t) + x_q \cos(\omega t) \quad (\text{A.3})$$

$$x_b = x_d \sin\left(\omega t - \frac{2\pi}{3}\right) + x_q \cos\left(\omega t - \frac{2\pi}{3}\right) \quad (\text{A.4})$$

$$x_c = x_d \sin\left(\omega t + \frac{2\pi}{3}\right) + x_q \cos\left(\omega t + \frac{2\pi}{3}\right) \quad (\text{A.5})$$

A.2 Park transformation with zero-sequence component

A.2.1 abc to dqz transformation matrix

$$\begin{bmatrix} x_d \\ x_q \\ x_z \end{bmatrix} = \frac{2}{3} \begin{bmatrix} \sin(\theta) & \sin\left(\theta - \frac{2\pi}{3}\right) & \sin\left(\theta + \frac{2\pi}{3}\right) \\ \cos(\theta) & \cos\left(\theta - \frac{2\pi}{3}\right) & \cos\left(\theta + \frac{2\pi}{3}\right) \\ \frac{1}{2} & \frac{1}{2} & \frac{1}{2} \end{bmatrix} \begin{bmatrix} x_a \\ x_b \\ x_c \end{bmatrix} \quad (\text{A.6})$$

A.2.2 dqz to abc transformation matrix

$$\begin{bmatrix} x_a \\ x_b \\ x_c \end{bmatrix} = \begin{bmatrix} \sin(\theta) & \cos(\theta) & 1 \\ \sin(\theta - \frac{2\pi}{3}) & \cos(\theta - \frac{2\pi}{3}) & 1 \\ \sin(\theta + \frac{2\pi}{3}) & \cos(\theta + \frac{2\pi}{3}) & 1 \end{bmatrix} \begin{bmatrix} x_d \\ x_q \\ x_z \end{bmatrix} \quad (\text{A.7})$$

A.3 Transformation between global and local ref. frame

Here is a short explanation for transformation between global and local reference frame in phasor domain models, which is mentioned in Chapter 4.

First, it is useful to define the angle between the global D-axis and the global voltage V_G , δ :

$$\delta = \arctan\left(\frac{V_{Q,G}}{V_{D,G}}\right) \quad (\text{A.8})$$

Then, the local dq frame is defined such that the local d -axis is aligned with the global voltage, V_G . This way, the local q -voltage becomes zero. This alignment corresponds with the convention where the local d -current controls active power and the local q -current controls reactive power, where the local q -voltage is zero.

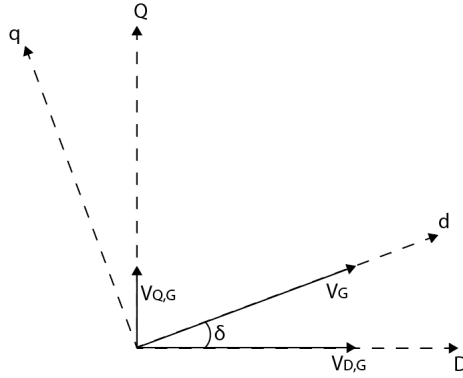


Figure A.1: Alignment of reference frames for transformation between global to local reference frame.

The equations to transform the global quantities, $x_{D,Q}$, to the local quantities, $x_{d,q}$, can be derived as:

$$x_d = x_D \cos(\delta) + x_Q \sin(\delta) \quad (\text{A.9})$$

$$x_q = x_D \sin(\delta) - x_Q \cos(\delta) \quad (\text{A.10})$$

For a current injector component, as explained in Chapter 4, the local currents have to be transformed to global currents. However, OpenModelica accepts the transformation equations in the same form as Equations (A.9) and (A.10) and solves them for the global quantities; hence no inverse transformation is needed.

Appendix B

AC-side switching models

B.1 Model parameters

Table B.1: 2L-VSC parameters

Parameter	Value
Base apparent power	20 kVA
Base voltage	400 V
Base frequency	50 Hz
Series inductance	0.15 pu
Series resistance	0.01 pu
Switching frequency	10 kHz

B.2 Simulink switching model implementation

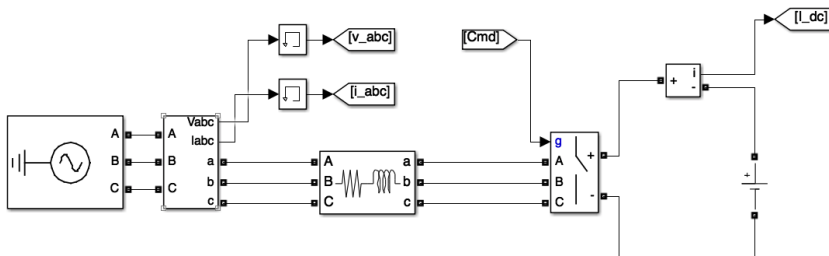


Figure B.1: The implementation of the AC side in a 2L-VSC switching model in Simulink.

B.2.1 PMW generator

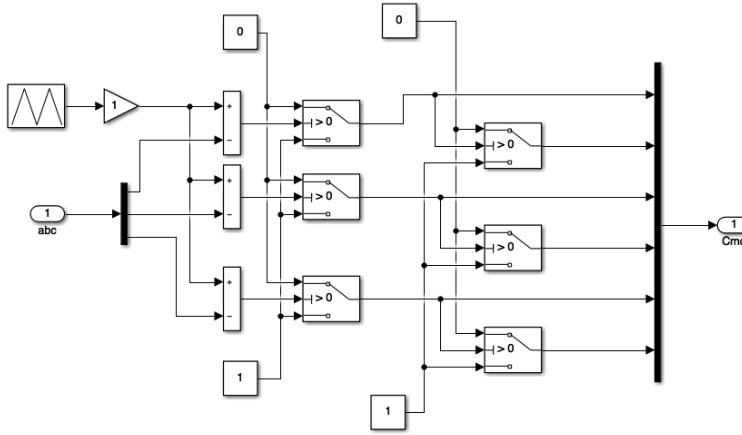


Figure B.2: The implementation of a PWM signal generator in Simulink.

B.2.2 Current controller

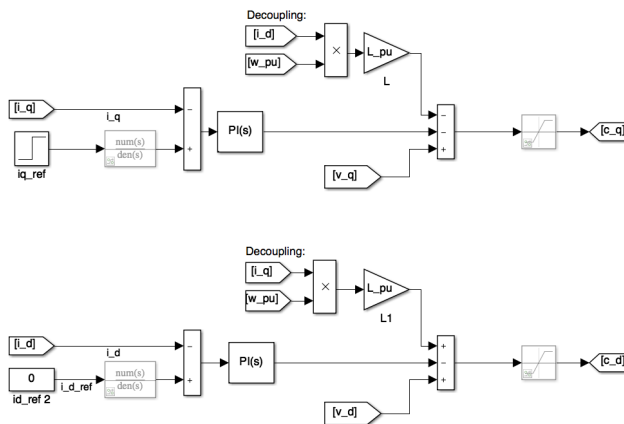


Figure B.3: Implementation of the current controller in Simulink.

B.2.3 dq transformation

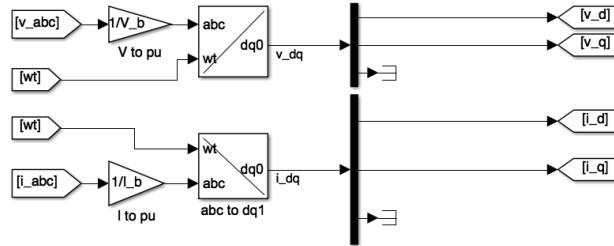


Figure B.4: Implementation of the dq-transformation in Simulink.

B.2.4 inverse dq transformation

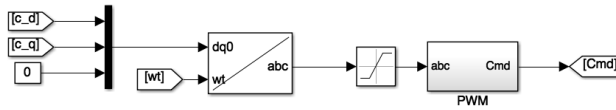


Figure B.5: Implementation of the inverse dq-transformation in Simulink.

B.2.5 Ideal PLL

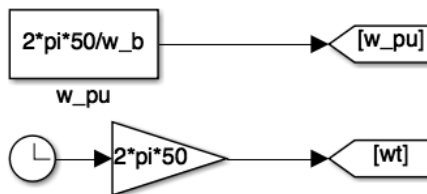


Figure B.6: Implementation of the ideal PLL in Simulink.

B.3 OpenModelica switching model implementation

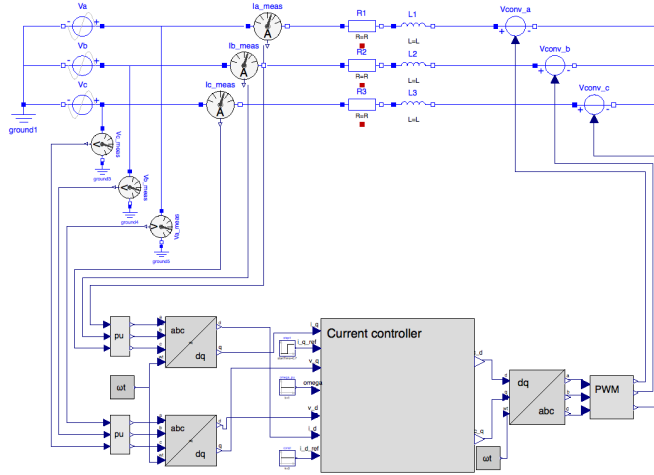


Figure B.7: Implementation of the switching model in OpenModelica.

B.3.1 PWM generator

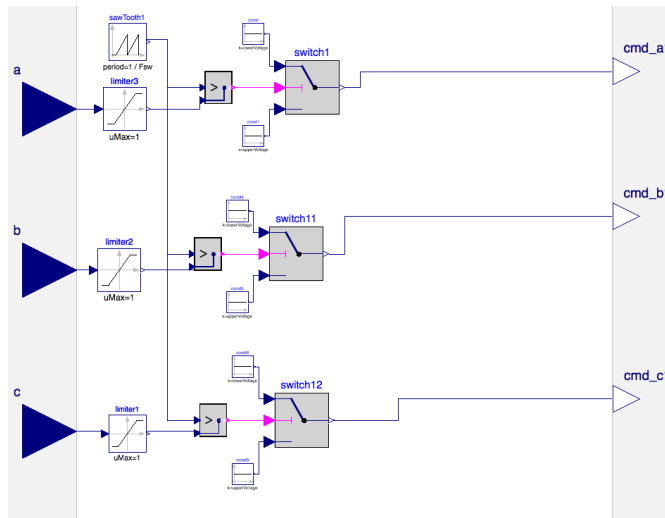


Figure B.8: Implementation of the PWM generator in OpenModelica.

B.3.2 Current controller

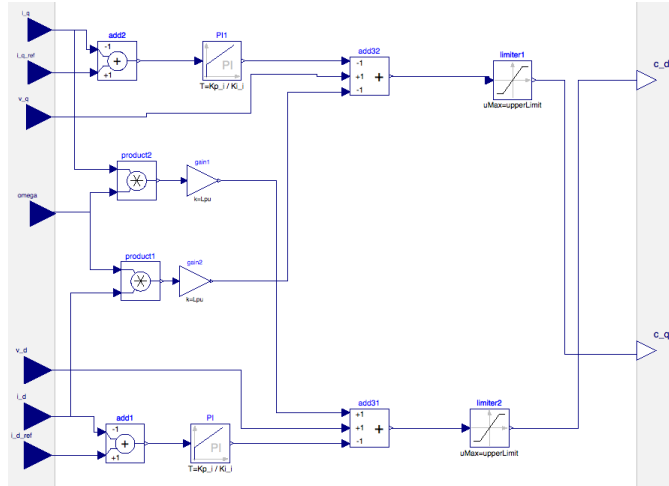


Figure B.9: Implementation of the current controller for the switching model in OpenModelica.

B.3.3 dq transform

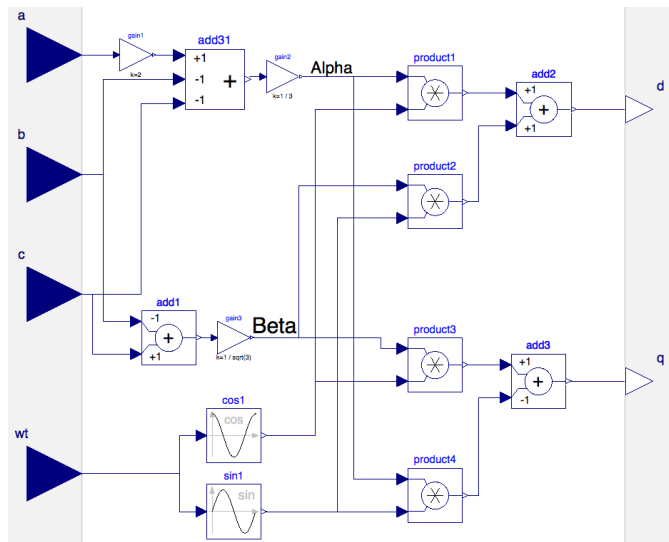


Figure B.10: Implementation of the dq-transform for the switching model in OpenModelica.

B.3.4 Inverse dq transform

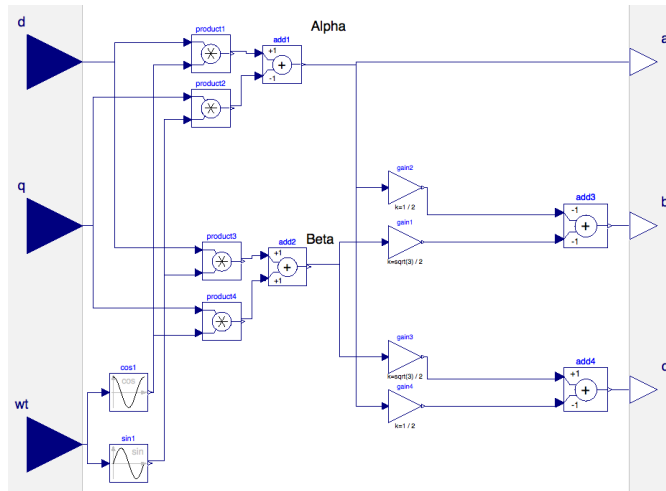


Figure B.11: Implementation of the inverse dq-transform for the switching model in OpenModelica.

B.3.5 Ideal PLL

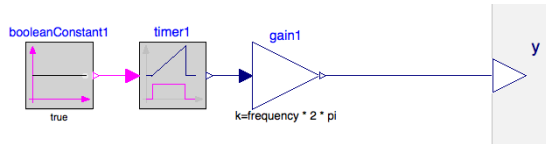


Figure B.12: Implementation of the ideal PLL in OpenModelica.

OpenModelica and Opal-RT

C.1 Power Pin to 3ph grid interface

Figure C.1 shows the interface that is built to make three phase time domain models work with ePHASORSIM. An HVDC model using three-phase quantities is built to illustrate the use of this interface and included later in this Appendix.

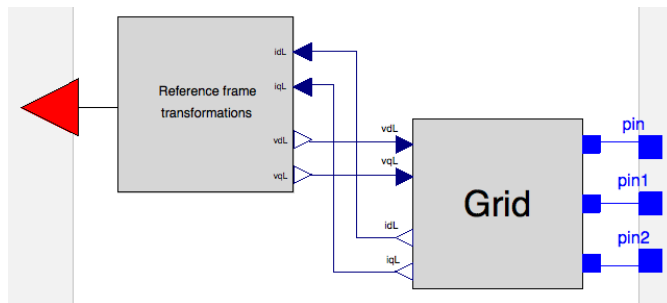


Figure C.1: The outer level of the PowerPin to 3ph grid class.

C.1.1 Reference frame transformation

The reference frame transformation class in Figure C.1 transforms between the local dq quantities of the component connected to the Grid and transforms it into the global DQ coordinates used by the Power Pin. The implementation of the class can be seen in Figure C.2.

```

1 block RefFrameTransform
2   Real delta;
3   Real Isre;
4   Real Isim;
5 ▶ Modelica.Blocks.Interfaces.RealInput IdL annotation( ... );
7 ▶ Modelica.Blocks.Interfaces.RealInput IqL annotation( ... );
9 ▶ Modelica.Blocks.Interfaces.RealOutput vdL annotation( ... );
11 ▶ Modelica.Blocks.Interfaces.RealOutput vqL annotation( ... );
13 ▶ OpalRT.NonElectrical.Connector.PwPin p annotation( ... );
15 equation
16   ///ANGLE CALCULATION////////////////////////////////////
17   delta = atan2(p.vi, p.vr);
18   ///POWER PIN CURRENTS////////////////////////////////////
19   p.ir = Isre;
20   p.ii = Isim;
21   ///TRANSFORMATIONS////////////////////////////////////
22   // Transforms currents between local and global:
23   IdL = Isre * cos(delta) + Isim * sin(delta);
24   IqL = Isre * sin(delta) - Isim * cos(delta);
25   // Transforms grid voltage between local and global:
26   vdL = p.vr * cos(delta) + p.vi * sin(delta);
27   vqL = p.vr * sin(delta) - p.vi * cos(delta);
28 ▶ annotation( ... );
32 end RefFrameTransform;

```

Figure C.2: Implementation of the reference frame transformation class.

C.1.2 Grid

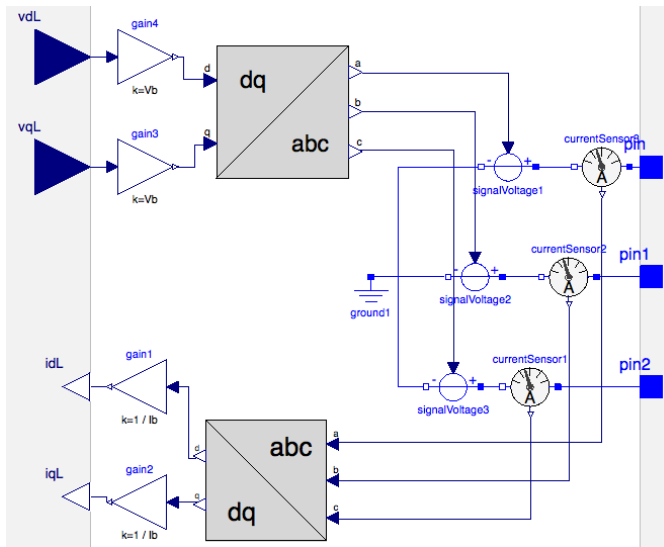


Figure C.3: Implementation of the Grid class used by the PowerPin to 3ph grid interface.

C.2 Implementation of VSC_BASE block

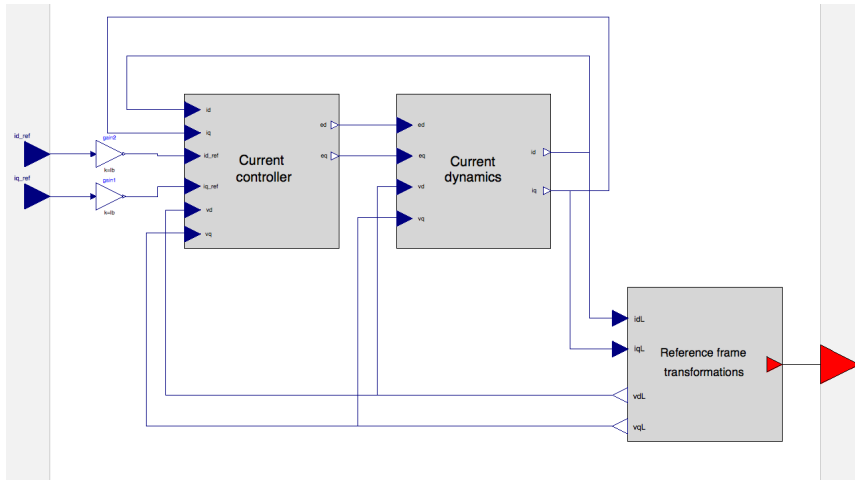


Figure C.4: Implementation of the VSC_BASE block in OpenModelica including dq-current dynamics, controllers and transformation between local and global reference frame.

C.3 HVDC model for ePHASORSIM

This section will present an HVDC model developed for real-time simulations using the Power Pin to 3ph grid interface developed earlier in this Appendix.

The model uses the MMC and cable parameters found in Appendix E. The power base and voltage base are both changed accordingly in the excel file used. The overall grid setup used to test this system is shown in Figure C.5.

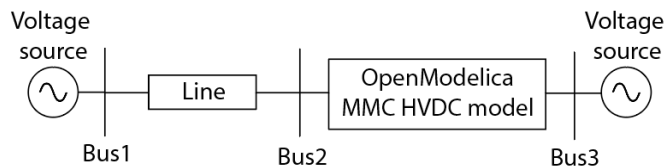


Figure C.5: The example grid used to test the MMC based HVDC model.

The GenUnit implementation can be seen in Figure C.6. The main differences from this model to the other example models are the use of the Power Pin to 3ph grid interface and the use of two power pins, one for each MMC station. When using two Power Pins, the model type in the FMU Glossary has to be Type 7 for HVDC.

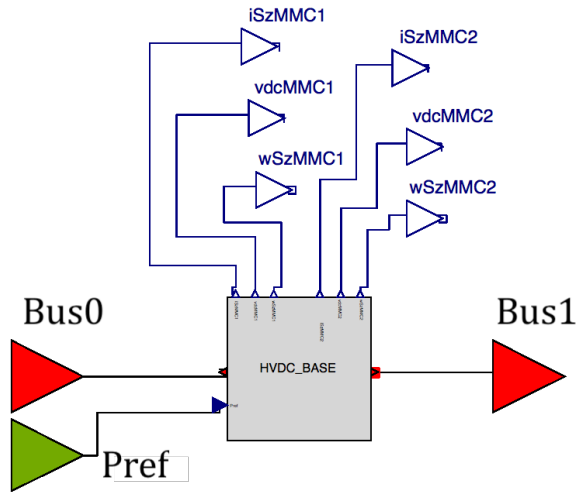


Figure C.6: The GenUnit implementation of the HVDC model.

Figure C.7 shows the HVDC_BASE implementation in the developer library. The MMC and cable implementations are the same as in Appendix D, but some additional outputs are added to the MMC for plotting during real-time simulations.

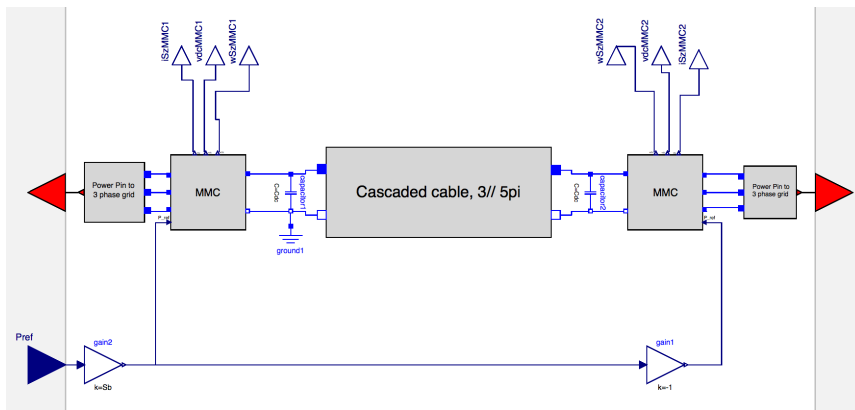


Figure C.7: The HVDC_BASE implementation in the Developer library.

The model runs when testing it at $\Delta t = 100\mu s$ with both Dassl and Rungekutta solver in OpenModelica. However, in Simulink, after the FMU compiled, the model only runs at $\Delta t = 25\mu s$ or lower regardless of solvers. This will be further mentioned in the discussion in Chapter 7.

The complete excel implementation of this system can be seen in Figure C.8.

	A	B	C	D	E	F								
1	Excel file version	v1.5												
2	Name	Template												
3	Frequency (Hz)	50												
4	Power Base (MVA)	1059												
5														
<div style="border: 1px solid black; padding: 2px; display: inline-block;">Do not edit this field</div>														
<div style="display: flex; justify-content: space-between; border-bottom: 1px solid black;"> General Pins Bus Vsource Line HVDC + </div>														
	A	B	C	D	E	F								
1	outgoing	Vmag	1/Vmag		2/Vmag									
2	outgoing	Vang	1/Vang		2/Vang									
3	incoming	Pref	hvd1/Pref											
4	outgoing	iSzMMC1	hvd1/iSzMMC1											
5	outgoing	vdcMMC1	hvd1/vdcMMC1											
6	outgoing	wSzMMC1	hvd1/wSzMMC1											
7	outgoing	iSzMMC2	hvd1/iSzMMC2											
8	outgoing	vdcMMC2	hvd1/vdcMMC2											
9	outgoing	wSzMMC2	hvd1/wSzMMC2											
10														
<div style="display: flex; justify-content: space-between; border-bottom: 1px solid black;"> General Pins Bus Vsource Line HVDC + </div>														
	A	B	C	D	E	F	G							
1	Bus	Base Voltage (V)	Voltage (V, pu)	Angle (deg)	Type									
2	1	271893	1	0	SLACK									
3	2	271893	1,026	-0,04	PQ									
4	3	271893	1	-0,01	PQ									
<div style="display: flex; justify-content: space-between; border-bottom: 1px solid black;"> General Pins Bus Vsource Line HVDC + </div>														
	A	B	C	D	E	F	G							
1	Bus	ID	Voltage (V, pu)	Angle (deg)	Rs (ohm, pu)	Xs (ohm, pu)								
2		1 v1	1	0	0	0								
3		3 v3	1	0	0	0								
4														
<div style="display: flex; justify-content: space-between; border-bottom: 1px solid black;"> General Pins Bus Vsource Line HVDC + </div>														
	A	B	C	D	E	F	G	H						
1	From bus	To bus	Type	ID	R (pu)	X (pu)	B (pu)							
2		1	2 LN_PI	ln1	3,50E-03	4,00E-02	0,7							
3														
<div style="display: flex; justify-content: space-between; border-bottom: 1px solid black;"> General Pins Bus Vsource Line HVDC + </div>														
	A	B	C	D	E	F	G	H	I	J	K	L	M	N
1	name	bus0	bus1	Sb	Vb	La	Ra	Lf	Rf	Vbdc	Csm	N	fb	Cdc
2	hvd1	2	3	1,06E+09	271893	0,05	0,001	0,06	0,001	6,40E+05	0,01	400	50	1,67E-06
3														
<div style="display: flex; justify-content: space-between; border-bottom: 1px solid black;"> General Pins Bus Vsource Line HVDC + </div>														

Figure C.8: The excel implementation of a grid containing the HVDC model built in OpenModelica.

C.4 RT-LAB / ePHASORSIM guide

This section will add a description on how to set up a grid model for real-time simulations using RT-LAB using the VSC model as an example.

C.4.1 Excel implementation of example system

Figure C.9 shows a single line diagram of the simple test system including the OpenModelica built VSC model used to in this example.

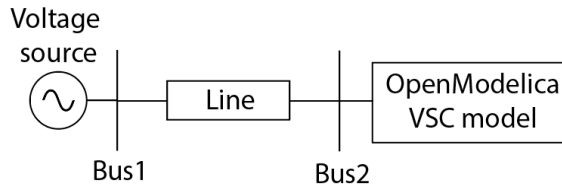


Figure C.9: Example system using the VSC model.

The complete excel implementation of the system can be seen in Figure C.10 including all sheets needed to describe the system in Figure C.9 with the parameters used.

	A	B	C	D	E
1	Excel file version	v1.5			
2	Name	Template			
3	Frequency (Hz)	50			
4	Power Base (MVA)	0,02			
5					

General Pins Bus Vsource Line VSC +

	A	B	P	Q	R	S
1	outgoing	Vmag				
2	outgoing	Vang				
3	incoming	idref				
4	incoming	iqref				
5						

General Pins Bus Vsource Line VSC +

	A	B	C	D	E	F
1	Bus	Base Voltage (V)	Voltage (V, pu)	Angle (deg)	Type	
2	1	400	1	0	SLACK	
3	2	400	1,026	-0,04	PQ	
4						
5						

General Pins Bus Vsource Line VSC +

	A	B	C	D	E	F
1	Bus	ID	Voltage (V, pu)	Angle (deg)	Rs (ohm, pu)	Xs (ohm, pu)
2	1	v1	1	0	0	0
3						
4						
5						

General Pins Bus Vsource Line VSC +

	A	B	C	D	E	F	G
1	From bus	To bus	Type	ID	R (pu)	X (pu)	B (pu)
2	1	2	LN_PI	ln1	3,50E-03	4,00E-02	0,7
3							
4							
5							

General Pins Bus Vsource Line VSC +

	A	B	C	D	E	F	G	H	I	J	K
1	name	bus0	Vb	Sb	fb	Lpu	Rpu				
2	cnv1	2	400	20000	50	0,15	0,01				
3											
4											
5											

General Pins Bus Vsource Line VSC +

Figure C.10: The complete excel implementation of the example system using the VSC.

C.4.2 Preparing the system model in RT-LAB

When the excel file is prepared and the VSC model is built according to the guide in Chapter 4, the next step is to prepare the real-time simulation model in the RT-LAB software.

Figure C.11 shows a picture of the laboratory equipment used to perform the real-time simulation of the described example system. The setup consists of a cabinet including one computer with the RT-LAB software and Simulink installed and the real-time simulator

from Opal-RT. The computer and the real-time simulator are connected in the back of the cabinet.

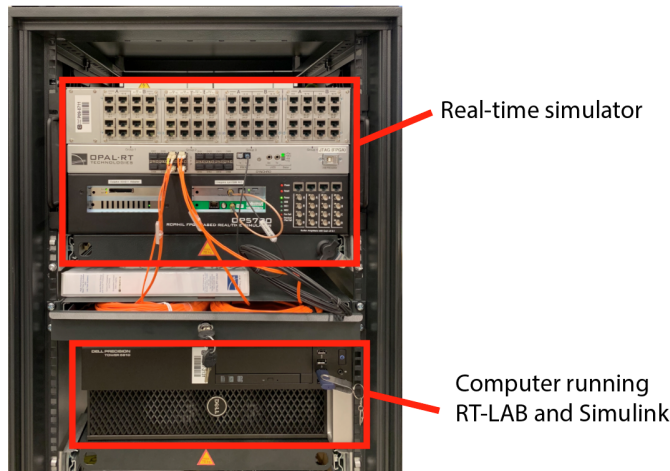


Figure C.11: The laboratory set up for real-time simulations.

When opening the RT-LAB software, the interface showed in Figure C.12 will appear.

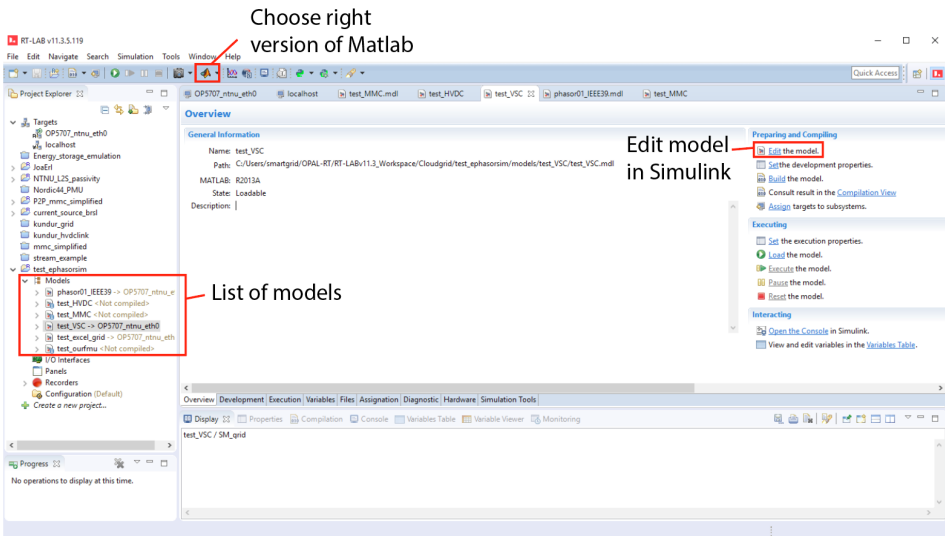


Figure C.12: The interface of RT-LAB.

After making a folder with a .mld Simulink file for the project, it will appear under the list of models. Then, choose the right version of Matlab. In this case, the right version was the 2013 32-bit version. Next, hit "Edit" to open Simulink and prepare the model in

Simulink.

Figure C.13 shows the Simulink window that appears after hitting "Edit" in the VSC model.

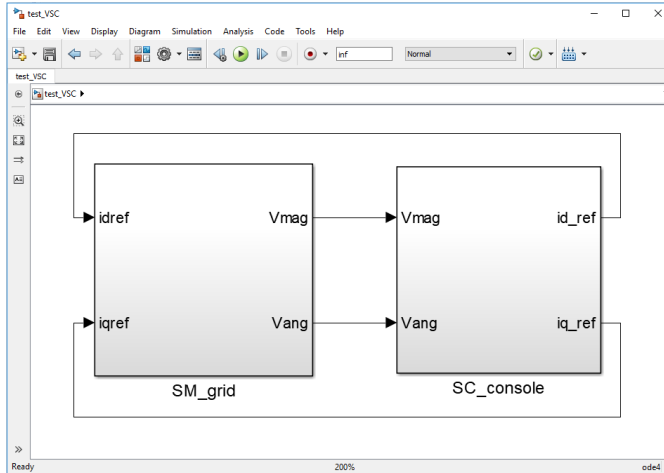


Figure C.13: The outer level of the VSC model in Simulink.

The model consists of two sub-systems, one called "SC_console" where the user can monitor the scopes and input signals to the model and one called "SM_grid" containing the ePHASORSIM solver. The sub-system contains licensed software blocks developed by Opal-RT to be used by the real-time simulator, such as the "Solver" and "OpComm" blocks.

Figure C.14 shows the implementation of the SC_console sub-system. The "OpComm" block is an interface between inputs and outputs used by the real-time simulator.

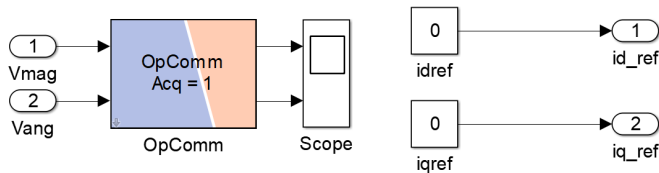


Figure C.14: The SC_console sub-system of the VSC test model.

Figure C.15 shows the implementation of the SM_grid sub-system using the "Solver" block and another "OpComm" block.

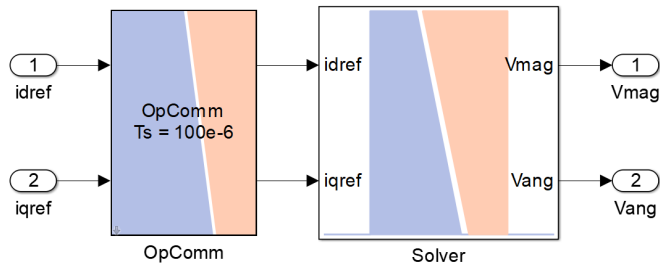


Figure C.15: The SM_grid sub-system of the VSC test model.

The "Solver" block is where the excel file name and the FMU folder name containing the VSC FMU are entered, as shown in Figure C.16. This "Solver" block is the core of ePHASORSIM. It is important that both the excel file describing the power system and the FMU folder are placed inside the same project folder as the .mld Simulink file. The "Solver" block then reads the excel file and adds the input and output ports to the block according to what is defined under the "Pins" sheet in the excel file.

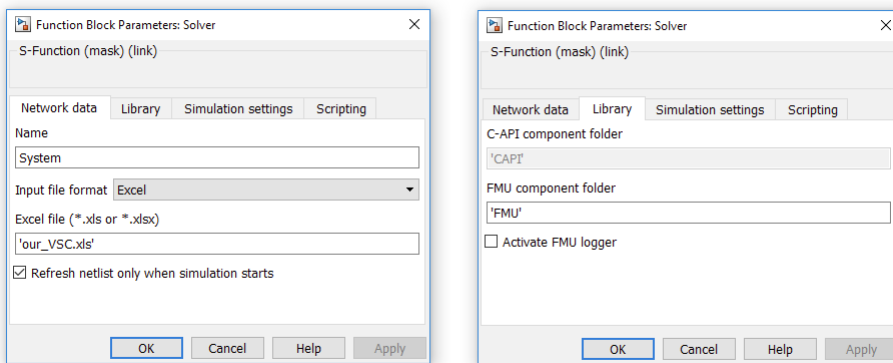


Figure C.16: Settings inside the "Solver" block for the Excel file and the FMU folder.

Additionally, under "Simulation settings" in the "Solver" block, "Dynamic simulation only (without power-flow)" has to be selected and the time step of the solver has to be entered, as shown in Figure C.17.

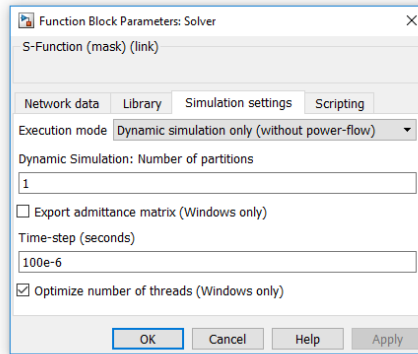


Figure C.17: Settings under the "Simulation settings" tab in the "Solver" block.

At this point, the grid model, including the OpenModelica-built VSC model should be ready to be compiled for a real-time simulation. The model can also be tested in Simulink before it is ultimately built and compiled for the real-time simulator. However, before building the model, the simulation time has to be set to "inf" in the Simulink window.

The next steps are to build the model for the real-time simulator. This is done by hitting "Build" in the RT-LAB interface as seen in Figure C.12. If the model builds successfully, the next step is to hit "Load" to load the model to the real-time simulator. Then, the last step is to hit "Execute" to start the real-time simulation. A window will appear with the compiled model where the scopes and user inputs, which in this case are the dq-current references, will appear, as shown in Figure C.18.

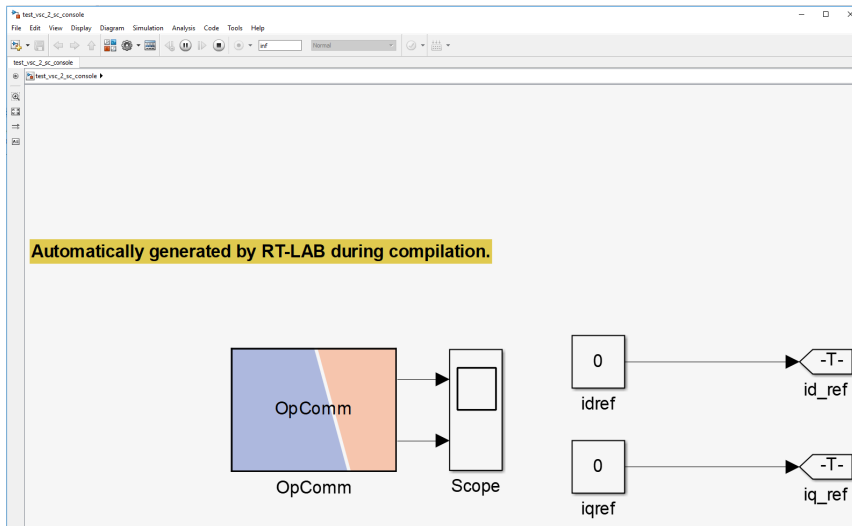


Figure C.18: The window that appears after the "Execute" button is clicked.

Figure C.19 shows a screenshot during a successful real-time simulation where the upper scope shows the voltage magnitudes at the two buses and the lower scope shows the voltage angles of the two buses in the system.

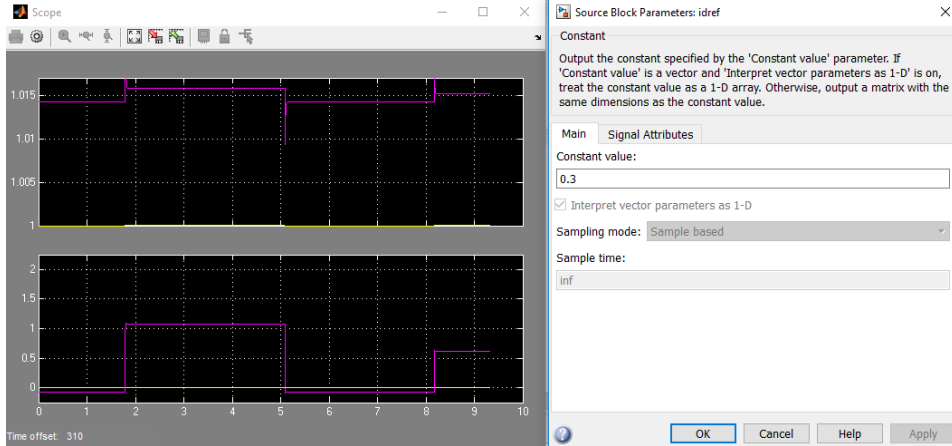


Figure C.19: Screenshot during a successful real-time simulation containing the VSC model.

Appendix D

OpenModelica implementation

D.1 MMC model

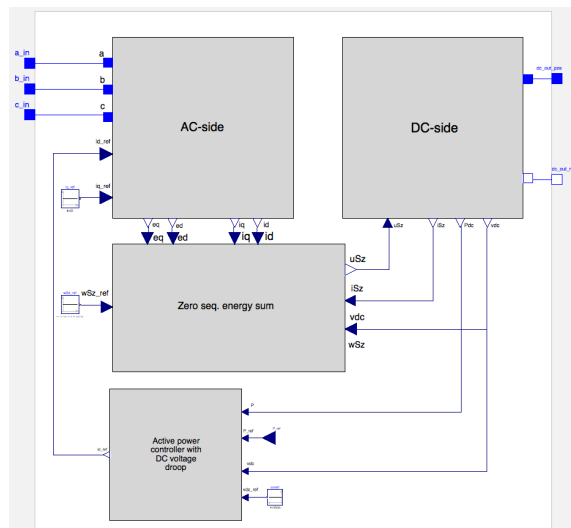


Figure D.1: Implementation of the MMC model.

D.2 AC-side

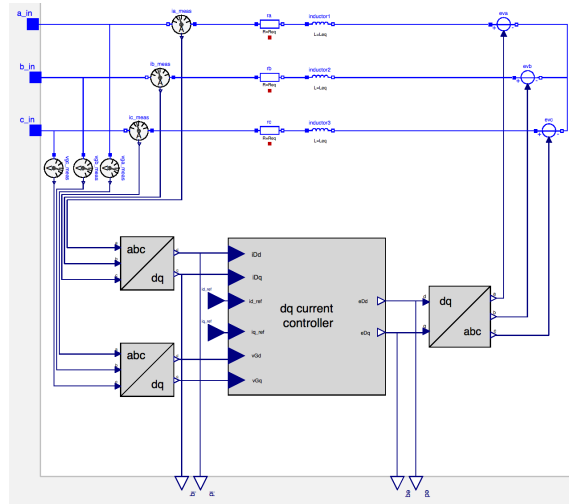


Figure D.2: Implementation of the AC-side of the MMC model.

D.2.1 dq current controller

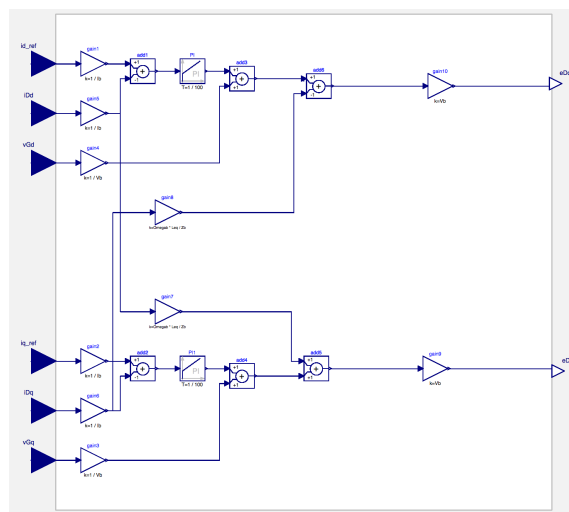


Figure D.3: Implementation of the dq-current controller.

D.2.2 Park transform

```

278 class abc_to_dq_transform_sinusoidal
279   import Modelica.Constants.pi;
280   parameter Real fb = fb;
281   parameter Real w = 2 * pi * fb;
282   Modelica.Blocks.Interfaces.RealInput a annotation( (..) );
283   Modelica.Blocks.Interfaces.RealInput b annotation( (..) );
284   Modelica.Blocks.Interfaces.RealInput c annotation( (..) );
285   Modelica.Blocks.Interfaces.RealOutput d annotation( (..) );
286   Modelica.Blocks.Interfaces.RealOutput q annotation( (..) );
287   equation
288     d = 2 / 3 * (a * sin(w * time) + b * sin(w * time - 2 * pi / 3) + c * sin(w * time + 2 * pi / 3));
289     q = 2 / 3 * (a * cos(w * time) + b * cos(w * time - 2 * pi / 3) + c * cos(w * time + 2 * pi / 3));
290   annotation( (..) );
291 end abc_to_dq_transform_sinusoidal;

```

Figure D.4: Implementation of the Park transform.

D.2.3 Inverse park transform

```

301 class dq_to_abc_transform_sinusoidal
302   import Modelica.Constants.pi;
303   parameter Real fb = fb;
304   parameter Real w = 2 * pi * fb;
305   Modelica.Blocks.Interfaces.RealInput d annotation( (..) );
306   Modelica.Blocks.Interfaces.RealInput q annotation( (..) );
307   Modelica.Blocks.Interfaces.RealOutput a annotation( (..) );
308   Modelica.Blocks.Interfaces.RealOutput b annotation( (..) );
309   Modelica.Blocks.Interfaces.RealOutput c annotation( (..) );
310   equation
311     a = d * sin(w * time) + q * cos(w * time);
312     b = d * sin(w * time - 2 * pi / 3) + q * cos(w * time - 2 * pi / 3);
313     c = d * sin(w * time + 2 * pi / 3) + q * cos(w * time + 2 * pi / 3);
314   annotation( (..) );
315 end dq_to_abc_transform_sinusoidal;

```

Figure D.5: Implementation of the inverse Park transform.

D.3 DC-side

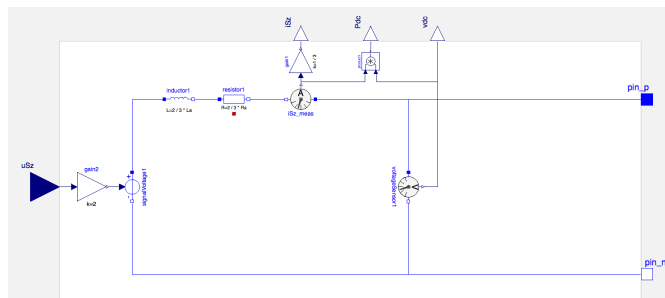


Figure D.6: Implementation of the DC-side of the MMC model

D.4 Zero sequence energy sum

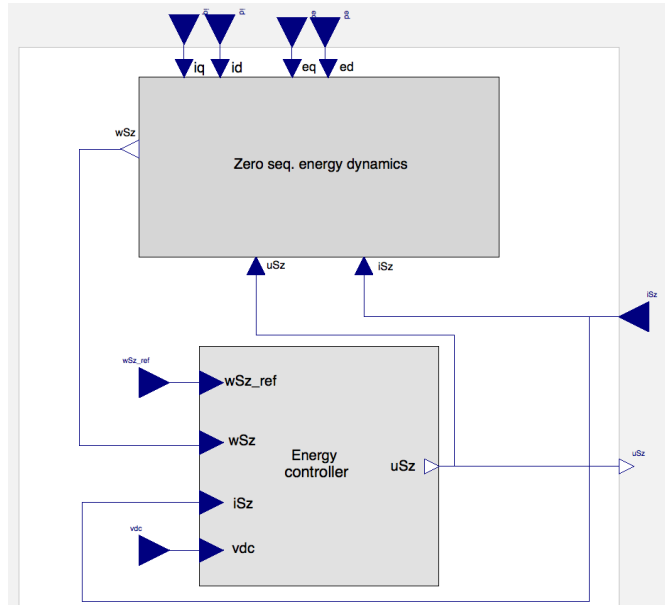


Figure D.7: Implementation of the zero sequence energy sum block in the MMC model.

D.4.1 Zero sequence energy dynamics

```

452 model ZERO_seq_energy_dynamics
453   Modelica.Blocks.Interfaces.RealInput id annotation(
454     Modelica.Blocks.Interfaces.RealInput iq annotation(
455       Modelica.Blocks.Interfaces.RealInput eq annotation(
456         Modelica.Blocks.Interfaces.RealInput ed annotation(
457           Modelica.Blocks.Interfaces.RealOutput wSz annotation(
458             Modelica.Blocks.Interfaces.RealInput uSz annotation(
459             Modelica.Blocks.Interfaces.RealInput iSz annotation(
460
461   initial equation
462     wSz = 10240000;
463     iSz = 0;
464   equation
465     der(wSz) = (-0.5 * (ed * id + eq * iq)) + 2 * uSz * iSz;
466     annotation(
467   end ZERO_seq_energy_dynamics;
468

```

Figure D.8: Implementation of the zero sequence energy dynamics

D.4.2 Energy controller

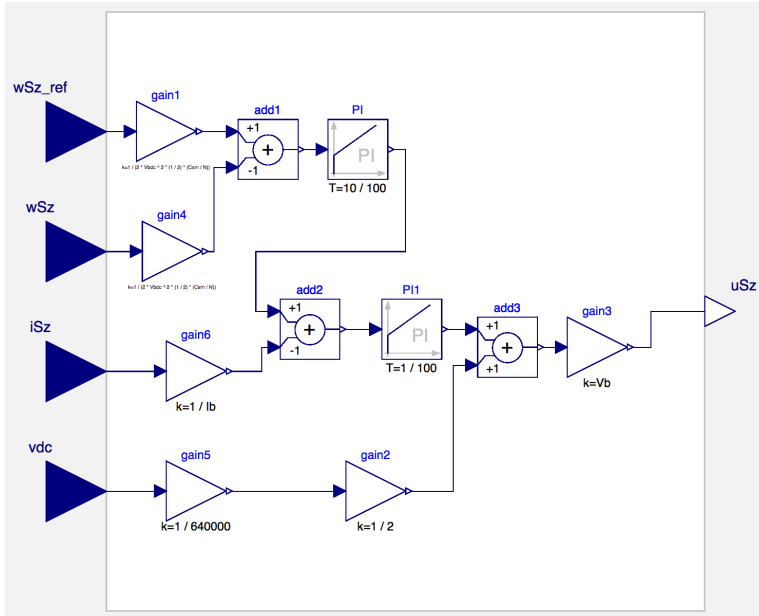


Figure D.9: Implementation of the zero sequence energy controller.

D.5 Power controller

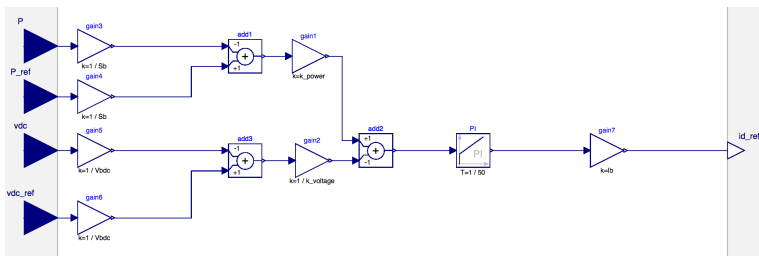


Figure D.10: Implementation of the active power controller with DC voltage droop.

D.6 Wind farm model

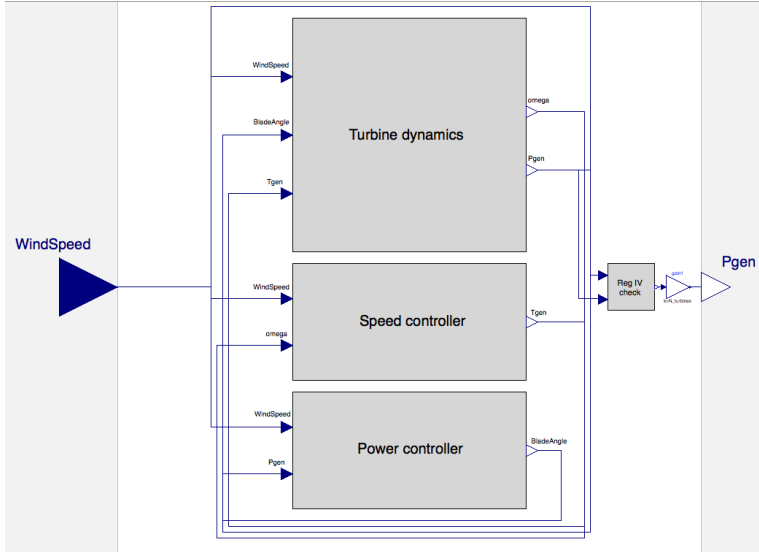


Figure D.11: Overview of the wind turbine model used to represent a wind farm.

D.6.1 Turbine dynamics

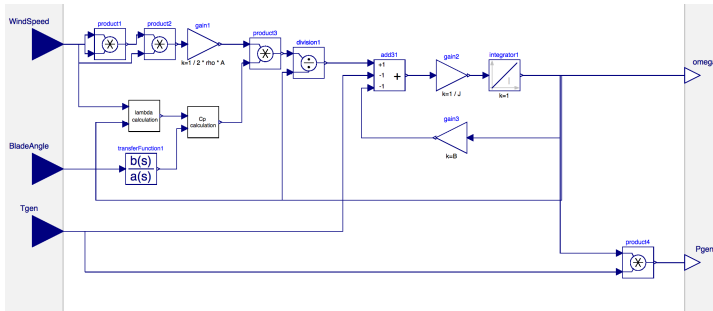


Figure D.12: Implementation of the turbine dynamics block.

D.6.2 Turbine speed controller

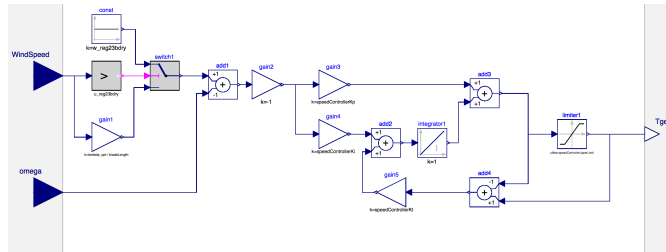


Figure D.13: Implementation of the speed controller in the turbine model.

D.6.3 Turbine power/pitch controller

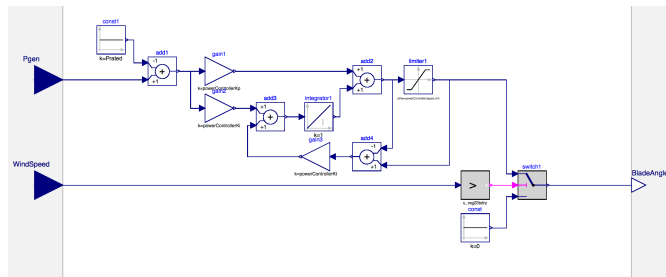


Figure D.14: Implementation of the power controller in the turbine model.

D.6.4 Region IV check

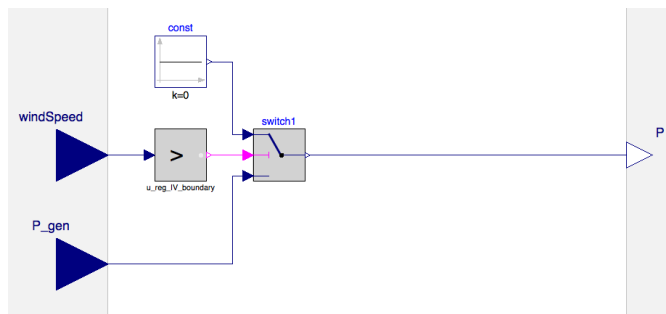


Figure D.15: Logic block to turn off the power production when wind speed is above the limit for region IV.

D.6.5 Coupling the wind farm model electrically

Figure D.16 shows how the wind farm model can be coupled with electrical components by translating the power to a DC current source at a specific voltage.

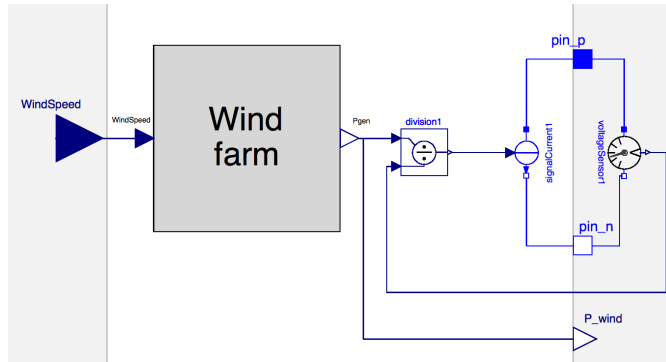


Figure D.16: Coupling of the wind farm model with electrical components.

The setup in Figure D.16 was successfully tested combined with an MMC model connected to an ideal grid, as showed in Figure D.17.

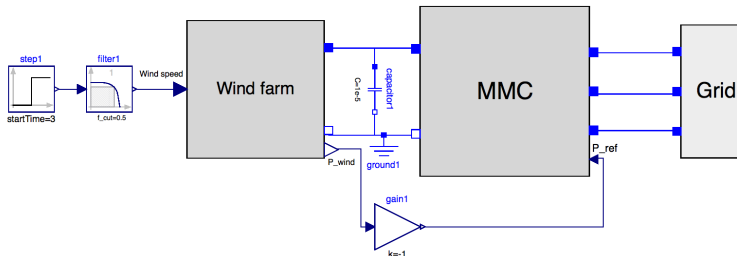


Figure D.17: Test of the wind farm model coupled with electrical components.

D.7 HVDC cable model

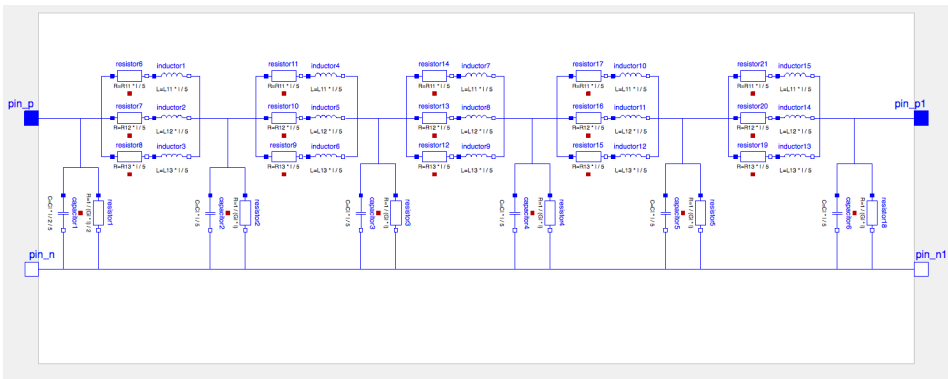


Figure D.18: Implementation of a cable model with 3 parallel branches and 5 pi sections.

D.8 Energy storage model

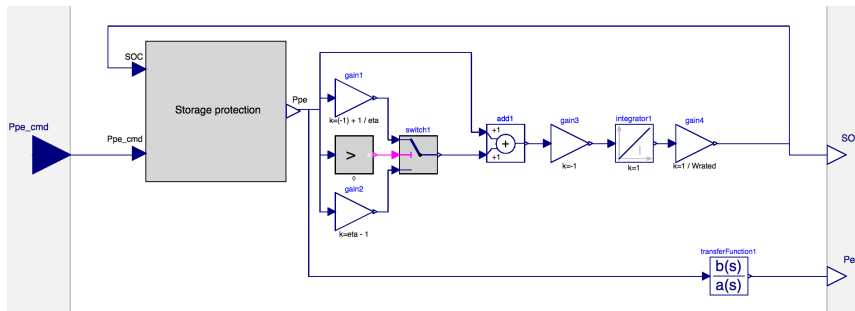


Figure D.19: Implementation of the storage model.

D.8.1 Storage protection

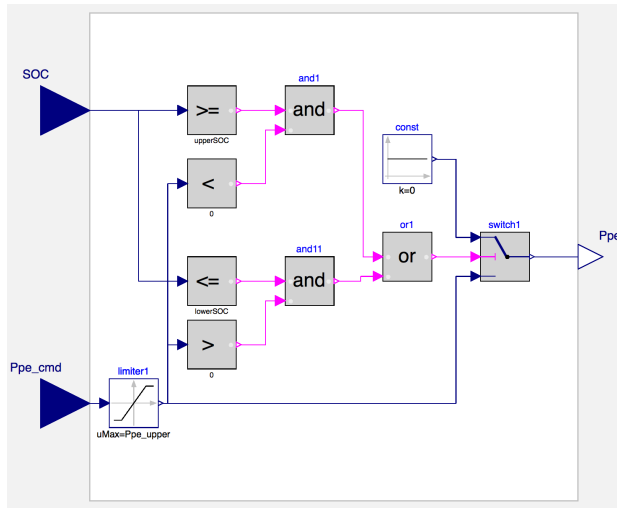


Figure D.20: Implementation of the storage protection.

D.9 Transformer model

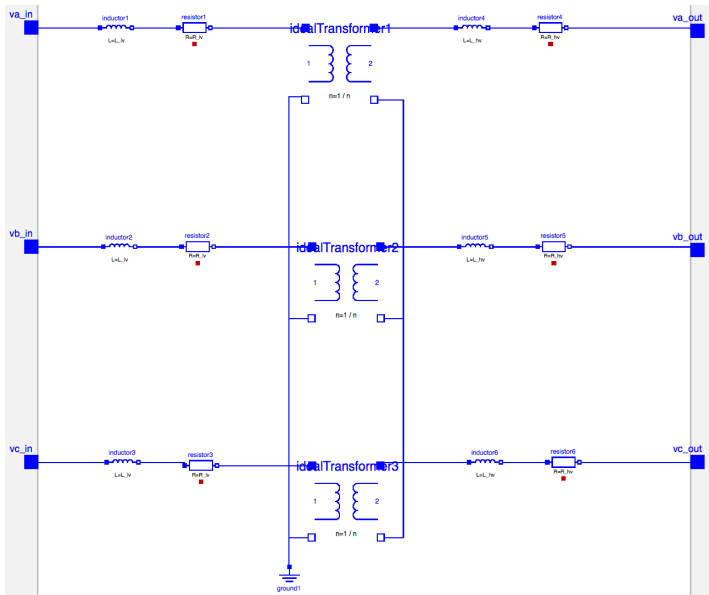


Figure D.21: Implementation of the transformer model in OpenModelica.

Appendix E

System parameters

This section includes the parameters used in all models in Test cases 1 to 3.

E.1 HVDC parameters

E.1.1 MMC parameters

Table E.1: MMC parameters

Parameter	Value
Base power	1059 MVA
Nominal voltage	333e3 V
Base voltage	271 893 V
Base DC voltage	640 000 V
Base frequency	50 Hz
Arm inductance, L_a	0.05 H
Grid side inductance, L_f	0.06 H
Arm resistance, R_a	0.001 Ω
Grid side resistance, R_f	0.001 Ω
Sub-module capacitance, C_{sm}	0.01 F
Number of sub-modules, N	400
DC capacitance, C_{dc}	1.672e-6 F

Table E.2: MMC controller parameters

Parameter	Value
Proportional gain, current controller	1
Time constant, current controller	1/100 s
Proportional gain, Power controller	0.1
Time constant, Power controller	1/50 s
Power controller power droop constant, MMC1	1
Power controller voltage droop constant, MMC1	1/3
Power controller power droop constant, MMC2	1
Power controller voltage droop constant, MMC2	1/10
Power controller power droop constant, MMC3	1
Power controller voltage droop constant, MMC3	1
Proportional gain, circulating current controller	-1
Time constant, circulating current controller	1/100 s
Proportional gain, energy controller	10
Time constant, energy controller	1/10 s
Initial stored energy	10.24 MJ

E.1.2 Cable parameters

The parameters used for the cable are the same as the parameters used in reference [99], where an HVDC connection of similar power levels as those used in this Thesis was considered. Note that the parameters are divided by 5 and used in 5 pi-sections. Although this does not correspond to the vector fitting method described in Chapter 5, this was the best data available.

Table E.3: Cable parameters

Parameter	Value
R_{11}	1.1724e-1 Ω/km
R_{12}	8.2072e-2 Ω/kmV
R_{13}	1.1946e-2 Ω/km
G_l	7.6330e-11 S/km
C_l	0.1983e-6 F/km
L_{11}	2.2851e-4 H/km
L_{12}	1.5522e-3 H/km
L_{13}	3.2942e-3 H/km
Cable length	100 km

E.2 Wind farm parameters

Table E.4: Wind farm parameters

Parameter	Value
Turbine rated power	7 MW
Total turbine inertia, J	4e6 kg m ²
Friction constant, B	2e3 Nm/(rad/s)
Blade length	75 m
Blade angle time constant	1 s
Optimal tip speed ratio	8.1 rad/s/m/s
Number of turbines in wind farm 1	70
Number of turbines in wind farm 2	60
Maximum C_p	0.48

Table E.5: Wind turbine controller parameters

Parameter	Value
Proportional gain, speed controller	1e6/0.1
Integral gain, speed controller	1e6/0.1/10
Kt, speed controller	1
Upper and lower limit, speed controller	5e6, 0
Proportional gain, pitch controller	2.5/1e6
Integral gain, pitch controller	30/1e6/100
Kt, pitch controller	1
Upper and lower limit, pitch controller	30, 0

E.3 Energy storage parameters

Table E.6: Energy storage parameters

Parameter	Value
Rated power, P_{rated}	250 MW
Rated charging/discharging time, t_{rated}	1 hour
Charge/Discharge efficiency, η	0.9304
Rated storable energy	$P_{rated} \cdot t_{rated}$ J
Upper SOC limit	0.9
Lower SOC limit	0.2
Delay time constant	10ms

Additional results

F.1 Test case 2: Dimensioning of energy storage

This section shows some additional results related to Test case 2 to illustrate the dimensioning process of the energy storage that led to the values of $T = 1000s$ for the filter time constant and $P_{rated} = 250MW$ for the rated power of the energy storage that is further used in test case 3.

F.1.1 Varying filter time constant with $P_{rated} = 250MW$

The first tweak to test case 2 is to show the effects of changing the filter time constant. Two simulations are performed in addition to one with the final values.

Figure F.1 shows the effect on the combined power from the wind farm and storage when keeping the rated power of the energy storage at the final value of 250MW. As can be seen from the results, the final value of the filter time constant of $T = 1000s$ has the smoothest power profile.

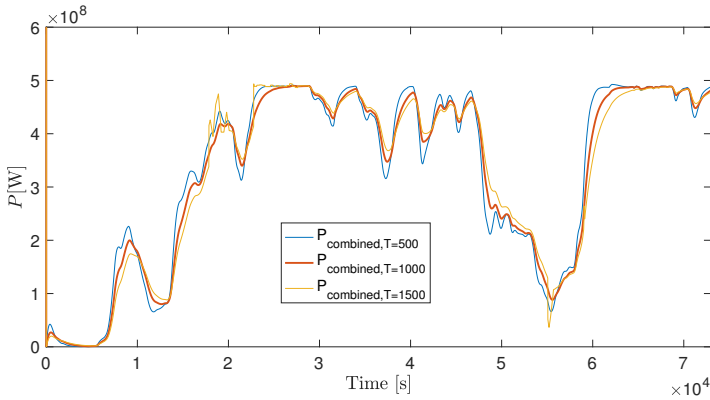


Figure F.1: Effects on the combined wind farm and storage power when varying the filter time constant of Test case 2.

One interesting event in Figure F.1 is right before $t = 2e4s$ where the power curve for $T = 1500s$ starts fluctuating more rapidly, which is the opposite of the desired behavior. This event can be explained by looking at the state of charge in Figure F.2 where the curve for $T = 1500s$ hits the upper limit of 0.9 around that time. This means that the storage unit cannot be further charged, and any excess power goes directly to the output. In other words, higher filter time constants put higher demands on the energy storage, and, therefore, it has to be dimensioned according to the storage rated power.

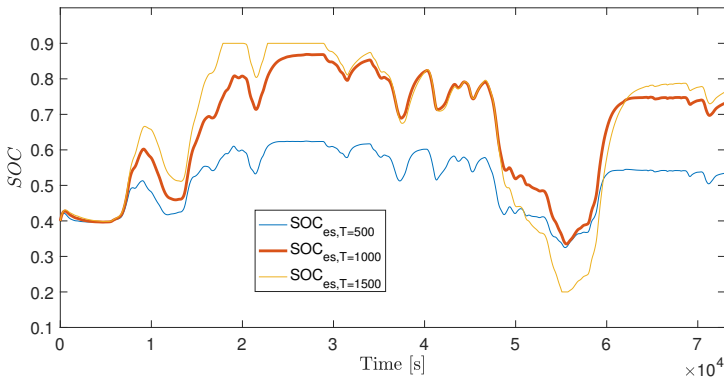


Figure F.2: Effects on the SOC when varying the filter time constant of Test case 2.

Figure F.2 also shows how the final values are those where the energy storage system is best utilized. If the time constant becomes too small, as with $T = 500s$, the energy storage system is not utilized to its fullest, because the state of charge is nearly constant. This may indicate that the storage unit is over-rated.

F.1.2 Varying P_{rated} with constant filter time constant

The following results aim to show the effects of changing P_{rated} while the filter time constant is kept at the final value of $T = 1000s$.

Figure F.3 shows how decreasing P_{rated} leads to a less smooth power curve because the energy storage can not deliver nor absorb enough power to smooth the power from the wind. Additionally, increasing P_{rated} from an already well-dimensioned power level of $P_{rated} = 250MW$ does not have any effect. This is because the required power is already delivered and absorbed, and it does not change by increasing the maximum available power.

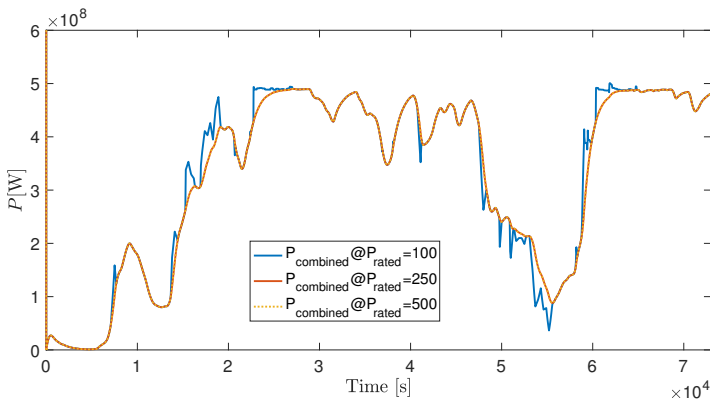


Figure F.3: Effects on the combined wind farm and storage power when varying the rated power of the energy storage in Test case 2.

Figure F.4 complements the description of the power results by showing how the SOC for the case with the lowest P_{rated} caps at the maximum SOC of 0.9 and the minimum SOC 0.2, thus it can not deliver nor absorb the power needed. The plot for the higher P_{rated} also indicates that the storage may be over-rated.

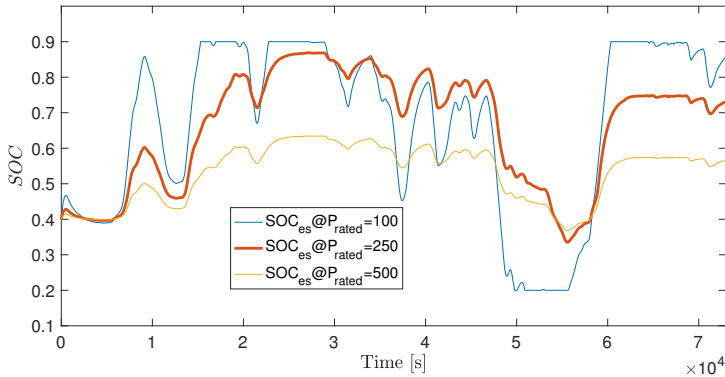


Figure F.4: Effects on the SOC when varying the rated power of the energy storage in test case 2.

F.1.3 Increasing both filter time constant and P_{rated}

For further illustrative purposes, the rated power of the energy storage is increased to $P_{rated} = 500\text{MW}$ to match the rated power of the wind farm at 490MW . The time constant was increased accordingly to see how much smoother the combined power output could become with these values. Figure F.5 shows the effects on the combined power, where the new values, plotted in orange, are compared to the selected values for test case 3 of $T = 1000\text{s}$ and $P_{rated} = 250\text{MW}$. The results show a slightly smoother power profile, and Figure F.6 of the state of charge shows that the combination of values leads to good utilization of the energy storage device. These results will be further discussed in Chapter 7.

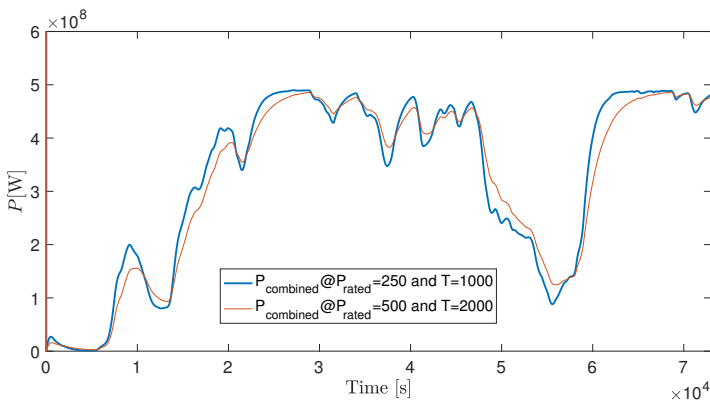


Figure F.5: Effects on the combined wind farm and storage power when increasing both the filter time constant and the rated power of the energy storage in Test case 2.

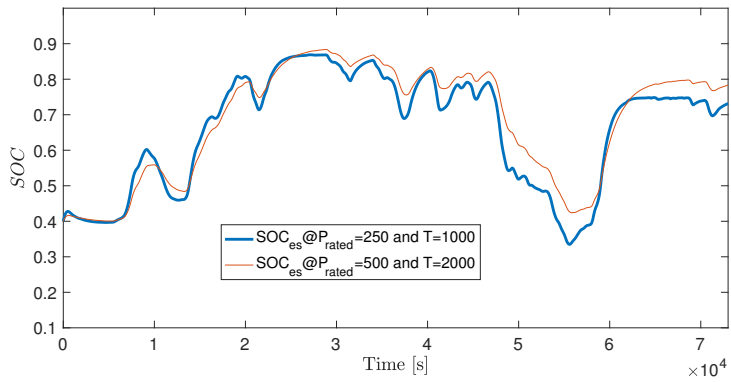


Figure F.6: Effects on the SOC when increasing both the filter time constant and the rated power of the energy storage in Test case 2.

Appendix **G**

OSSES2019 paper

This appendix contains the paper that was submitted and accepted for presentation at the OSSES2019 conference based on this Thesis and Erling Vatn Tranulis's Thesis. The paper starts on the next page.

Modeling of Multiterminal HVDC Offshore Grids with Renewable Energy and Storage Integration by Opensource Tools

Joachim Espvik
*Department of Electric
Power Engineering,
Norwegian University of
Science and Technology*
Trondheim, Norway
joachim_espvik@hotmail.com

Erling Vatn Tranulis
*Department of Electric
Power Engineering,
Norwegian University of
Science and Technology*
Trondheim, Norway
erling.v.t@gmail.com

Elisabetta Tedeschi
*Department of Electric
Power Engineering,
Norwegian University of
Science and Technology*
Trondheim, Norway
elisabetta.tedeschi@ntnu.no

Santiago Sanchez Acevedo
*Energy Systems
SINTEF Energy Research
Trondheim, Norway*
santiago.sanchez@sintef.no

Abstract—With increasing offshore wind penetration levels, more secure and flexible offshore electrical transmission systems are needed to ensure security of supply to onshore users. When considering long distances of electrical power transmission, HVDC grids based on the modular multilevel converter (MMC) are a solution for present and future large scale offshore wind integration. As HVDC grids are developing into large and complex systems, dynamic analysis of the systems is useful to gain knowledge on the interactions between the different components in the grids. This paper uses the open source tool OpenModelica as modeling environment to demonstrate the potential of the tool in modeling such HVDC systems. A three-terminal HVDC system with offshore wind and energy storage integration is implemented in OpenModelica, and the dynamics of the system are investigated through four simulation cases. The main focus of this paper is dynamics and operation related to the HVDC system. The simulation results show that the MMCs can improve the most rapid power fluctuations using its internal storage capabilities, while an external energy storage system provides a more constant power flow over more extensive periods, in addition to improving the operation of the HVDC system. All models used in this paper are made publicly available to anyone for any purpose, including future studies of larger HVDC grids.

Index Terms—Offshore wind power, Energy storage system, Multiterminal HVDC, MMC, Open source, OpenModelica, Dynamic modeling, Transient simulations

I. INTRODUCTION

Over the last 10 years, the installed capacity of offshore wind power has dramatically increased from 1 to 18 GW in Europe [1]. Furthermore, projections of future installation levels coupled with economic considerations and maritime spatial planning predict increasing distances to shore of future offshore wind farms [2], [3]. When transporting electrical energy in submarine cables over such long distances, economic and technical considerations make high-voltage direct current (HVDC) the preferred choice for electrical power transmission [4].

This work was partly funded by the Norwegian Research Council and DNV-GL through the NFR contract n. 250493 - within the Integrated approach to the Design and Control of Offshore HVDC Networks (IDeCON) project.

As the number of wind farms with HVDC connections to shore increases, the power system also becomes increasingly dependent on secure power supply through these HVDC connections. To ensure security of supply from these wind farms, it is useful to connect the HVDC terminals in an offshore HVDC grid [5]. This increases the flexibility of the system, as power flows in HVDC grids can be rerouted through different paths to shore. This allows power transfer from the wind farms to shore even if one of the HVDC connections is out of operation, thus, increasing the reliability of the system.

In such HVDC grids, the modular multilevel converter (MMC) is becoming the preferred power electronic converter for converting between AC and DC due to its many benefits [6]. The MMC is capable of reversing the power flow without reversing the polarity of the DC voltages by DC current reversal. Additionally, features like modularity and scalability make the MMC advantageous compared to other voltage source converter (VSC) topologies. The MMC also has an inherent capability of storing energy internally in the converter [7], which can benefit the system in which it is connected.

Another crucial aspect for offshore wind power integration is the varying power production due to the intermittency in wind speed. The varying power production from wind farms can be classified into three categories [8]. The first being the most rapid variations due to, e.g., wind gusts on the time scale of seconds. The second variation is short-term variations on the scale of minutes to hours while the third and last variation is seasonal variations. To meet this challenge, an energy storage system can be integrated into the HVDC grid to complement the power production from the offshore wind farms and further improve the overall system.

However, because HVDC grids are developing into large and complex systems with many different components, it is useful to test the system to gain knowledge on the interactions between the various components. When investigating the dynamics and testing the controllers of such large systems, it is not directly feasible to run tests on full-scale systems.

Therefore, hardware-in-the-loop (HIL) testing is often used to test HVDC grids in laboratory environments [9]. HIL combines software based simulation models that replicate the behavior of the physical components with actual physical components.

The Modelica modeling language is a tool especially used in the automobile industry for HIL testing [10], [11]. An emerging tool based on the Modelica language is OpenModelica, which is open-source and allows integration of models developed in different physical domains. Additionally, OpenModelica supports the Functional Mock-up Interface (FMI) standard that allows models developed in OpenModelica to be shared across multiple platforms and tools, and be used in, e.g., HIL testing. This makes the modeling of an HVDC grid in OpenModelica a timely investigation area, including possibilities for laboratory testing and verification.

In this paper, a model of a three-terminal HVDC grid with offshore wind and energy storage integration, including MMCs, HVDC cables, wind farms, and an energy storage system, is analyzed and implemented in OpenModelica. The topic of energy storage integration in the HVDC grid is investigated using simulations of the system to demonstrate the potential of the open source tool in such analyses. Additionally, the internal storage capabilities of the MMC are studied to investigate how the MMC can contribute to the HVDC grid support compared to an external offshore energy storage system.

As an additional contribution to the knowledge community, all models introduced in the paper are made publicly available to anyone for any purpose through the following URL: <https://github.com/joachimesp/OpenModelica-HVDC-NTNU>. Additionally, an MMC model and a point-to-point HVDC model built for Opal-RTs real-time simulator, ePHASORSIM, are added to the folder for illustration purposes on how to build models for the real-time simulator. This allows models to be used in future laboratory experiments with HIL testing.

Further details of the models developed and test cases presented hereafter can be found in [12], [13].

The remainder of the paper is organized as follows: Section II introduces the OpenModelica software with the description of a preliminary assessment of its performance. Next, Section III describes the three-terminal HVDC system with all models used to build the system. Section IV introduces the different simulation cases, their purpose, and results. Section V includes a discussion and Section VI concludes.

II. THE OPENMODELICA SOFTWARE

The Modelica modeling language is a vendor-independent standard, thus there exists multiple implementations of modeling tools using the modeling language, such as Dymola, MathModelica and IDA. However, these implementations are not open source, which makes OpenModelica an emerging tool.

One of the features used in this paper was the use of electrical components in the built-in standard library of OpenModelica. This reflects the acausal modeling approach in the

software, meaning dynamics of an electrical circuit can be modeled by drawing the circuit with circuit components and not with generic blocks as in causal modeling.

Preliminary tests were carried out to verify that OpenModelica is able to capture high frequency dynamics in the range of several kilohertz. This was done by building two 10kHz 2L-VSC models, one in OpenModelica and one in MATLAB Simulink to compare their results. The tests showed that the captured dynamics of the two models were very similar [12], [13]. Since such dynamics are of significantly higher frequency than the simulations in this paper, it was assumed that OpenModelica could accurately capture all dynamics of interest.

III. SIMULATION SYSTEM DESCRIPTION

The final goal of this paper is to investigate the dynamics of the system in fig. 1 by implementing it in OpenModelica. The topology is chosen because it is the system with the lowest complexity that allows studying the interactions between the key components in an HVDC grid, including an energy storage system.

The system in fig. 1 includes two wind farms, WF1 and WF2, three HVDC MMC converters connected by two HVDC cables and an energy storage system (ESS) connected near WF2.

WF1 consists of 70 turbines with a rated power of 7MW each, while WF2 consists of 60 turbines with a rated power of 7MW each. Both cables are of 100km length. The rated values of the energy storage will be dimensioned in simulation case 2 later in the paper. A table with all the key parameters used in the different models is included in the Appendix. For further details on the controller parameters used in this paper, the reader can refer to the appendices in [12], [13].

The models used for each component are presented in this section.

A. Energy-based MMC model

As explained in the introduction, the MMC is one of the key components in an HVDC grid, and it is used for converting between AC and DC in the grid. Figure 2 shows a schematic of the circuit of the MMC that is built of multiple submodules.

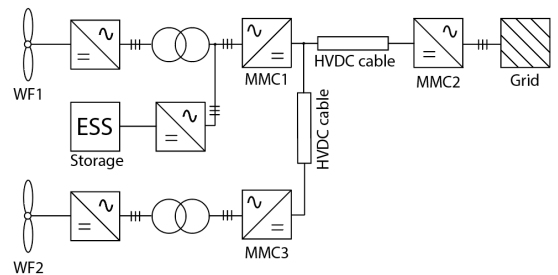


Fig. 1. Three-terminal HVDC system with offshore wind and storage integration under analysis.

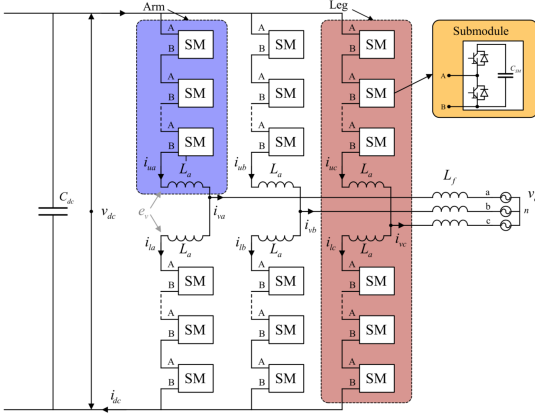


Fig. 2. A schematic of the MMC from [15].

Each submodule is, in this case, a half bridge with two IGBTs and a capacitor. Additionally, the MMC consists of an arm inductor for each arm, L_a , and an inductor on each phase of the AC-side, L_f . The MMC is operated such that the voltage of each submodule is inserted at the output voltage in steps, resulting in a waveform close to a sine on the AC-side, e_v . The output voltage waveform is generated with respect to the grid voltage, represented by voltage sources in the schematic, to produce a flow of active and reactive power across the grid side inductors.

In [14], a comparison of all available MMC models in the literature with varying level of complexity was done, and the conclusion led to a recommendation for using average value models for network-level studies. Average models are more computationally efficient compared to the more complex models, and they can reproduce the dynamics of the MMC accurately without detailed modeling of the internal structure of the MMC. Average models represent the MMC through controllable voltage and current sources on the AC and DC side, effectively meaning that effects of the pulse width modulation within the converter are averaged out over the switching period.

Furthermore, in this paper, the contribution of the internally stored energy in the MMC is studied. Therefore, an energy-based MMC model that includes the dynamics of the internally stored energy in the MMC was chosen.

When deciding on the how to model the MMC, it was desirable that the model should have steady state time invariant (SSTI) states. SSTI states facilitate linearized state space representations for eigenvalue analysis. Although this feature was not directly utilized in this work, it still makes the model more attractive for members of the industry and researchers wishing to make use of such techniques for stability analysis or tuning purposes. Furthermore, this makes control of the model easier.

Hence, the simplified zero-sequence MMC model from [15]

was chosen. The model couples states that oscillate at the same frequency in equation sets, which are subsequently transformed into a synchronous rotating reference frame (SRF). It is assumed that the modulation indices are calculated in a manner which compensates for the oscillations in the circulating voltage, referred to as "compensated modulation" [15]. This modeling approach is of great utility when deriving energy-based MMC models that provide great insight into the energy dynamics they introduce [16].

B. The energy-based model schematic

Figure 3 shows the overview of the circuit implementation of the model as well as the associated control schemes.

The AC-side of the MMC is represented by a stiff grid voltage, v_g^{abc} , equivalent AC resistances, $R_{eq} = R_f + \frac{1}{2}R_a$, and inductances, $L_{eq} = L_f + \frac{1}{2}L_a$, as well as a controlled voltage source, e_v^{abc} , representing the voltage driving the AC-side currents, i_v^{abc} . The currents on the AC-side are controlled by an inner vector control of the transformed dq-currents [17]. The reference for the d-current comes from the outer power controller with DC voltage droop based on the measured power, P_{dc} , and voltage, V_{dc} . Droop control allows multiple MMCs in the grid to contribute to the DC voltage regulation. In this study, only the active power of the converter was of interest, and therefore, the reference for the q-current, controlling reactive power, was set to zero for all simulations executed in this paper.

The AC- and DC-sides are coupled using an energy balance equation, which accounts for the internal energy storage capability of the MMC, by modeling the zero-sequence energy sum, $w_{\Sigma,z}$ based on the equivalent arm capacitance, C_{eq} . This energy is controlled using a zero-sequence energy sum controller, including a controller for the circulating current, i_{cz} .

The DC-side is modeled using a controllable voltage source for the circulating voltage, $v_{c,z}$, as well as equivalent arm resistances, $\frac{2}{3}R_a$, and inductances $\frac{2}{3}L_a$, and a DC-side capacitor, C_{dc} . The current source in fig. 3 represents, e.g., the DC current from another MMC in a point-to-point HVDC connection.

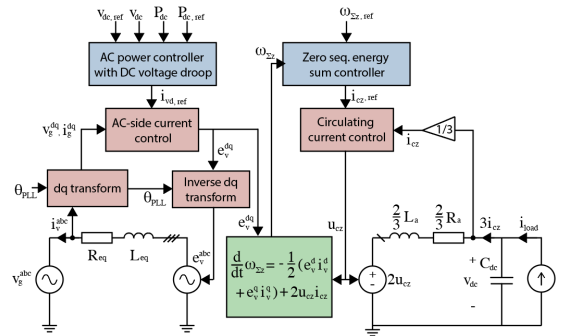


Fig. 3. Overview of the MMC model.

C. Wind farm model

The wind farm model is represented in aggregated form based on the dynamics of a single wind turbine, assuming all turbines are operated equally. Figure 4 shows a schematic including the variables used in the turbine model.

The basis for the model is the dynamic equation for torque balance between the turbine blades, T_{wind} , the electrical generator, T_{gen} , the frictional torque, $B\omega$, and the torque associated with the acceleration of the turbine and generator $J\frac{d}{dt}\omega$ which can be expressed as follows:

$$J\frac{d}{dt}\omega = T_{wind} - T_{gen} - B\omega \quad (1)$$

where J is the total inertia in turbine and the generator and ω is the rotational speed of the turbine.

The turbine mechanical power, $P_{turbine}$, can be expressed by the turbine torque, T_{wind} , as

$$P_{turbine} = \omega T_{wind} \quad (2)$$

Alternatively, the turbine power can be expressed as a fraction of the power available in the wind through the power coefficient C_p .

$$P_{turbine} = C_p P_{wind} = C_p \frac{1}{2} \rho A u^3 \quad (3)$$

where ρ is the air density, A is the area swept by the blades and u is the wind speed.

When considering the aerodynamics of the turbine blades, it is useful to define the tip speed ratio λ as:

$$\lambda = \frac{\omega \ell}{u} \quad (4)$$

where ℓ is the length of the turbine blades.

The power coefficient represents the aerodynamics of the turbine blades, and it can be expressed as a function of the tip speed ratio λ and the blade angle β representing the pitch of the blades [18]:

$$C_p(\lambda, \lambda_{ai}, \beta) = 0.5176 \left(\frac{116}{\lambda_{ai}} - 0.4\beta - 5 \right) \exp\left(\frac{-21}{\lambda_{ai}}\right) + 0.0068\lambda \quad (5)$$

where

$$\lambda_{ai}(\lambda, \beta) = \left(\frac{1}{\lambda + 0.08\beta} - \frac{0.035}{\beta^3 + 1} \right)^{-1} \quad (6)$$

Because this paper models the wind farm in an aggregated form, a gain representing the total number of turbines, $N_{turbines}$, is added to the power output from the model.

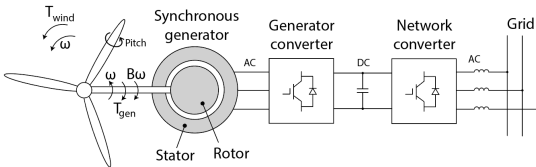


Fig. 4. A schematic of a Type IV turbine showing the basic variables used in the turbine model.

1) *Turbine controllers:* The turbine model has two control loops: one speed controller and one pitch controller.

The speed controller controls the torque of the electrical generator to regulate the speed of the turbine. This is done to maintain an optimal tip speed ratio, λ , optimizing the power coefficient, C_p , for wind conditions up to the rated wind speed, u_{rated} .

The pitch controller is activated for wind conditions above the rated wind speed. It is used to control the blade angle, β , to shed excess power when the wind speeds are above the rated value.

D. Energy storage model

The energy storage model consists of three power flows; one describing the output from the power electronics, P_{pe} , one describing the losses in the storage system, P_{loss} and one power flow that represents the power at the storage terminals, P_{es} . The equations describing the storage system are as follows:

$$P_{es} = P_{pe} + P_{loss} \quad (7)$$

$$W_{es} = \int -P_{es} \quad (8)$$

$$SOC = \frac{W_{es}}{W_{rated}} \quad (9)$$

$$0 \leq SOC \leq 1 \quad (10)$$

where SOC is the state of charge, describing how much of the total capacity the storage unit is charged, and W_{es} is the accumulated energy stored in the unit.

Two charging states of the storage unit are defined; a charging and a discharging state. The equations describing the storage unit when it is discharging are:

$$P_{pe} > 0 \quad (11)$$

$$P_{pe} = \eta \cdot P_{es} \quad (12)$$

$$P_{loss} = \left(\frac{1}{\eta} - 1 \right) \cdot P_{pe} \quad (13)$$

where η is the charging and discharging efficiency of the energy storage system, hence assumed to be equal.

Next, the equations describing the unit when it is charging are:

$$P_{pe} < 0 \quad (14)$$

$$P_{es} = \eta \cdot P_{pe} \quad (15)$$

$$P_{loss} = (\eta - 1) \cdot P_{pe} \quad (16)$$

Also, to represent the delay in the storage system, a first-order transfer function is added to the power output of the storage. The filter time constant use in this paper is $T_{delay} = 10ms$. This is a small time constant that represents a fast energy storage system as, e.g., electrochemical energy storage systems. Examples of such electrochemical energy storage systems are lithium-ion and lead-acid [19], [20].

Additionally, a storage protection system is added to limit the state of charge between 20% and 90%. Also, the protection system prevents the storage system from charging and discharging beyond the rated power.

E. HVDC cable model

The HVDC cable used for this study is a circuit representation of a frequency dependent cascaded pi representation from [21]. This model captures the behavior of the frequency dependent parameters as resistances and inductances for a wide range of frequencies in addition to the effects of the hyperbolic correction factors in an actual cable. These aspects can be crucial in long cable implementations such as those used in offshore applications.

IV. SIMULATION CASES AND RESULTS

A. Simulation case 1: Contribution of the MMC through the internal storage

Since the MMC contains several submodules connected in cascade, each comprising a capacitor, the MMC has some energy storage capability characterized by short charge and discharge periods. Control of this stored energy could thus be executed to improve power dynamics that occur over relatively short periods ranging from milliseconds to a couple of seconds depending on the energy requirement.

To investigate the support capability of the MMC with regards to power dynamics, two test cases were simulated. In the first test-case, the MMC attempts to smoothen out power variations arising from the turbine dynamics caused by wind speed fluctuation. In the second, the MMC attempts to reduce the response time of the HVDC system upon a step in power reference.

1) *Responding to turbine dynamics:* To investigate the improving impact an MMC can have on the power dynamics of a wind turbine caused by wind speed fluctuation, this aspect of fig. 1 was investigated using the isolated sub-system, corresponding to the model depicted in fig. 5.

The wind speed was varied around the rated wind speed of the controllers with a maximum variation of $0.2m/s$ to induce power fluctuation relating to the turbine dynamics. The controller used to determine $w_{\Sigma,z,ref}$ was a PI controller, taking $P_{WF} - P_{ref}$ as input. To ensure that the controller did not deplete the capacitors, the admissible energy range was determined to be $0.7 \leq w_{\Sigma,z,ref} \leq 1.3$. The simulation was run twice. The first time the aforementioned control was implemented and in the second, $w_{\Sigma,z,ref}$ was set equal to 1, i.e. no contribution from the internal storage in the MMC.

2) *Results:* The power delivered to the grid, together with the p.u. wind speed and rotational speed of the wind turbine, are depicted in fig. 6.

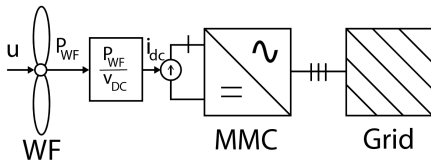


Fig. 5. Test case used to isolate the power dynamics of the turbine and MMC for Simulation case 1.

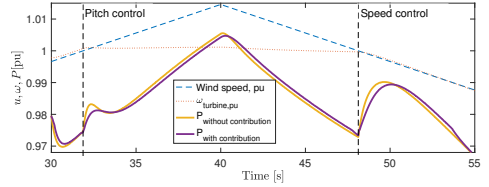


Fig. 6. Response of the powers delivered to the grid with and without contribution from the MMCs internal storage for Simulation case 1.

The most interesting section of this power dynamic is for $30s \leq t \leq 35s$. During this period, the wind speed increases from below the rated value, i.e. the threshold value for the pitch controller to above the threshold value. Upon crossing this threshold, the turbine operation is changed from speed control to pitch control. The pitch angle controller is activated to shed the excess power. However, because of the delay of 1 second associated with the pitching of the blade angles, for a small time period, this extra power is fed into the converter. Additionally, the speed controller decelerates the angular velocity of the turbine releasing some of its kinetic energy.

When $w_{\Sigma,z,ref}$ is kept constant at 1 pu, this power fluctuation flows directly through the converter without being absorbed. However, when the converter is allowed to vary $w_{\Sigma,z,ref}$, this excess energy is absorbed by the converter, (fig. 7). This dampens the power fluctuation by reducing the fluctuation from 0.009 p.u. to 0.006 p.u.

Subsequently, while $t \leq 48s$ the wind speed increases and decreases within the same control region. When the wind speed increases the converter absorbs energy and when the wind speed falls the converter releases energy, as shown in fig. 7. However, the time periods are so long that this energy absorption (and release) only manifest as a negligible impacts on the power response, see fig. 6.

When $48s \leq t \leq 54s$, the wind speed is reduced below the threshold value, and the speed controller is activated. Thus, the rotational speed of the turbine decelerates releasing some of the rotational kinetic energy stored in the inertia of the turbine to be converted and released as electrical energy into the converter. Once again, the energy absorption only causes negligible impact on the power profile. Afterwards, the converter has reached its lower energy limit and cannot release more energy. Therefore, the two power profiles converge.

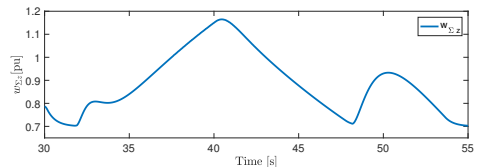


Fig. 7. Response of the internal stored energy in Simulation case 1.

3) *Response to steps in power reference:* To investigate if the MMC could improve the power step response of the HVDC system, the sub-system depicted in fig. 8 was analyzed.

MMC2 controls the power flow to Grid 3. A step in power reference from 0.7 to 0.8 was executed at $t = 1$ s. The simulations were run twice. During the first simulation $w_{\Sigma,z,ref}$ was controlled by a PI controller and in the second $w_{\Sigma,z,ref}$ was set equal to 1.

4) *Results:* Figure 9 shows the difference in response of the internal energies of the MMC when using the two control strategies.

The p.u. powers delivered to Grid 3 are displayed in fig. 10 with and without control of $w_{\Sigma,z,ref}$, thereby with and without contribution from the MMCs internally stored energy.

As can be seen, when the energy controller controls $w_{\Sigma,z,ref}$ to release energy upon a step in the power reference, the stored converter energy starts to decline and the output power of the converter reaches the power level around its reference faster than when $w_{\Sigma,z,ref}$ is set constant to 1 pu.

In both cases, $w_{\Sigma,z,pu}$ declines upon the step, causing the power leaving the converter to exceed the power entering the converter from the HVDC cable. However, when $w_{\Sigma,z,ref}$ is maintained at 1, the rate of change of the converter energy declines after 1 ms. Therefore, the difference between the power delivered to the grid and the power entering the converter decreases, until the converter starts to recharge at $t = 4.3$ ms after the step. Because of the recharging of the converter, there is some additional delay before the converter output energy rises again, but subsequently, it exponentially approaches its reference. When $w_{\Sigma,z,ref}$ is controlled, the power delivered to the grid overshoots and subsequently oscillates below its reference. This oscillatory behaviour was reduced in [13], by releasing the energy in an exponentially decaying manner based on the size of the step in power reference. This reduced the overshoot from 14% of the step size to 6% of the step size and reduced the undershoot by almost 3 orders of magnitude.

This simulation shows that control of the zero-sequence energy can reduce the power step response time of the HVDC system.

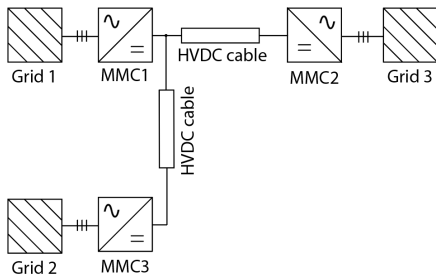


Fig. 8. System build to investigate MMC induced improvements of power step responses of HVDC systems for Simulation case 1.

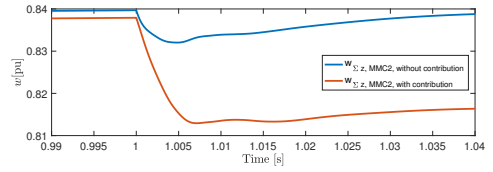


Fig. 9. Response of the stored energy in the MMC for Simulation case 1.

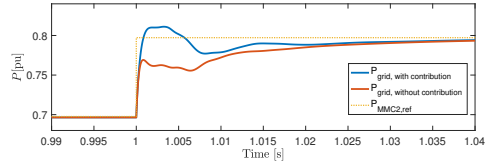


Fig. 10. Response of powers in the system for Simulation case 1.

B. Simulation case 2: Energy storage dimensioning

Simulation case 2 aims at pre-sizing the energy storage system before it is integrated into the three-terminal HVDC system in Simulation case 3. Simulation case 2 uses a configuration where the power from the wind farm is filtered through a large first order filter, as shown in fig. 11. The difference between the filtered power and the actual power is sent as a reference for the energy storage system. This way, the combined power from the wind farm and the energy storage will have a much smoother profile than the power from the wind farm alone when the energy storage and the filter are properly dimensioned.

To dimension the energy storage rated power, the real wind speed profile shown in fig. 12 was used. These are actual wind speed data measured at Roosevelt station over approximately 20 hours.

1) *Results:* Figure 13 shows the power from WF1, the power from the energy storage, and the combined storage and wind farm power output after dimensioning of the energy storage rated power and the filter time constant.

These results and the interaction between the wind farm and the energy storage were considered satisfactory and led to the choice of a P_{rated} of 250MW for the energy storage, assuming a time constant of $T = 1000$ s for the first order filter used to filter the power output from the wind farm.

Additionally, the state of charge was used as an indicator

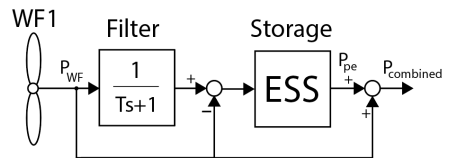


Fig. 11. Simulation setup for Simulation case 2.

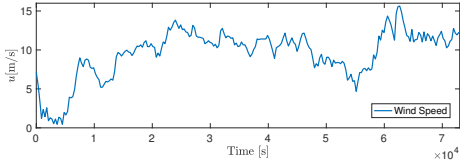


Fig. 12. The wind speed variation used for dimensioning.

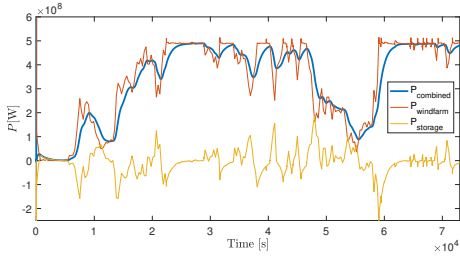


Fig. 13. Power from wind turbine, energy storage and combined power from Simulation case 2.

during the process of finding the rated values. From fig. 14, it can be seen that the state of charge varies in the whole range between its limits of 0.2 and 0.9 without capping at the limits during the simulation. This was regarded as an indicator that the storage was not over- nor under-dimensioned, resulting in proper utilization of the available capacity.

C. Simulation case 3: Three-terminal HVDC system with wind power and energy storage integration

To study the short term effects of integrating an energy storage system offshore near one of the wind farms in fig. 15, the configuration of Simulation case 2 was added to WF1 and the energy storage system in the final simulation system showed in fig. 15.

The offshore AC-grids are modeled by voltage sources as stiff grids, and the power outputs from the wind farm models and energy storage model are applied at the references of their respective MMC.

Two events are introduced to study the differences in responses of the system when an event occurs at WF1 with an energy storage system nearby and WF2 without an energy storage system. A sudden drop in wind speed from 10 m/s to

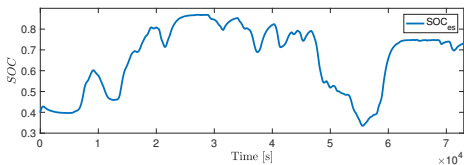


Fig. 14. The state of charge (SOC) of the energy storage from Simulation case 2.

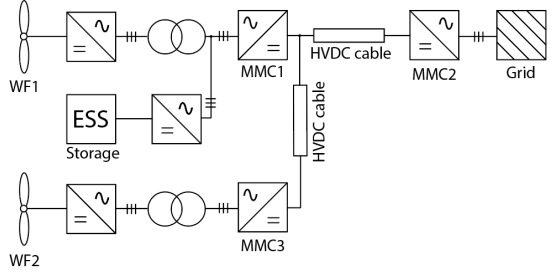


Fig. 15. Simulation system of Simulation case 3. Figure 1 repeated for convenience.

5m/s is introduced first at WF1 at $t = 30$ s then at WF2 at $t = 60$ s.

In this simulation case, $w_{\Sigma,z,ref}$ is kept constant at 1pu for all of the MMCs.

1) *Results:* Figure 16 shows the response of the power from WF1, WF2 and the energy storage when a sudden drop in wind speed is introduced. From the figure, it can be seen how the energy storage system quickly reacts after the power from WF1 drops, to maintain a *more* constant power to MMC1.

Figure 17 shows the response of the MMC powers under the same conditions. From the figure it can be seen how the power delivered to shore from MMC2 is *more* constant when there is a drop in wind speed at WF1 with an energy storage system compared to when there is a drop at WF2, which has no energy storage system.

Figure 18 shows the response of the DC voltages at the MMC terminals when a sudden drop in wind speed is introduced. It can be seen that the response of the DC voltages is improved for the event at WF1 at $t = 30$ s compared to the event at WF2 at $t = 60$ s due to the fast contribution of

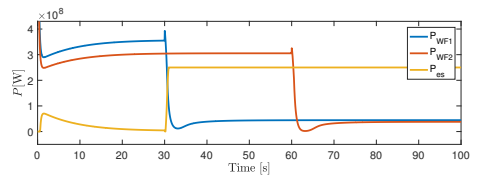


Fig. 16. The response of the wind farm powers and energy storage powers when two sudden drops in wind speed are introduced in Simulation case 3.

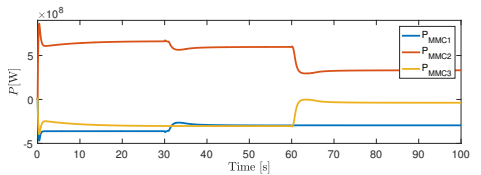


Fig. 17. Response of the MMC powers during two sudden drops in wind speeds is introduced in Simulation case 3.

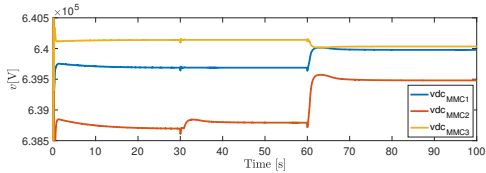


Fig. 18. The response of the DC voltages during two sudden drops in wind speeds is introduced in Simulation case 3.

the energy storage system. In the first case, the *more* constant power output from MMC1 means that the DC voltage levels do not have to be adjusted when there is a drop in the wind speed compared to the case when the wind speed drops at WF2.

Figure 19 shows the response of the zero-sequence energy sum in the MMCs when a sudden drop in wind speed is introduced. The response of the energies are also improved for the case of an event at WF1 at $t = 30$ s compared to WF2 at $t = 60$ s due to the fast contribution of the energy storage system.

V. DISCUSSION

A. The internal storage contribution of the MMC

As seen from the results, the internally stored energy in the MMCs is not large enough to account for the short term variations in the wind with the values used in this paper. However, the internal storage can be increased by either increasing the number of sub-modules in the MMC or by increasing the rated voltage of each sub-module or a combination of both.

However, because the MMC can improve fast responses as the step response of the converter, it may be beneficial to use the MMC to smooth the most rapid variations in the wind from e.g. wind gusts and tower shadowing, as studied in [22]. Possibly, these capabilities could also be used for other purposes such as power oscillation damping, improve voltage behaviour, increasing the life span of batteries by eliminating ripple or providing initial frequency response and system inertia [23]–[26].

B. Justification for offshore storage placement

In this study, the energy storage system was placed offshore near one of the wind farms. This was done to study the effects on the HVDC system when having a storage system

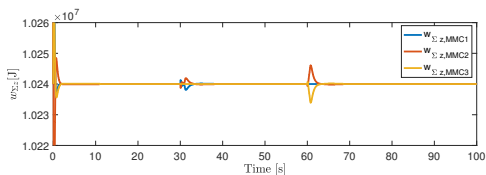


Fig. 19. The response of the zero-sequence energy of the MMCs during two sudden drops in wind speeds in Simulation case 3.

offshore, and directly compare a wind farm complemented with energy storage to a wind farm without energy storage. The configuration was practical for directly comparing the effects of events at both wind farms without changing the configuration of the system model.

Further, one can argue that in addition to improved operation of the HVDC system, the energy storage system can be placed offshore to fully utilize the flexibility of HVDC grids. By having the energy storage near the wind farm, the same constant power profile can be delivered regardless of the power flow direction to shore. This may be beneficial in cases where, e.g., different countries are connected by the HVDC grid. The offshore placement of the energy storage system allows the same power to flow to country x as country y , without having separate energy storage systems connected at the onshore terminals of both countries.

However, the topic of offshore versus onshore placement of the energy storage and its multiple techno-economic implications were not the main focus of this paper, and should, therefore, be addressed in separate studies.

C. Storage dimensioning

Dynamic simulations using only one wind speed series are used for pre-sizing of the energy storage system to be used further in the paper. As the dimensioning of the storage was not the main focus of this paper, the approach was chosen for its simplicity, and without presumption of generality, mainly to demonstrate one practical usage of simulations in the OpenModelica software. It should, therefore, be clarified that this approach is very simple compared to actual dimensioning of energy storage systems for real wind farms.

Also, the chosen rated power of the energy storage system was 250MW, which corresponds to around half of the rated power from the wind farm nearby, containing 70 turbines with a rated power of 7MW. The rated power from the energy storage system is therefore not enough to cover the rated power from the wind farm, and it is therefore just a complement to the wind farm production resulting in more constant operation. Economic considerations relating how this can be used to financially justify the ESS investment and considerations recommending a smaller energy storage system sizing were left outside the scope of this paper. The results from simulation case 2 when using a rated power of the same as the wind farm did not show a good enough increase in performance to justify the potential increases in costs of a larger energy storage system.

D. Using OpenModelica for real-time HIL testing

To further address the usage of the OpenModelica for model sharing through the Functional Mock-up Interface (FMI) standard and usage in real-time HIL testing, preliminary testing was performed at the National Smart Grid laboratory in Trondheim. A review of the available literature revealed the lack of information on how to build and prepare OpenModelica models for one of Opal-RT's real-time simulators, ePHASOR-SIM. However, a short guide inside the software was found,

but this guide lacked some important details. Therefore, this aspect was investigated further to increase the usefulness of the OpenModelica software in the context of modeling HVDC grids for real-time HIL testing.

Multiple models, including a model of an MMC and a point-to-point HVDC connection using MMCs were implemented in OpenModelica, exported for the real-time simulator and successfully run in a larger system model with the real-time simulator. The approach is further described in [12], [13], and by following the included guide, HVDC grid models developed in OpenModelica can be used for real-time HIL simulations for future experimental validation and testing. The guide found in [12], [13] adds to the information found inside the software.

The real-time simulation models are added to the aforementioned GitHub folder for illustration purposes. However, to have complete access to all components in the model, the Opal-RT Modelica Developer library is needed. This library is handed out by Opal-RT's customer support upon request.

VI. CONCLUSIONS

In this paper, a three-terminal HVDC system with offshore wind and energy storage integration was modeled in OpenModelica, including the key components in an HVDC grid. The paper started by introducing the open source modeling software OpenModelica with a preliminary assessment of the performance of the software. The software was tested for the fast dynamics of a switching model of a 10kHz 2L-VSC with comparison to Simulink. The results showed that OpenModelica successfully reproduced these fast dynamics.

Next, the models for the MMC, the wind farms, the HVDC cables, and the energy storage system were described and a description of the simulation cases studied in the paper was presented.

The first simulation case showed that the internal energy of an MMC can improve the step response of the active power delivered to the grid from a three-terminal HVDC system. Further, the second simulation case showed that the contribution of the MMCs is very small when considering short term variations in the wind. Therefore, it is recommended to consider using the MMC for smoothing the most rapid changes in power due to wind gusts, tower shadowing, etc.

The third simulation used real wind speed data to pre-dimension an external energy storage system to smooth the hourly variations in power production due to changes in wind speeds. Lastly, the fourth and final simulation case combined the three terminal HVDC system with two wind farms and an energy storage system to study the short term effects of having an energy storage system at one wind farm. The results using a fast energy storage system showed that the overall operation of the HVDC system was improved when using an energy storage system, leading to smaller transients in the responses of the DC voltage and internal energy storage when wind speeds suddenly dropped.

Additionally, models developed in the software were tested in the National Smart Grid laboratory with Opal-RT's real-time

simulator ePHASORSIM. This allows for future experimental testing and validation using HIL simulations.

All simulations were performed in the open source tool OpenModelica, and the models were made publicly available to anyone for any purpose, e.g. future studies including more HVDC terminals. This paper can be used as a reference for the use of such models.

VII. ACKNOWLEDGMENTS

The authors would like to express their gratitude towards Dr. Yongtao Yang in DNV GL for his guidance and advisory in the development of this paper and the associated Master's Theses.

REFERENCES

- [1] Wind Europe, "Wind in power 2018: Annual combined onshore and offshore wind energy statistics," 2018.
- [2] Wind Europe, "Wind energy in Europe: scenarios for 2030," 2017.
- [3] H. Björklund, "Strong winds, high yield," in ABB review - special report 60 years of HVDC. pp. 22–25, 2014.
- [4] M. P. Bahrman and B. K. Johnson, "The ABCs of HVDC transmission technologies," in IEEE Power and Energy Magazine, vol. 5, no. 2, pp. 32–44, March–April 2007. doi: 10.1109/MPAE.2007.329194
- [5] Weixing Lu and Boon-Teck Ooi, "Optimal acquisition and aggregation of offshore wind power by multiterminal voltage-source HVDC," in IEEE Transactions on Power Delivery, vol. 18, no. 1, pp. 201–206, Jan. 2003. doi: 10.1109/TPWRD.2002.803826
- [6] R. Marquardt, "Modular multilevel converter: An universal concept for HVDC-Networks and extended DC-Bus-applications," The 2010 International Power Electronics Conference - ECCE ASIA -, Sapporo, 2010, pp. 502–507. doi: 10.1109/IPEC.2010.5544594
- [7] K. Ilves, S. Norrga, L. Harnefors and H. Nee, "On energy storage requirements in modular multilevel converters," in IEEE Transactions on Power Electronics, vol. 29, no. 1, pp. 77–88, Jan. 2014. doi: 10.1109/TPEL.2013.2254129
- [8] A. Taffese, A. Endeganew, S. Sanchez, E. Tedeschi, "Reducing rapid wind farm power fluctuations using the modular multilevel converter", unpublished.
- [9] D. Van Hertem, O. Gomis-Bellmunt and J. Liang, "HVDC grids", Wiley Online Library, 2016.
- [10] D. Winkle and C. Gühmann, "Hardware-in-the-Loop simulation of a hybrid electric vehicle using Modelica/Dymola," in Proceedings of the 22nd international battery, hybrid and fuel cell Electric Vehicle Symposium (EVS-22), Yokohama, Japan, pp. 1054–1063, 2006.
- [11] M. Otter, C. Schlegel and H. Elmqvist, "Modeling and realtime simulation of an automatic gearbox using Modelica," in Proceedings of ESS, pp. 19–23, Citeseer, 1997.
- [12] J. Espvik, "Modeling of multiterminal HVDC grids with renewable energy and storage integration by opensource tools for HIL applications", M.S. thesis, Norwegian University of Science and Technology, Trondheim, June 2019.
- [13] E. Tranulis, "Modeling of the MMC and its energy dynamics in an offshore HVDC perspective using OpenModelica", M.S. thesis, Norwegian University of Science and Technology, Trondheim, June 2019.
- [14] S. Khan, E. Tedeschi, "Modeling of MMC for fast and accurate simulation of electromagnetic transients: a review," in Energies, vol. 10, no. 8, 2017. doi: 10.3390/en10081161
- [15] G. Bergna-Diaz, J. A. Suul and S. D'Arco, "Energy-based state-space representation of modular multilevel converters with a constant equilibrium point in steady-state operation," in IEEE Transactions on Power Electronics, vol. 33, no. 6, pp. 4832–4851, June 2018. doi: 10.1109/TPEL.2017.2727496
- [16] G. Bergna, J. A. Suul and S. D'Arco, "State-space modelling of modular multilevel converters for constant variables in steady-state," 2016 IEEE 17th Workshop on Control and Modeling for Power Electronics (COMPEL), Trondheim, 2016, pp. 1–9. doi: 10.1109/COMPEL.2016.7556695
- [17] C. Bajracharya, M. Molinas, J. A. Suul, T.M. Undeland, Tore M, "Understanding of tuning techniques of converter controllers for VSC-HVDC," in Nordic Workshop on Power and Industrial Electronics (NORPIE/2008), June 9–11, 2008, Espoo, Finland, 2008.

APPENDIX

[18] S. Heier, "Grid integration of wind energy: onshore and offshore conversion systems", John Wiley & Sons. 2014.

[19] H. Hesse, M. Schimpe, D. Kucevic and A. Jossen, "Lithium-ion battery storage for the grid a review of stationary battery storage system design tailored for applications in modern power grids", in *Energies*, vol. 10, no. 12, 2017.

[20] B. McKeon, J. Furukawa, Jun and S. Fenstermacher, "Advanced lead-acid batteries and the development of grid-scale energy storage systems", in *Proceedings of the IEEE*, vol. 102, no. 6, pp. 951–963, 2014.

[21] J. Beerten, S. D'Arco and J. A. Suul, "Frequency-dependent cable modelling for small-signal stability analysis of VSC-HVDC systems," in *IET Generation, Transmission & Distribution*, vol. 10, no. 6, pp. 1370-1381, 21 4 2016. doi: 10.1049/iet-gtd.2015.0868

[22] A. Taffese, A. Endegnanew, S. Sanchez, E. Tedeschi, "Reducing rapid wind farm power fluctuations using the modular multilevel converter", unpublished.

[23] A. A. Taffese, E. Tedeschi and E. de Jong, "A control scheme for utilizing energy storage of the modular multilevel converter for power oscillation damping," 2017 IEEE 18th Workshop on Control and Modeling for Power Electronics (COMPEL), Stanford, CA, 2017, pp. 1-8. doi: 10.1109/COMPEL.2017.8013415

[24] A. E. Leon, "Short-term frequency regulation and inertia emulation using an MMC-Based MTDC System," in *IEEE Transactions on Power Systems*, vol. 33, no. 3, pp. 2854-2863, May 2018. doi: 10.1109/TPWRS.2017.2757258

[25] J. Freytes et al., "Dynamic analysis of MMC-based MTDC grids: use of MMC energy to improve voltage behavior," in *IEEE transactions on power delivery*, vol. 34, no. 1, pp. 137-148, Feb. 2019. doi: 10.1109/TPWRD.2018.2868878

[26] I. Puranik, L. Zhang and J. Qin, "Impact of low-frequency ripple on lifetime of battery in MMC-based battery storage systems," 2018. 10.1109/ECCE.2018.8558061.

[27] C. A. Bharadwaj and S. Maiti, "Modular multilevel converter based hybrid energy storage system," 2017 IEEE PES Asia-Pacific Power and Energy Engineering Conference (APPEEC), Bangalore, 2017, pp. 1-6. doi: 10.1109/APPEEC.2017.8308983

TABLE I
SYSTEM PARAMETERS

Component	System parameters		
	Parameter	Value	Unit
MMC	S_n	1059	MVA
MMC	V_n	333	kV
MMC	$R_{a,pu}$	0.005	p.u.
MMC	$R_{f,pu}$	0.00285	p.u.
MMC	$L_{a,pu}$	0.08	p.u.
MMC	$L_{f,pu}$	0.16428	p.u.
MMC	$C_{eq,pu}$	0.8	p.u.
MMC	$C_{DC,pu}$	0.051637	p.u.
HVDC cable	C_l	0.1983	$\mu\text{F}/\text{km}$
HVDC cable	G_l	$7.6330 \cdot 10^{-11}$	S/km
HVDC cable	R_{1l}	$1.1724 \cdot 10^{-1}$	Ω/km
HVDC cable	R_{2l}	$8.2072 \cdot 10^{-2}$	Ω/km
HVDC cable	R_{3l}	$1.1946 \cdot 10^{-2}$	Ω/km
HVDC cable	L_{1l}	$2.2861 \cdot 10^{-1}$	mH/km
HVDC cable	L_{2l}	1.5522	$[\text{mH}/\text{km}]$
HVDC cable	L_{3l}	3.2943	$[\text{mH}/\text{km}]$
Turbine	P_{rated}	7	MW
Turbine	J	$4 \cdot 10^6$	kgm^2
Turbine	B	$2 \cdot 10^6$	$\text{sN}^{-1}\text{m}^{-1}$
Turbine	ℓ	75	m
Turbine	ρ	1.2	kgm^{-3}
Turbine	λ_{opt}	8.1	p.u.
Turbine	C_{pmax}	0.48	p.u.
Turbine	u_{rated}	11.14	ms^{-1}
Turbine	T_{pitch}	1	s
ESS	P_{rated}	250	MW
ESS	t_{rated}	1	hour
ESS	η	0.9304	hour
ESS	$SOC_{lim,upper}$	0.9	p.u.
ESS	$SOC_{lim,lower}$	0.2	p.u.
ESS	T_{delay}	10	ms